

Multimode Collocated Vibration Control with Multiple Piezoelectric Transducers

Ivan Giorgio

▶ **To cite this version:**

Ivan Giorgio. Multimode Collocated Vibration Control with Multiple Piezoelectric Transducers. Mechanical engineering [physics.class-ph]. Università degli studi di Roma I, 2008. English. NNT : . tel-00798635

HAL Id: tel-00798635
https://theses.hal.science/tel-00798635

Submitted on 9 Mar 2013

HAL is a multi-disciplinary open access archive for the deposit and dissemination of scientific research documents, whether they are published or not. The documents may come from teaching and research institutions in France or abroad, or from public or private research centers.

L'archive ouverte pluridisciplinaire **HAL**, est destinée au dépôt et à la diffusion de documents scientifiques de niveau recherche, publiés ou non, émanant des établissements d'enseignement et de recherche français ou étrangers, des laboratoires publics ou privés.

Ivan Giorgio

Multimode Collocated Vibration Control with Multiple Piezoelectric Transducers



June 2008



SAPIENZA
UNIVERSITÀ DI ROMA

PhD in
THEORETICAL AND APPLIED MECHANICS
XX Cycle

MULTIMODE COLLOCATED VIBRATION CONTROL WITH MULTIPLE PIEZOELECTRIC TRANSDUCERS

by

Ivan Giorgio

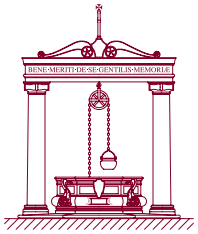
Thesis submitted in conformity with the requirements
for the Degree of

Doctor of Philosophy

Tutor:
prof. Dionisio Del Vescovo

Printed on August 18, 2008

Ivan Giorgio: *Multimode Collocated Vibration Control with Multiple Piezoelectric Transducers,* © June 2008



Dipartimento di Meccanica
e Aeronautica

Abstract

Multimode Collocated Vibration Control with Multiple Piezoelectric Transducers

In this thesis a new approach is presented to control vibrations for one- and two-dimensional mechanical structures, as beam or thin plates, by means of several piezoelectric transducers shunted with a proper electric network system. The governing equations for the whole system are coupled to each other through the direct and converse piezoelectric effect. The mechanical equations are expressed in accordance with the modal theory considering n vibration modes, that in need of control, and the electrical equations reduce to the one-dimensional charge equation of electrostatics for each of n considered piezoelectric transducers. In this electromechanical system, a shunting electric device forms an electric subsystem working as multi-degree of freedom damped vibration absorber for the mechanical subsystem. Herein, it is introduced a proper transformation of the electric coordinates in order to approximate the governing equations for the whole shunted system with n uncoupled, single mode piezoelectric shunting systems that can be readily damped by the methods reported in literature. A further numerical optimisation problem on the spatial distribution of the piezoelectric elements allows to achieve an effective multi-mode damping. Numerical case studies of two relevant systems, a double clamped beam and a fully clamped plate, allow to take into account issues relative to the proposed approach for vibration control. Laboratory experiments carried out in real time on a beam clamped at both ends consent to validate the proposed technique.



"The unexamined life is not worth living"

(Plato, *The Apology of Socrates* [38a])

Whoever limiting his worldly ambitions
finds satisfaction in the speculative life
has in the approval of an enlightened and competent judge
a powerful incentive to labours,
the benefits of which are great but remote,
and therefore such as the vulgar altogether fail to recognise.

To such a judge and to his gracious attention
I now dedicate this work.

Preface

The immediate reason to draw up this thesis is the necessity to summarise all the work done by me in three years of study, in accordance with my duty, given that[1]:

> *"... non fa scïenza,*
> *sanza lo ritenere avere inteso."*

Two are criteria that have driven me to write this thesis: *comprehensibility* and *synthesis*. I have chosen to provide both examples and explanations in order to satisfy the first criterion, albeit these involve a larger length of this work. It is true that Abbot Terrasson tells us that *if the size of a book were measured not by the number of its pages but by the time required to understand it, then we could say about many books that they would be much shorter if they were not so short*. Examples and explanations certainly make easier to understand the written but they also involve some inopportune effects. In fact, if we are concerned with the distinctness and the comprehensibility of a voluminous whole of speculative cognition that yet coheres in one principle, then we could just as legitimately say that *many books would have turned out much more distinct if they had not been intended to be quite so distinct* that is, "clear" in the popular sense —plenty of examples. For the aids to distinctness, while helpful in parts of a book, are often distracting in the book as a whole. They keep the reader from arriving quickly enough at an overview of the whole; and with all their bright colours they do cover up and conceal the articulation of the dissertation. However, if we are concerned with the synthesis, it is worth saying that examples and explanations are necessary for a popular publication but this report is written primarily for engineers, and they do not

[1] Dante Alighieri (1265–1321). *La Divina Commedia*, Par., V, 41–42.

need of these facilities. Hence, as good as always, I have tried to achieve a right balance taking into account all these points of view.

Acknowledgments

I would like to thank my supervisor *Dionisio Del Vescovo*, for his many suggestions and constant support during this research. I am also thankful to *Antonio Culla* and *Corrado Maurini* for their guidance and friendly encouragement, which gave me a better perspective on my own results and provided many useful references.

Of course, I am grateful to my parents for their patience and *love*. Without them this work would never have come into existence. In particular I would like to acknowledge the "*Laboratoire de Modélisation en Mécanique*" (*CNRS-UMR* 7607, University of Paris 6).

Rome, Italy *Ivan Giorgio*
June 2008

Contents

Introduction 1

I Vibration Control Using Piezoelectric Transducers 11
- I.1 Modal Approach to Modelling . . . 12
- I.2 An Independent Modal-Space Shunt Damping Technique . . . 15
  - I.2.1 Linear Transformation for Independent Control . . . 21
  - I.2.2 Piezoelectric Placement for Independent Control . . . 23
- I.3 Two-Equation Systems Uncoupled . . . 24
- I.4 Controllability and Observability . . . 26
- I.5 Vibration Control with a Single Piezoelectric Transducer . . . 27
- I.6 Generalised Passive Approach . . . 27
  - I.6.1 Parallel Configuration . . . 28
  - I.6.2 Series Configuration . . . 34
  - I.6.3 Comparisons . . . 38
- I.7 Generalised Hybrid Approach . . . 41
  - I.7.1 A Passive Shunt Circuit with Compensating Action . . . 44
- I.8 Generalised Active Control . . . 45
  - I.8.1 Optimal Control in the Time Domain . . . 48
  - I.8.2 Pole Allocation with State Feedback Control . . . 49
  - I.8.3 State Estimation . . . 50
- I.9 Control and Observer Spillover . . . 52

II Physical System Models 54
- II.1 First Order Theory of Thin Plates . . . 54
  - II.1.1 Introduction . . . 54
  - II.1.2 Hamiltonian Formulation . . . 57
- II.2 Piezoelectric Transducers . . . 59

II.2.1 General Notices 59
II.2.2 Equations of Plate with Transducers 64
II.3 Modal Analysis 68
II.4 Finite Element Model 69

III Numerical Simulations **72**
III.1 Clamped-Clamped Beam Case Study 72
III.1.1 Numerical Results 77
III.2 Fully Clamped Plate Case Study 83
III.2.1 Piezoelectric Transducer Allocation 83
III.2.2 Numerical Results and Comparisons 86

IV Laboratory Experiments **93**
IV.1 Experimental Set Up 93
IV.1.1 Mobility Estimations 94
IV.2 System Identification 97
IV.2.1 Mechanical Parameters 97
IV.2.2 Piezoelectric Parameters 102
IV.3 Control Validation 107
IV.3.1 The Control System 107
IV.3.2 Results 108

Conclusions **112**

A Rectangular Plates **115**
A.1 Newtonian Formulation 115
A.2 Hamiltonian Formulation 119
A.3 Vibration of Fully Clamped Plates 121
A.4 Modal Analysis with the Finite Element Model 130

Bibliography **143**

List of Figures

1 Crystals without a permanent polarisation 5
2 Ferroelectric crystals 6

I.1 Block diagram of the electro-mechanical system 24
I.2 Shunt circuit in parallel configuration 28
I.3 Root locus for parallel shunt circuit 32
I.4 Mobilities for parallel shunt circuit 34
I.5 Shunt circuit in series configuration 35
I.6 Mobilities for series shunt circuit 39
I.7 Sensitivity functions for fixed points method 39
I.8 Sensitivity functions for pole allocation method 40
I.9 Ratio between the mobility peaks for passive circuit 41
I.10 Shunt circuit with compensating action 44
I.11 Mobilities with different compensating actions 46
I.12 Sensitivity functions with different compensating actions 46
I.13 Mobilities for active control 50
I.14 Sensitivity functions for active control 51
I.15 Block diagram of the observer estimate 52

II.1 Plate representation 55
II.2 Scheme of the piezoelectric transducers 60
II.3 A detail of the scheme for modelling the system with FEM . . . 70

III.1 Piezoelectric transducers placement on the beam 75
III.2 SIMULINK model 76
III.3 Beam mobility for passive approach in parallel configuration . 79
III.4 Beam mobility for passive approach in series configuration . . 80
III.5 Beam mobility for hybrid approach in parallel configuration . . 80

III.6 Beam mobility for active approach 81
III.7 Beam impulse response for passive approach in parallel configuration 81
III.8 Beam impulse response for hybrid approach in parallel configuration 82
III.9 Beam impulse response for active approach 82
III.10 Smart Plate 83
III.11 Piezoelectric placement index 85
III.12 Plate mobility for passive approach in parallel configuration . . 87
III.13 Plate mobility for hybrid approach in parallel configuration . . 88
III.14 Plate mobility for active approach 88
III.15 Plate impulse response for passive approach in parallel configuration 89
III.16 Plate impulse response for hybrid approach in parallel configuration 89
III.17 Plate impulse response for active approach 90
III.18 Electrical scheme for current flowing control 90
III.19 Comparison of the proposed and the current flowing control . 92

IV.1 Beam representation 94
IV.2 Mobility of the beam actuated by the first piezo-element 96
IV.3 Mobility of the beam actuated by the second piezo-element . . 96
IV.4 Mobility of the beam actuated by the third piezo-element . . . 97
IV.5 Regenerated mobility of the beam actuated by the first piezo-element 99
IV.6 Nyquist plot of mobility of the beam actuated by the first piezo-element 99
IV.7 Regenerated mobility of the beam actuated by the second piezo-element 100
IV.8 Nyquist plot of mobility of the beam actuated by the second piezo-element 100
IV.9 Regenerated mobility of the beam actuated by the third piezo-element 101
IV.10 Nyquist plot of mobility of the beam actuated by the third piezo-element 101

IV.11 Regenerated impedance of the first piezo-transducer 104
IV.12 Nyquist plot of impedance of the first piezo-transducer 104
IV.13 Regenerated impedance of the second piezo-transducer 105
IV.14 Nyquist plot of impedance of the second piezo-transducer . . . 105
IV.15 Regenerated impedance of the third piezo-transducer 106
IV.16 Nyquist plot of impedance of the third piezo-transducer 106
IV.17 FRF function of the beam to measure coupling coefficients . . . 108
IV.18 Simulink model for the real-time application 109
IV.19 Inertance with control of the first and the second mode 109
IV.20 Inertance with control of the first and the third mode 110
IV.21 Inertance with control of the second and the third mode 110

A.1 Convention for loads acting on the plate 116
A.2 Plate characteristic functions 129
A.3 First mode shape of the plate 130
A.4 Second mode shape of the plate 131
A.5 Third mode shape of the plate 131
A.6 Fourth mode shape of the plate 132
A.7 Fifth mode shape of the plate 132
A.8 First mode rotation around the axis X of the plate 133
A.9 Second mode rotation around the axis X of the plate 133
A.10 Third mode rotation around the axis X of the plate 134
A.11 Fourth mode rotation around the axis X of the plate 134
A.12 Fifth mode rotation around the axis X of the plate 135
A.13 First mode rotation around the axis Y of the plate 135
A.14 Second mode rotation around the axis Y of the plate 136
A.15 Third mode rotation around the axis Y of the plate 136
A.16 Fourth mode rotation around the axis Y of the plate 137
A.17 Fifth mode rotation around the axis Y of the plate 137

List of Tables

II.1 Voigt notation 62

III.1 Piezoelectric properties 73
III.2 Specifications of the piezoelectric transducers 74
III.3 Plate specifications 84
III.4 Parameters of the current flowing circuits used for comparison 91

IV.1 Damping ratio of the bending modes 98
IV.2 Resonance frequencies of the beam 102
IV.3 Curve-fitting estimated piezoelectric coupling coefficients . . . 103
IV.4 Curve-fitting estimated piezoelectric capacitances 103
IV.5 Measured piezoelectric coupling coefficients 107
IV.6 Predicted piezoelectric coupling coefficients 107

A.1 SS mode parameters 127
A.2 SA mode parameters 127
A.3 AS mode parameters 127
A.4 AA mode parameters 128

Introduction

Piezoelectric materials have been a great expansion in the engineering application of structural control. One reason for this is that it may be possible to create certain types of systems capable of adapting to or correcting for changing operating conditions. The advantage of incorporating these special types of material into the structure is that the sensing and actuating mechanism becomes part of the structure.

In the last years the employ of structures more and more thin had made arise numerous issues regarding vibrations. The challenge of reliability and durability of mechanical structures is an important task for engineers, the design of systems leading to the efficient control of structural vibrations in order to reduce fatigue load, crack propagation and damage appears to be an attractive opportunity. Then the object of this dissertation is to investigate the possibility to reduce vibrations. Thus, the topics presented in this research work are chiefly concerned with application to mechanical vibrations, system identification, automotive, railway and aerospace industries. To take into account a possible effective control, piezoelectric transducers are employed. This is primarily due to their abilities but also to the growing availability of more efficient piezoelectric ceramics. Smart structures using piezoelectric material are successfully employed in reducing vibration [Alessandroni et al., 2005; Dosch et al., 1992; Anderson and Hagood, 1994; Hollkamp and Starchville, 1994; Badel et al., 2006; Wu, 1998; Tang and Wang, 2001; dell'Isola and Vidoli, 1998; Thorp et al., 2001]. Piezoelectric materials produce a voltage when strained and conversely strain when undergone to a voltage. This property is very interesting, because a piezoelectric element can be indifferently used either as a sensor or an actuator. Moreover, these piezoelectric element skills can be simultaneously employed to obtain a collocated sensor-actuator

control and to achieve with ease a stable control. The piezoelectric transducers coupled to mechanical structures can convey the mechanical energy flow toward electric network systems where it is dissipated: it is a piezoelectric shunt-damping. The use of the *piezoelectric shunt damping* technique for vibration reduction in one and two dimensional flexible structures is a very common practice because of the strong electromechanical coupling associated with currently available piezoelectric transducers. In this technique the piezoelectric transducers, bonded on the flexible structure, are shunted by a passive electric network that acts as a damped vibration absorber for the host mechanical structure. A classical application of this method is a single resonant piezoelectric shunting system studied in [Hagood and Flotow, 1991; Wu, 1996]. The damper is formed by a piezoelectric element shunted with an inductor and a resistor. The external shunt circuit with the inherent piezoelectric capacitance is a RLC circuit. Its natural frequency is imposed equal to one natural frequency of the host mechanical structure by maximising the energy exchange. The resistance role is to maximise the electric dissipation of the energy coming from the mechanical structure. Its main drawback is the requirement of high-value inductors, 10–1000 H, working at high-voltage. For this reason, passive components are simulated by active circuits, synthetic impedances or alternatively admittances, which require an external feeding. Subsequent applications involve one piezoelectric transducer coupled with a multi-resonant electric network to damp a set of mechanical modes. Hollkamp's circuit is one of this kind [Hollkamp, 1994]. The shunt circuit consists of a set of branches whose main is an RL circuit. The other branches are RLC shunts. The number of controlled mechanical modes is equal to the number of the branches. An issue of this technique is the necessity of retuning the circuit when a branch is added. Indeed, in [Hollkamp, 1994] is proposed no closed-form tuning solution. Further approaches use multiple piezoelectric transducers by shunting each of them to a proper multi-resonant electric network [Moheimani et al., 2004]. In practice, to account for the undesired cross influence of the shunt circuits on the mechanical modes to be controlled, a fine-tuning is due.

In [dell'Isola and Vidoli, 1998; Andreaus et al., 2004; Maurini et al., 2004; Alessandroni et al., 2005] systems with periodically distributed piezoelectric

transducers and modular shunting networks are considered. This approach adopts homogenised continuum modelling and looks for periodic lumped electric systems having, in the continuum limit, the same dynamic behaviour of the mechanical structure to be controlled. The drawback of this "continuum mechanics" approach is the requirement of a high number of piezoelectric elements and complicated shunting networks, in order to approach the continuum limit. Moreover, different types of structures, *e.g.* beams or plates, demand the solution of specific design problems. The theoretical and numerical results provided optimal electric networks for damping flexural vibrations of beams [Andreaus et al., 2004; Maurini et al., 2004] and plates [Alessandroni et al., 2005]; in reference [dell'Isola et al., 2004] a first experimental implementation is presented.

The interpretation of piezoelectric shunt damping systems as a feedback control problem allows to employ this technique to realise collocated vibration active control in which piezoelectric transducers are used both as sensors and actuators. In [Tang and Wang, 2001], it is proposed the use of "negative capacitance" carrying out with an active devise op-amp based. Other applications perform active control systems no-collocated, as reported in [Rizet et al., 2000], where the implementation of a modal filtering on a *DSP* board is proposed to control the flexural vibrations of a beam.

Semi-active techniques [Badel et al., 2006; Niederberger and Morari, 2006] develop non-linear switching shunting to avoid the use of high-value inductors and to obtain a wide-band damping, with reduced power requirements. As showed in [Niederberger and Morari, 2006], the switch shunt is less performing but more robust than the standard RL shunt.

In conclusion, as underlined in [Chopra, 2002; Moheimani, 2003], the development of efficient and reliable techniques for control with multiple piezoelectric transducers remains an open problem.

The aim of this study is to extend the resonant shunting techniques to control multiple modes with multiple piezoelectric transducers by an electric network which connects the whole set of piezoelectric elements. The key idea in this thesis is to make the whole shunted system equivalent to a set of independent, single resonant piezoelectric shunting systems. Therefore, it is possible to use the widely investigated methods presented in literature.

A Brief Digression on Piezoelectricity

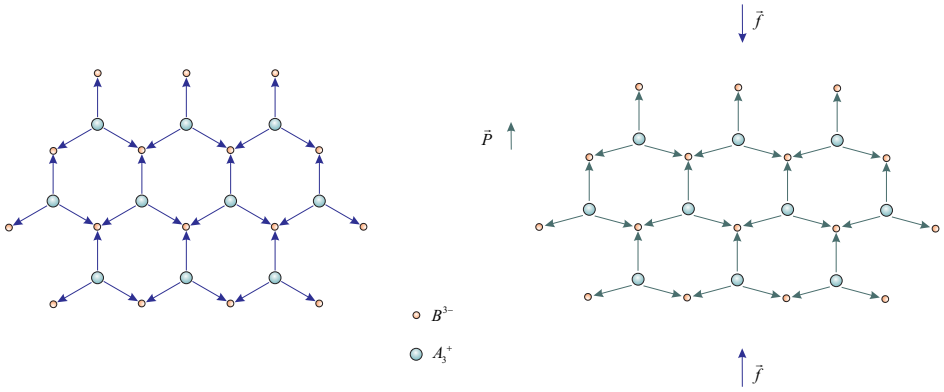
In 1880, the brothers Pierre and Jacques Curie predicted and demonstrated piezoelectricity[2]. They showed that crystals of tourmaline, quartz and Rochelle salt (sodium potassium tartrate tetrahydrate) generate electrical polarisation from mechanical stress. Quartz and Rochelle salt exhibited the most piezoelectricity. Converse piezoelectricity was mathematically deduced from fundamental thermodynamic principles by Lippmann in 1881. The Curies immediately confirmed the existence of the "converse effect", and went on to obtain quantitative proof of the complete reversibility of electro-elasto-mechanical deformations in piezoelectric crystals. More exactly the piezoelectricity is the aptitude of a material to show polarisation charges on certain faces as a result of the application of mechanical stress. This effect is called direct piezoelectric or piezo-generator. It is reversible, indeed, if one imposes an external electric-field vector, the body will be strained in a way that depends on the direction and magnitude of electric vector. This is inverse piezoelectric effect or piezo-motor. The deformation is of the order of nanometres, nevertheless piezoelectric materials find useful applications such as the production and detection of sound, generation of high voltages, electronic frequency generation, microbalance, and ultra-fine focusing of optical assemblies.

Necessary condition for existence of the piezoelectric phenomenon is the anisotropy of the material. Piezoelectric materials are crystals not having a crystallographic symmetric centre. Punctual groups not-centre-symmetric are 21 of the 32 crystallographic classes and, more exactly, if one represents them by an international standard, are

$$
\begin{gathered}
1,\ 2,\ 3,\ 4,\ 6,\\
m, mm2, 3m, \bar{4}, 4mm, \bar{4}2m, \bar{6}, 6mm, \bar{6}2m, \bar{4}3m,\\
222,\ 32,\ 422,\ 622,\ 23,\ 432.
\end{gathered}
$$

The piezoelectric phenomenon is possible only for 20 of these because the 432, that belongs to the cubic system, even though not centre-symmetric, shows characteristics of symmetry combining do not allow any piezoelectric effect.

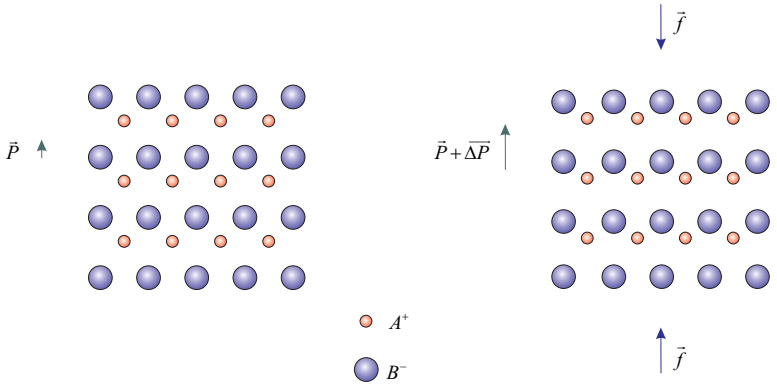
[2]The word is derived from the Greek $\pi\iota\varepsilon\zeta\acute{\varepsilon}\omega$, which means I squeeze or press.



1.1: Unloaded crystal. 1.2: Loaded crystal.

Figure 1: The subfigure 1.1 shows a crystal having a ternary symmetry axis with lack of external loads. In this crystal are depicted electric dipole moments on a proper crystallographic plane. The vector sum of electric dipole moments is zero for each group of vectors. The subfigure 1.2 shows a crystal undergone a compression by force, $\vec{f}$, that generates a polarisation, $\vec{P}$. The total vector sum of electric dipole moments is not more zero.

The piezoelectric phenomenon can be explained by two different examples. The former is characterised by the presence of some electric dipole moments for each elementary cell, whose vector sum is zero. If one applies a mechanical or electric load in a given direction, a polar moment not-null arises. Figure 1 sketches a simplified illustration of this case. A hydrostatics pressure does not allow the piezoelectric phenomenon because the load is the same in all directions. The quartz (SiO_2) is a member of this class. The latter is distinguished, in lack of external perturbations, by an electric dipole moment not-null, and so by only one permanent polar axis. Figure 2 depicts a sketch of this second mechanism. They have a related property known as pyroelectricity. This property, known as early as the 19th century and named by David Brewster in 1824, is the aptitude of certain mineral crystals to generate electrical charge on their surfaces in case they undergo an uniform heating. This electric charge is proportional to the difference of temperature and it is the result of electric dipole magnitude variation. It is worth to note that even crystals not pyroelectric can show a superficial electric charge if it is heated not uniformly, as consequence of internal stress due to thermal ex-



2.1: Unloaded crystal. 2.2: Loaded crystal.

Figure 2: The subfigure 2.1 shows a crystal lattice having a permanent polarisation, that is ferroelectric one in an undeformed state, where the polarisation is due to the position not symmetric of the ion A^+. The subfigure 2.2 shows a lattice in presence of a compression force, $\vec{f}$, that produced a variation of polarisation, $\Delta\vec{P}$, the piezoelectric induced polarisation.

pansion. Only 10 of the 20 not-symmetric-centre classes, written above, are pyroelectric. These crystals, differently by those not having polar axis, shows piezoelectric properties even in case of hydrostatics pressure. Examples of pyroelectric crystals are the tourmaline[3] and zinc oxide (ZnO).

Ferroelectric materials are particular pyroelectric crystals which have got the ability to invert own electric dipole moment through the application of electric field with appropriate strength. The presence of a dipole moment not-null, however, is not sufficient to guarantee the ferroelectricity. Besides, not all pyroelectric crystals can be ferroelectric; the electric field necessary to obtain the inversion of dipole could be too strong and cause the breaking of material. The graph of induced polarization[4], $\vec{P}$, or of stored charge, Q, versus to applied voltage, V, in ferroelectrics has a hysteretic cycle, in contrast to other dielectrics that show a linear relationship. There is in this cycle a residual polarisation $\vec{P}_r$, whose verse is depend on history of V, that is the

[3]Tourmaline have general formulae: $AX_3Y_6(BO_3)_3Si_6O_{18}(O,OH,F)_4$. In this A means calcium or sodium; X means aluminium, iron, lithium or magnesium; Y means aluminium, and less usually chrome or iron.

[4]The polarisation is a vector quantity defined as the electric dipole moment per unit of volume. Also called dielectric or electric polarisation.

polarisation for V null. It occurs, moreover, to note a polarisation of saturation, $\vec{P}_s$, referring to high applied electric field[5]. The ferroelectric property is typical at low temperatures because enhancing the thermic agitation motion the arrangement of dipoles is destroyed. Over a certain temperature, called transition temperature or Curie point, T_c, the material has a paraelectric behaviour or, easier, not-ferroelectric. The symmetry of the paraelectric phase, being stable over T_c, is centre-symmetric and the transition that turns out for cooling implies easily a reduction of symmetry, passing to a punctual group not-centre-symmetric. This transition occurring at T_c is, indeed, an example of phase transition order-disorder. Into ferroelectric crystals there are regions in which adjacent electric moments are uniformly arrayed. These regions are called *domains*. These have variable dimensions but usually are about tens or a hundreds of angstroms; the thickness of boundary can be only one reticular constant too. Inside each domain dipoles are arranged according to a unique crystallographic axis. The total polarisation of a ferroelectric material is the vector sum of polarisation of each domain. If one applies an external electric field, such a field tries to align all dipoles in direction of the same field. The condition of saturation is achieved when the alignment is whole. The Rochelle salt ($KNaC_4H_4O_6 \cdot 4H_2O$), the lithium niobate ($LiNbO_3$) are examples of ferroelectric crystals. Often ferroelectric oxides are used in capacitors for their high dielectric constants, in particular near to T_c.

Very important in applications are piezoelectric ceramics made of ferroelectric micro-crystals, each of them being organised in many domains. These materials are turned artificially piezoelectric; they are heated up to Curie point and undergone, during the cooling, the high electric-field vector, that lines up dipoles producing a stable polarisation in limits of the mechanical, thermic or electric load of the material. During the process of the polarisation, the ceramic is subjected to an expansion in the direction of electric field and a compression in the two orthogonal directions. Such variations of dimension remain even after the removal of the electric-field vector. The orientation process of dipoles referred to as "poling", is analogous to the process by which a piece of soft iron can be magnetised by a magnetic field.

[5] For instance the barium titanate ($BaTiO_3$) has a saturation polarisation of 0.26 C m^{-2} at temperature of 296 K.

When the ceramic reaches the Curie point, it loses utterly and permanently its piezoelectric properties. The Curie point provides the upper limit of the temperature that can be achieved by a piezo-ceramic. The polarisation process of the piezo-ceramics is explained by its ferroelectric properties. In the ceramics, as it is comprehensible, a perfect alignment will never be obtained, because of mechanical stresses and of defects in grains of the material that does not allow the shift of the polar axis in the direction more favourable. At first the piezo-ceramic was isotropic, owing to the random orientation of micro-crystals; after the application of the electric field such isotropy is destroyed in the direction of the polarisation axis, but it is maintained in the plane orthogonal to it. Such a material is called orthotropic. It is undeniable that materials naturally piezoelectric have not grains with preferential directions of polarisation, and so they have reduced capacity of macroscopic deformation. The advantages of ceramic materials are summarised, without a doubt, in high efficiency of transformation electro-mechanic, even above 50%, in a good workable, in a lot of shapes obtainable, in a mass production. The greater disadvantages are linked up to the possibility of depolarisation; certainly, significant electric fields in opposite directions to the polarisation, or high alternating electric fields, or also important mechanical stresses, as well as temperatures higher than Curie point involve the loss of the piezoelectric property. It is important to note the phenomenon of the aging that is the decrease of the piezoelectric properties with the pass of time from the polarisation. Solid solutions of lead titanate-zirconate $Pb(Ti, Zr)O_3$, usually pointed out with short form PZT, is the most popular piezoelectric material in use. The success of these alloys stays on remarkable inducible polarisation and in a high transition temperature, 493–623 K, that allows the variation of their chemical composition by thermic treatments at high temperatures, changing as a result also heavily any physic properties without a decay of piezoelectric features. A PZT material shows strains of about 0.1% of the original dimension. They are divided into hard and soft PZT. The former has a narrow hysteretic cycle, resists to high mechanical or electric loads, and besides ages more slowly. It is suitable to be employed as generator and transducer with high voltage or power. The latter has a large sensitivity and high dielectric constants but the depolarisation and the heating turn out easy. It is used as

sensor or transducer with high impedance.

Other materials with piezoelectric effect are piezo-polymers, as the polyvinyl difluoride, $PVDF$, and copolymers of vinylidene fluoride, VDF, trifluoroethylene, $TrFE$, e tetrafluoroethylene $TeFE$. Even they undergo a process of poling completely analogous to that of piezo-ceramics. They are used at high frequencies, in contrast with piezo-ceramics that cannot be used because too fragile. These materials have a wide range of frequency of employment, a low acoustic impedance, a high elastic deformation, as well as a high dielectric strength[6]. They have, however, low acting temperatures and a modest efficiency in the electro-mechanical conversion. In other words they are more right as sensors rather than actuators. There are notable differences between $PVDF$ and PZT materials. For instance, on average, PZT is approximately four times as dense, forty times stiffer, and has a permittivity one hundred times as great as that of $PVDF$. Therefore, $PVDF$ is much more compliant and lightweight, making it more attractive for sensing applications, lessening the insertion error. In contrast, PZT is often preferred as an actuator since it exhibits a greater induced strain [Moheimani, 2003].

Finally there are piezo-composites too, or rather materials made of polymers and piezo-ceramics.

Features of better consideration in a piezoelectric material are:

a) high efficiency of electro-mechanical transformation;

b) wide range of frequency of employment;

c) good stability at variation of environment conditions as the temperature or the humidity;

d) easily workable;

e) several shapes obtainable.

Damages due to aging are typical of sensors and are negligible for actuators, because in actuators the material undergoes an electric-field vector with the same direction of the polarisation. A further issue in piezoelectrics

[6]The maximum electrical field that a material can withstand without rupture; usually specified in volts per millimetre of thickness. Also known as electric strength.

is given by the creep. This last, however, is very small, at its maximum value achieved in few hours it differs of 1% from last driven motion.

In the end, it is useful to note that electrostrictive materials are not piezoelectric and possess no spontaneous polarisation. The electrostriction is a form of elastic deformation of a dielectric induced by an applied electric field, associated with those components of strain which are independent of reversal of field direction, in contrast to the piezoelectric effect. It is found in all dielectric materials although their deformations are usually too small, approximately between 10^{-7}% and 10^{-5}% of the original dimension, to utilise practically. Electrostrictive ceramics, based on a class of materials known as relaxor ferroelectrics, however, show strains comparable to piezoelectrics, 0.1% of the original dimension, and have already found application in many commercial systems. When correctly used they can be virtually loss free up to hundreds of kilohertzs.

CHAPTER I

Vibration Control Using Piezoelectric Transducers

> Knowledge is of no value unless you put it into practice.
>
> ANTON CHEKHOV (1860–1904)
> *Russian playwright*

STRUCTURAL vibration control is to implement energy dissipation devices or control systems into structures to reduce excessive vibration. Specifically, this chapter deals with control of one- and two-dimensional structures to reduce vibrations related to multiple mechanical modes by shunting several piezoelectric transducers with a multi-port electric system. Since each of the piezoelectric transducers integrate actuation and sensing capabilities within a single transducer, a collocated control is obtained. The electric network can be a passive electrical impedance system that acts to increase the mechanical damping. In spite of the passive nature of this control, however, this network is commonly made with an active electrical device that establishes a certain relationship between voltage and current at its terminals because of actualisation issues; in fact, it turns out that very large inductors, even about hundreds henries, are required. This technique, called "*virtual passive approach*", implements in an active manner the behaviour of passive damping systems. It is possible for the collocated nature of the piezoelectric transducers, see [Juang and Phan, 1992]. Besides, it is argued in [Moheimani, 2003] that the shunt damping technique can be interpreted as a multi-variable feedback control problem, in which the impedance, or alternatively the ad-

mittance of the electrical multi-port shunt, constitutes the feedback controller. Herein, following this approach the control signal is assumed the current flowing through each piezoelectric transducer and the measurement is assumed the voltage on the same piezoelectric element. Thus, considering that even for passive damping systems it is advantageous to mimic them with active devices, the restriction of the passivity for the controller can be removed by implementing also purely active control in which this arrangement is used to obtain better performance.

I.1 Modal Approach to Modelling

Linearly elastic continua, such as beams or plates, can be modelled with the same general formulation. Let $w(\mathbf{x},t)$ be the displacement field, defined for all point $\mathbf{x}$ over a domain $\mathscr{A}$ denoting the region occupied by system. The partial differential equation describing the behaviour of these systems is

$$\mathfrak{L}\left[w(\mathbf{x},t)\right]+\frac{\partial}{\partial t}\mathfrak{D}\left[w(\mathbf{x},t)\right]+\mathfrak{M}(\mathbf{x})\frac{\partial^2 w}{\partial t^2}(\mathbf{x},t)=f(\mathbf{x},t) \tag{I.1}$$

in which $\mathfrak{L}$ and $\mathfrak{M}$ are linear homogeneous differential operators respectively of orders $2k$ and $2m$ with $k>m$ with respect to the spatial coordinate x_i. They constitute a model of the stiffness and the mass density of system. $\mathfrak{D}$ is a linear homogeneous differential operator of order $2k$ similar to $\mathfrak{L}$, used to model a viscous damping. The term f describes an external distributed or point load; in case of a point force, f is of type $F_j(t)\delta(\mathbf{x}-\mathbf{x}_j)$ acting at point $\mathbf{x}_j$, with δ the Dirac delta. The equation (I.1) is completed with the following boundary conditions

$$\mathscr{B}_r\left[w(\mathbf{x},t)\right]=0 \qquad r=1,2,\dots k \tag{I.2}$$

which must be satisfied at every point of the boundary $\partial\mathscr{A}$ of the domain $\mathscr{A}$. In Eqs. (I.2) $\mathscr{B}_r$ are linear differential operators of orders ranging from zero to $2k-1$.

As above mentioned, piezoelectric devices can be used to reduce the vibrations of one or two dimensional systems and with the target of obtaining a collocated control by means of a set of n_p piezoelectric transducers, they can be used simultaneously as sensors and actuators. The Eq. (I.1) can be

rewritten

$$\mathfrak{L}_p\left[w(\mathbf{x},t)\right] + \frac{\partial}{\partial t}\mathfrak{D}_p\left[w(\mathbf{x},t)\right] + \mathfrak{M}_p(\mathbf{x})\frac{\partial^2 w}{\partial t^2}(\mathbf{x},t) = \\ = f_d(\mathbf{x},t) + \sum_{h=1}^{n_p}\mathfrak{P}_h\left[\wp_h(\mathbf{x})\right]\frac{d\phi_h}{dt}(t) \quad \text{(I.3)}$$

where $f_d(\mathbf{x},t)$ is the disturbance load to the structure; the second term on the right hand side of Eq. (I.3) involves that each of n_p piezoelectric patches applies a forcing input proportional to the time derivative of the flux linkage ϕ_h, *i.e.* the terminal voltage of the h-th transducer. In particular $\mathfrak{P}_h$ is a linear homogeneous differential operator and $\wp_h(\mathbf{x})$ is a spatial function of piezoelectric localisation that takes the value one where the piezoelectric element is placed and zero everywhere else. As an example of $\mathfrak{P}_h$, for two dimensional bending problems, it can be considered proportional to the Laplacian operator [Koshigoe and Murdock, 1993]. Besides the subscript p in operators $\mathfrak{L}_p$ and $\mathfrak{M}_p$, and $\mathfrak{D}_p$, indicates the presence of the piezoelectric transducers which cause a slight difference. As a first order of approximation, each piezoelectric transducer is, according to Norton's theorem, electrically equivalent to a strain dependent charge generator in parallel with a capacitance C_h and a resistance R_h [Yang and Jeng, 1996]. Dynamic equations for transducers, implying the charge conservation, can thus be expressed as

$$Q_h(t) = C_h\frac{d\phi_h}{dt}(t) + \frac{1}{R_h}\phi_h(t) + \int_{\mathscr{A}_h}\mathfrak{P}_h\left[w(\mathbf{x},t)\right]d\mathscr{A}_h \qquad h = 1,2,\dots n_p \quad \text{(I.4)}$$

in which Q_h is the induced charge and each $\mathfrak{P}_h$, that represents the piezoelectric effect, is integrated on the region $\mathscr{A}_h$ occupied by the h-th transducer. In ordinary applications, the internal resistance R_h is very large and can be neglected.

To simplify the theoretical analysis, a normalised flux linkage is defined

$$\psi_h = \sqrt{C_h}\,\phi_h \qquad h = 1,2,\dots n_p \quad \text{(I.5)}$$

Substituting (I.5) in equation (I.3) can then be obtained

$$\mathfrak{L}_p\left[w(\mathbf{x},t)\right] + \frac{\partial}{\partial t}\mathfrak{D}_p\left[w(\mathbf{x},t)\right] + \mathfrak{M}_p(\mathbf{x})\frac{\partial^2 w}{\partial t^2}(\mathbf{x},t) = \\ = f_d(\mathbf{x},t) + \sum_{h=1}^{n_p}\mathcal{P}_h\left[\wp_h(\mathbf{x})\right]\frac{d\psi_h}{dt}(t) \quad \text{(I.6)}$$

where $\mathcal{P}_h = (1/\sqrt{C_h})\mathfrak{P}_h$. Besides, the Eq. (I.4) becomes

$$\mathcal{Q}_h(t) = \frac{d\psi_h}{dt}(t) + \frac{1}{R_h\, C_h}\psi_h(t) + \int_{\mathscr{A}_h} \mathcal{P}_h\left[w(\mathbf{x},t)\right] d\mathscr{A}_h \qquad h = 1,2,\dots n_p \quad \text{(I.7)}$$

being $\mathcal{Q}_h(t) = (1/\sqrt{C_h})Q_h(t)$.

The displacement, w, of the considered system may be expanded in the series

$$w(\mathbf{x},t) = \sum_i W_i(\mathbf{x})\,\eta_i(t) \qquad \text{with } i = 1,2,\dots \quad \text{(I.8)}$$

where $W_i(\mathbf{x})$ are the mode shapes of the i-th normal mode of the undamped system removing excitation f_d and under *short circuit condition*, $\dot{\phi}_h = 0$, $h = \{1,\dots n_p\}$[1], *i.e.* the eigenfunctions that are obtained by solving the eigenvalue problem

$$\mathfrak{L}_p\left[W(\mathbf{x})\right] = \lambda\, \mathfrak{M}_p(\mathbf{x}) W(\mathbf{x}) \quad \text{(I.9)}$$

with its associated boundary conditions deduced from the (I.2). In order to make the decomposition unique, the eigenfunctions are normalised to one. The coefficient $\eta_i(t)$ is the generalised coordinate describing the response of the i-th normal mode. In accord with the procedures based on the modal analysis, functions $\eta_i(t)$'s satisfy, taking n_m normal modes into account, n_m ordinary differential equations that in matrix form can be written as

$$\ddot{\boldsymbol{\eta}} + D\,\dot{\boldsymbol{\eta}} + \Omega^2\,\boldsymbol{\eta} - \tilde{\Gamma}\,\dot{\boldsymbol{\psi}} = \boldsymbol{f} \quad \text{(I.10)}$$

where, denoting each natural frequency of undamped oscillation under short circuit condition with ω_i, the $n_m \times n_m$ matrix Ω is defined as $\Omega_{ih} = \omega_i\,\delta_{ih}$ with δ_{ih} the Kronecker delta, the $n_m \times n_m$ damping matrix D is given by

$$D_{ih} = \int_{\mathscr{A}} W_i(\mathbf{x})\,\mathfrak{D}_p\left[W_h(\mathbf{x})\right] d\mathscr{A} \quad \text{(I.11)}$$

Note that the matrix D is symmetric if the operator $\mathfrak{D}_p$ is self-adjoint. However a very typical case is light damping, in this situation, it is possible to consider an approximate solution by neglecting the coupling of the normal coordinates due to damping and, thus, ignore the off-diagonal elements in the damping matrix D. The $n_m \times n_p$ *piezoelectric coupling* matrix $\tilde{\Gamma}$ whose entries $\tilde{\Gamma}_{ih}$ represent the coupling coefficient between the i-th normal mode shape

[1] The superscript dot denotes the derivative with respect to t.

and the h-th piezoelectric transducer, being the operator $\mathcal{P}_h$ self-adjoint, is defined by

$$\tilde{\Gamma}_{ih} = \int_{\mathscr{A}} W_i(\mathbf{x})\, \mathcal{P}_h\left[\wp_h(\mathbf{x})\right] d\mathcal{A} = \int_{\mathscr{A}} \wp_h(\mathbf{x})\, \mathcal{P}_h\left[W_i(\mathbf{x})\right] d\mathscr{A} \tag{I.12}$$

whilst the n_m-dimensional vector $\boldsymbol{f}$, representing mode forces, is given by

$$f_i(t) = \int_{\mathscr{A}} W_i(\mathbf{x})\, f_d(\mathbf{x}, t) d\mathscr{A} \tag{I.13}$$

In order to complete the description of considered electro-mechanic system the Eqs. (I.7) may be rewritten in compact form, using the expression (I.8) truncating higher frequency terms that lie out of the bandwidth of interest, keeping in mind the definition (I.12) and differentiating with respect to t, as follows

$$\ddot{\boldsymbol{\psi}} + \Xi\, \dot{\boldsymbol{\psi}} + \tilde{\Gamma}^{\mathrm{T}}\, \dot{\boldsymbol{\eta}} = \boldsymbol{\imath} \tag{I.14}$$

where the $n_p \times n_p$ matrix Ξ is defined as $\Xi_{ih} = \left[1/(R_h\, C_h)\right] \delta_{ih}$. The superscripted T indicates the transpose of a matrix. The column $\boldsymbol{\imath}$ represents the n_p-dimensional vector of normalised currents flowing through the piezoelectric elements.

For future reference, it is convenient to introduce the unit-frequency normalised coupling matrix $\Gamma = \Omega^{-1}\, \tilde{\Gamma}$, so that the governing equations for the electro-mechanic system can be summarised in the form

$$\begin{cases} \ddot{\boldsymbol{\eta}} + D\, \dot{\boldsymbol{\eta}} + \Omega^2\, \boldsymbol{\eta} - \Omega\, \Gamma\, \dot{\boldsymbol{\psi}} = \boldsymbol{f} \\ \ddot{\boldsymbol{\psi}} + \Xi\, \dot{\boldsymbol{\psi}} + (\Omega\, \Gamma)^{\mathrm{T}}\, \dot{\boldsymbol{\eta}} = \boldsymbol{\imath} \end{cases} \tag{I.15}$$

I.2 An Independent Modal-Space Shunt Damping Technique

It is indicated that the problem can be cast as a multi-variable feedback control problem. The model of a flexible structure integrating multiple piezoelectric transducers is made up considering as control signal the current flowing through each piezoelectric transducer and the voltage on the same piezoelectric element is the measurement. An alternative approach is to consider as control signal the terminal voltages and as electric degree of freedom to measure the charge. The chosen set up is primarily due to the following

aspects: the easiness to measure high voltage and to supply current with required accuracy on a piezoelectric element, as well as the minor influence of the hysteretic phenomena of the piezoelectric transducers driven by current source.

Introducing the problem, we made the assumption that the number of piezoelectric transducers, n_p, is different from the number of the modes, n_m, in need of control. At this point we want to relax this assumption and so consider $n_m = n_p = n$, in order to use each electric degree of freedom, ψ_h, to control one mechanical degree of freedom, η_i.

It is significant to examine an undamped system. To this end, Eqs. (I.15) become

$$\begin{cases} \ddot{\boldsymbol{\eta}} + \Omega^2 \boldsymbol{\eta} - \Omega \, \Gamma \, \dot{\boldsymbol{\psi}} = \boldsymbol{f} \\ \ddot{\boldsymbol{\psi}} + (\Omega \, \Gamma)^{\mathrm{T}} \, \dot{\boldsymbol{\eta}} = \boldsymbol{\imath} \end{cases} \tag{I.16}$$

Note that a small amount of mechanical damping is not relevant to design a proper shunt network system because it does not produce a significant change in the natural mechanica frequencies and modes. In addition, this damping has beneficial effect both on control performance and stability problem. It is strongly recommended that the piezoelectric coupling matrix Γ is not a singular matrix in order to avoid lack of controllability and observability. In general Eqs. (I.16) represent a set of $2n$ simultaneous linear second-order ordinary differential equations with constant coefficients. The analysis of such a set of equations is not a simple task, and we wish to explore means of facilitating it. To this end, the system can be express in a different set of generalised electric coordinates $\chi_k(t)$, $k = \{1, \dots n\}$, such that any coordinate $\psi_h(t)$, $h = \{1, \dots n\}$, is a linear combination of the new coordinates $\chi_k(t)$. Hence, let us consider the linear transformation

$$\boldsymbol{\psi} = U \boldsymbol{\chi} \tag{I.17}$$

in which U is a constant orthogonal square matrix, referred to as a *transformation matrix*. The matrix U can be regarded as an operator transforming the vector $\boldsymbol{\chi}$ into the vector $\boldsymbol{\psi}$. The key idea is to obtain a set of equations equivalent to Eqs. (I.16), consisting of n single mode piezoelectric shunting systems, that is to say n uncoupled systems of two coupled equations, each pair constituted by a mechanical equation and an electrical one [Hagood and

Flotow, 1991; Wu, 1996]. It means that each component of χ influences only the corresponding component of η and vice versa. In this case the electric coordinate transformation U is employed as a "mode-filter", making possible to control a single mechanical degree of freedom without any effect on the others. This uncoupling, thus, allows to use a single-mode vibration control very easy to realise by methods that have been widely investigated in the literature [Hagood and Flotow, 1991; Tang and Wang, 2001].

Because U is constant it also connects the vector $\dot{\chi}$ and the voltage vector $\dot{\psi}$ and in the same way the second derivatives. Inserting Eqs. (I.17) into Eqs. (I.16), it can write

$$\begin{cases} \ddot{\eta} + \Omega^2 \eta - \Omega \Gamma U \dot{\chi} = f \\ U\ddot{\chi} + \Gamma^{\mathrm{T}} \Omega \dot{\eta} = \iota \end{cases} \tag{I.18}$$

Next, premultiplying both sides of the second equation by U^{T}, the transpose of U, and applying the orthogonal properties of U, it obtains[2]

$$\begin{cases} \ddot{\eta} + \Omega^2 \eta - \Omega \mathcal{G} \dot{\chi} = f \\ \ddot{\chi} + (\Omega \mathcal{G})^{\mathrm{T}} \dot{\eta} = z \end{cases} \tag{I.20}$$

where the matrix $\mathcal{G} = \Gamma U$ is the *electro-mechanical coupling matrix* in the new electric coordinates, and thus the notation for a matrix $\mathcal{G}_{ik}$ has the row index labelling the i-th mechanical degree of freedom $\eta_i(t)$ and the column labelling the k-th electrical degree of freedom $\chi_k(t)$. The n-dimensional vector

$$z = U^{\mathrm{T}} \iota \tag{I.21}$$

has for elements the new electric forcing terms associated with the coordinates $\chi_k(t)$. Comparing Eqs. (I.20) with (I.16), it is possible to note that the form of the system does not change for the orthogonality assumption of the transformation matrix U. Besides, it is clear from equations (I.20) that if $\mathcal{G}$ were diagonal, recalling that Ω is diagonal, it would be possible to identify

[2] The matrix $U^{\mathrm{T}}U$ that multiplies the term $\ddot{\chi}$ can be interpreted in a more natural manner by considering the electric energy stored in the inherent piezoelectric capacitances. Indeed, this energy can be expressed in the form

$$\frac{1}{2}\dot{\psi}^{\mathrm{T}}\dot{\psi} = \frac{1}{2}\dot{\chi}^{\mathrm{T}}U^{\mathrm{T}}U\dot{\chi} \tag{I.19}$$

where $U^{\mathrm{T}}U$ is the capacitive matrix corresponding to the coordinates $\chi_k(t)$.

n single mode piezoelectric shunting systems. In view of this, the object of the transformation (I.17) is to produce a matrix $\mathscr{G}$ as diagonal as possible. In other words, the purpose is thus to allow a satisfactory coordination in control actions of all piezoelectric transducers so that they work together in an efficient way to control at the same time all mechanical degrees of freedom of interest, *i.e.* no control effort is used unnecessarily.

Remark I.1. Generally the piezoelectric coupling matrix Γ, whose properties depend on the configuration of piezoelectric transducers bonded on the host structure, is not diagonal therefore the Eqs. (I.16) are coupled through the piezoelectric coupling actions. In spite of it, if Γ were diagonal it would be possible to identify immediately n uncoupled systems of two coupled equations without recourse to transformation U. But there would be something inefficient with this arrangement. The action of a piezoelectric transducer is local and so, working each of them on only one mechanical degree of freedom, the global damping is very weak. In addition, it is difficult to find an optimal pattern of the piezoelectric set that makes Γ diagonal.

◇ ◇ ◇

Let $\mathbb{M}_n$ denote the vector space of all square matrices of order n over real field $\mathbb{R}$. It is useful to endow $\mathbb{M}_n$ with the habitual inner product

$$A \cdot B = \text{trace}(AB^{\text{T}}) \tag{I.22}$$

where A and B are any two elements of $\mathbb{M}_n$. Accordingly, let us define the Euclidean or Frobenius norm of A by the equations

$$\|A\| = (A \cdot A)^{\frac{1}{2}} = \sqrt{\sum_{i=1}^{m}\sum_{j=1}^{n} |A_{ij}|^2} \tag{I.23}$$

It gives also the distance of any matrix A from the null one.

We state here and prove later that given any square matrix Γ in $\mathbb{M}_n$ and a matrix U belonging to the orthogonal group $Orth(n)$, the problem of diagonalising $\mathscr{G} = \Gamma U$ admits solution if and only if the rows of Γ are mutually perpendicular. If it does not occur, an exact diagonalisation of $\mathscr{G}$ is not feasible, so that a different approach is desirable. Herein it is proposed to find the best transformation matrix U that makes $\mathscr{G}$ approximatively diagonal. Using

the point of view of the set theory, let $\mathbb{G}$ be the set of all possible *electro-mechanical coupling matrix* that is the set of the matrices ΓU as U varies over the orthogonal group $Orth(n)$ as well let $\mathbb{D}_n$ be the vector subspace of the diagonal matrices of order n, the wanted U is the matrix which identifies the Euclidean distance between these two sets. Such distance $d(\mathbb{G}, \mathbb{D}_n)$ between the sets $\mathbb{G}$ and $\mathbb{D}_n$ is defined as the infimum of all distances between any two of their respective elements, ΓU and D, and can be expressed as

$$d(\mathbb{G}, \mathbb{D}_n) = \inf_{U \in Orth(n)} \left\{ \inf_{D \in \mathbb{D}_n} \|\Gamma U - D\| \right\} \tag{I.24}$$

where the expression inside the curly brackets defines the orthogonal projection of ΓU onto $\mathbb{D}_n$ and indeed represents the closest diagonal matrix to ΓU. Thus, for any matrix U, there exists a unique matrix $D_{\Gamma U}$ that belongs to $\mathbb{D}_n$ that attain the infimum as D varies in $\mathbb{D}_n$. Therefore, this infimum is a minimum that can be written as

$$\epsilon = \min_{D \in \mathbb{D}_n} \|\Gamma U - D\| = \|\Gamma U - D_{\Gamma U}\| \tag{I.25}$$

The non-negative quantity ϵ identified by $\|\Gamma U - D_{\Gamma U}\|$ represents the error in the approximation of ΓU with a diagonal matrix.

To find the orthogonal projection $D_{\Gamma U}$ for a given matrix Γ and any orthogonal matrix U, let $\mathcal{B} = \{D_i : i = 1,2,\dots n\}$ be the standard basis of $\mathbb{D}$ consisted of n diagonal matrices with one in the ii-th entry and zero elsewhere. Then, since the matrix $D_{\Gamma U}$ can be written in the form

$$D_{\Gamma U} = \textstyle\sum_{h=1}^{n} \alpha_h D_h \tag{I.26}$$

the coefficients α_h can be obtained by using the orthogonality of the projection $(\Gamma U - D_{\Gamma U}) \cdot D_h = 0$ and the orthonormality of the unit matrices of the chosen basis $D_h \cdot D_k = \delta_{hk}$ to get $\alpha_h = \Gamma U \cdot D_h$. Thus, the orthogonal projection of ΓU over $\mathbb{D}$ is the operation of taking the diagonal part of the matrix ΓU.

The theorem of Weierstrass assures the existence of a matrix U that attain the infimum of the expression (I.24) as U varies in $Orth(n)$, it states in fact that the real valued continuous function of the matrix U, ϵ, assumes a minimum and a maximum value on the compact subset $Orth(n)$ of $\mathbb{M}_n$. Thus, the above

optimisation problem equivalently expressed in terms of squared distance becomes

$$d(\mathbb{G}, \mathbb{D}_n)^2 = \min_{U \in Orth(n)} \|\Gamma U - D_{\Gamma U}\|^2 \tag{I.27}$$

Taking the properties of the above inner product for granted, one can expand the cost function for the optimisation problem (I.27) as follows

$$\begin{aligned} \|\Gamma U - D_{\Gamma U}\|^2 &= (\Gamma U - D_{\Gamma U}) \cdot (\Gamma U - D_{\Gamma U}) = \\ &= \Gamma U \cdot \Gamma U - 2\Gamma U \cdot D_{\Gamma U} + D_{\Gamma U} \cdot D_{\Gamma U} \end{aligned} \tag{I.28}$$

Next, being the matrix U orthogonal, it is easy to check that

$$\Gamma U \cdot \Gamma U = \Gamma \cdot \Gamma \tag{I.29}$$

that is to say the norm of coupling matrix $\mathcal{G} = \Gamma U$ does not depend on transformation matrix U. Once again taking into account the orthogonality of the projection, it is possible to write

$$(\Gamma U - D_{\Gamma U}) \cdot D_{\Gamma U} = 0 \tag{I.30}$$

Therefore, introducing the Eqs. (I.29) and (I.30) into Eq. (I.28), it turns out that

$$\|\Gamma U - D_{\Gamma U}\|^2 = \Gamma \cdot \Gamma - D_{\Gamma U} \cdot D_{\Gamma U} \tag{I.31}$$

It is clear from the Eq. (I.31) that, for any fixed matrix Γ, the optimisation problem (I.27) is equivalent to the problem

$$\max_{U \in Orth(n)} \|D_{\Gamma U}\|^2 \tag{I.32}$$

It is appropriate to pause at this point and reflect on the last results. It turns out that any matrix $\mathcal{G}$ is associated with the transfer of power through the piezoelectric elements between the mechanical degrees of freedom, $\eta_i(t)$, and the electric degrees of freedom, $\chi_k(t)$, employed to control vibrations. The relation (I.29) shows that this power depend only on the matrix Γ and therefore the piezoelectric placement. The role of the transformation matrix U is thus not to increase the whole transferred power but to improve the way of exchanging energy between the two linked systems. In fact, the two equivalent optimisation problems (I.32) and (I.27) have the purpose to increase the sum of squared on-diagonal entries of the coupling matrix $\mathcal{G}$, *i.e.* to increase

the exchanged power between one mechanical mode and the corresponding electric degree of freedom that will be used to control the same mode, and simultaneously to decrease the sum of squared off-diagonal entries of $\mathscr{G}$, *i.e.* to decrease the exchanged power between a mechanical mode and the not corresponding electric degrees of freedom.

It remains to prove that if and only if Γ has the rows mutually perpendicular, there exists a matrix U that makes $\mathscr{G}$ exactly diagonal. First, suppose that Γ has the rows mutually perpendicular. Then taking the matrix U with unit columns aligned with the rows of Γ, it is easy to see the diagonality of $\mathscr{G} = \Gamma U$. Now, suppose that $\mathscr{G}$ is diagonal. Thus, it follows that the rows of $\mathscr{G}$ are mutually perpendicular. Finally, since the matrix U is orthogonal, also the rows of Γ are mutually perpendicular, indeed $\Gamma^{\mathrm{T}} = U\mathscr{G}^{\mathrm{T}}$.

Solving the optimisation problem (I.32), a matrix U that depends on a given Γ is obtained. Therefore, a further optimisation step can be performed varying Γ consistent with the constraints, to obtain an electro-mechanical coupling matrix $\mathscr{G}$ as close as possible diagonal. These two proposed step of optimisation, on U and Γ, are discussed in the following sections.

I.2.1 Linear Transformation for Independent Control

The optimisation problem (I.32) can be solved by using the method of Lagrange multipliers. To this end, let $\vartheta(U)$ the objective function

$$\vartheta(U) = D_{\Gamma U} \cdot D_{\Gamma U} \tag{I.33}$$

subject to the orthogonal constraint

$$UU^{\mathrm{T}} - I = O \tag{I.34}$$

where I is the identity matrix and O the zero matrix both of size n. Now, define the Lagrangian, Λ, as

$$\Lambda(U, S) = D_{\Gamma U} \cdot D_{\Gamma U} - (UU^{\mathrm{T}} - I) \cdot S \tag{I.35}$$

where S is a symmetric matrix of undetermined multipliers. Setting the partial derivatives of Λ with respect to U and S equal to zero, it is possible to write the system of equations

$$\begin{cases} SU = \Gamma^{\mathrm{T}} D_{\Gamma U} \\ UU^{\mathrm{T}} - I = O \end{cases} \tag{I.36}$$

which solved yields the stationary values for the objective function (I.33). In detail, the Lagrange multiplier matrix S can be expressed as

$$S = \Gamma^{\mathrm{T}} D_{\Gamma U} U^{\mathrm{T}} \tag{I.37}$$

Since the matrix S must be symmetric

$$S = \Gamma^{\mathrm{T}} D_{\Gamma U} U^{\mathrm{T}} = U D_{\Gamma U} \Gamma = S^{\mathrm{T}} \tag{I.38}$$

the first equation of the (I.36) becomes

$$(\Gamma U)^{\mathrm{T}} D_{\Gamma U} = D_{\Gamma U} \Gamma U \tag{I.39}$$

Finally, taking only the significant equations of the (I.39) and (I.34), the equation set that solved the problem (I.32) consists of the following equations

$$\begin{cases} \sum\limits_{r,h} \left(\Gamma_{ir}\Gamma_{ih} - \Gamma_{jr}\Gamma_{jh} \right) U_{ir} U_{jh} = 0 & \forall\ i < j \\ \sum\limits_{r} U_{ir} U_{jr} = \delta_{ij} & \forall\ i \geq j \end{cases} \tag{I.40}$$

that is a system of n^2 quadratic equations in n^2 unknown variables, U_{ij}. There is a geometric interpretation of this system. Each equation is a quadric in n^2-dimensional space and hence, the solution set is the intersection of these quadrics.

◇ ◇ ◇

On the other hand, multiplying S by S^{T}, or changing the order S^{T} by S, it is found a matrix symmetric and positive definite S^2 and thus S can be interpreted as the square root of this matrix, that is in a more compact form

$$S = \left(\Gamma^{\mathrm{T}} D_{\Gamma U} D_{\Gamma U} \Gamma \right)^{\frac{1}{2}} \quad \text{or} \quad S = U \left(D_{\Gamma U} \Gamma \Gamma^{\mathrm{T}} D_{\Gamma U} \right)^{\frac{1}{2}} U^{\mathrm{T}} \tag{I.41}$$

in which the orthogonal properties of the matrix U are used. Substituting the expressions (I.41) into the first equation of the (I.36) an implicit formula for U in terms of Γ can be expressed as follows

$$U = \left(\Gamma^{\mathrm{T}} D_{\Gamma U} D_{\Gamma U} \Gamma \right)^{-\frac{1}{2}} \Gamma^{\mathrm{T}} D_{\Gamma U} \tag{I.42}$$

or equivalently

$$U = \Gamma^{\mathrm{T}} D_{\Gamma U} \left(D_{\Gamma U} \Gamma \Gamma^{\mathrm{T}} D_{\Gamma U} \right)^{-\frac{1}{2}} \tag{I.43}$$

These two matrix expressions are very interesting because can be interpreted as the polar decomposition theorem but with a diagonal weighting matrix $D_{\Gamma U}$ which is not constant. Therefore, in view of a numerical solution the starting guess can be advantageously initialised to the orthogonal factor of Γ^{T} in accordance with the polar decomposition theorem.

It is undeniable that this first step of optimisation allows to obtain a matrix $\mathscr{G}$ that is the best approximation of a diagonal matrix for a given matrix Γ. Based on the above considerations, to improve the performance it is appropriate a further step of optimisation for the matrix Γ.

I.2.2 Piezoelectric Placement for Independent Control

An additional optimisation problem can be performed varying Γ through a placement modification of the piezoelectric transducers. This general purpose can be accomplished by acting in two different directions. On the one hand, we can improve the performance by a proper placement of the piezoelectric elements increasing the transfer of power through the piezoelectric elements, and on the other hand achieving a reasonable approximation for uncoupling of the Eqs. (I.20). In particular, the former target is to enhance the norm of the matrix Γ. The latter target is to diminish the error in the approximation of $\mathscr{G}$ with a diagonal matrix, see Eq. (I.25). It should be noted that such error vanishes as the rows of Γ tend to be mutually perpendicular, in this case indeed the matrix $\mathscr{G}$ is absolutely diagonal. To this end, consider the matrix $\Gamma\Gamma^{\mathrm{T}}$ can be uniquely decomposed into the sum of two matrices, its diagonal part, $D_{\Gamma\Gamma^{\mathrm{T}}}$ and its non-diagonal part, $N_{\Gamma\Gamma^{\mathrm{T}}}$[3]. In fact, the diagonal entries of $D_{\Gamma\Gamma^{\mathrm{T}}}$ are the squared lengths of the rows of Γ and each of them represents the whole power transferred related to the corresponding mechanical degree of freedom. Recall that the row indexes of Γ are associated with mechanical degrees of freedom and the column indexes with the piezoelectric transducers. Furthermore, the entries below or above the main diagonal of $N_{\Gamma\Gamma^{\mathrm{T}}}$ are all the dot products between any two different rows of Γ and vanish only if they are perpendicular. Hence, a natural objective function can be introduced

[3]The matrix $N_{\Gamma\Gamma^{\mathrm{T}}}$ is symmetric and belongs to the orthogonal complement $\mathbb{D}^{\perp}$ of $\mathbb{D}$ in $\mathbb{M}_n$, that is the set of all matrices that are orthogonal to every matrix in $\mathbb{D}$.

as

$$\mu(\Gamma) = \|D_{\Gamma\Gamma^{\mathrm{T}}}\| - b\|N_{\Gamma\Gamma^{\mathrm{T}}}\| \tag{I.44}$$

where b is a proper positive real weight. Now, in accordance with the above, the additional optimisation problem is to find the matrix Γ that maximises the objective function (I.44), that is

$$\max_{\Gamma\in\mathfrak{S}} \mu(\Gamma) \tag{I.45}$$

in which $\mathfrak{S}$ is the set of all possible Γ. Thus, the goal here is to find a matrix Γ whose rows approach to be of maximum length and mutually perpendicular. On the whole, these two proposed step of optimisation on U and Γ reduce the error ϵ decreasing the unnecessary control effort and simultaneously enhance the transfer power.

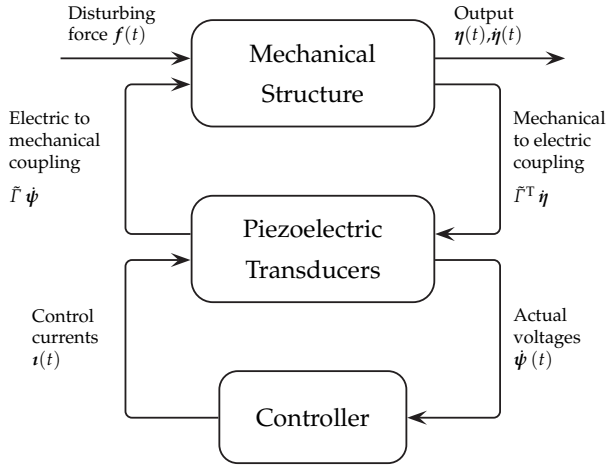


Figure I.1: Block diagram of the electro-mechanical system.

I.3 Two-Equation Systems Uncoupled

As indicated before, the idea of control is to impose certain currents on the piezoelectric transducers bonded on the considered structure, with a law that depends on the actual terminal voltages of the same transducers, so as to cause the system to exhibit satisfactory reduction of vibrations. The collocated feedback control system of Fig. I.1 can be regarded as representing such a system. In particular, equations (I.15) can be used to draw this block diagram.

The *reference input* is absent because it represents the desired output, *i.e.* no vibration. In Section I.2.1, a change of the electric variable has been introduced to obtain a set of n single mode piezoelectric shunting systems uncoupled. Hence, the equations (I.20) can be used in place of the equations (I.15). Now, recalling that $\mathscr{G}$ is quasi-diagonal and therefore neglecting its off-diagonal entries, it is possible to set $\mathscr{G}_{jk} = g_j \delta_{jk}$ and, thus, the equations (I.20) can be written in the scalar form

$$\begin{cases} \ddot{\eta}_j(t) + \omega_j^2 \eta_j(t) - \omega_j g_j \dot{\chi}_j(t) = f_j(t) \\ \ddot{\chi}_j(t) + \omega_j g_j \dot{\eta}_j(t) = z_j(t) \end{cases}, \qquad j = 1,2,\dots n \tag{I.46}$$

In feedback control, it is suitable to assume the control action $z_j = \boldsymbol{u}_j \cdot \boldsymbol{\imath}$ does not depend explicitly on t but on the electric degrees of freedom given by $\boldsymbol{\chi}$ and its derivatives. It is of great significance the case in which z_j depends on χ_j and its first derivative alone, or in detail

$$z_j = z_j(\chi_j, \dot{\chi}_j), \qquad j = 1,2,\dots n \tag{I.47}$$

It should be noted that Eqs. (I.47) do not restrict the functions z_j to being linear in the generalised coordinates χ_j and $\dot{\chi}_j$ and indeed this dependence can be linear or not. The reduced systems (I.46) with two degrees of freedom and the control laws (I.47) represent *closed-loop equations*. In contrast, Eqs. (I.46), in which the generalised action z_j depends explicitly on the time t and not on the generalised electric coordinates χ_j and/or $\dot{\chi}_j$, are referred to as *open-loop equations*. The open-loop equations represent a set of n uncoupled systems of two coupled equations. If the feedback control actions z_j are defined as in (I.47), then their effect is not to recouple the reduced systems. Hence, even the closed-loop equations are a set of n uncoupled systems. As a consequence, the design of the control laws (I.47) can be carried out with methods based on two degrees of freedom electro-mechanical systems. Before addressing this subject, it will prove convenient to calculate also the state equations equivalent to the (I.46). To this aim, the identities $\dot{\eta}_j(t) \equiv \dot{\eta}_j(t)$ are adjoined to Eqs. (I.46), so that, introducing the j-th state vector $\boldsymbol{w}_j(t) = [\eta_j(t),\ \dot{\eta}_j(t),\ \dot{\chi}_j(t)]^{\mathrm{T}}$, Eqs. (I.46) assume the following aspect

$$\dot{\boldsymbol{w}}_j(t) = \Lambda_j \boldsymbol{w}_j(t) + \mathbf{a}_j f_j(t) + \mathbf{b}_j z_j(t), \quad j = 1,2,\dots n \tag{I.48}$$

where

$$\Lambda_j = \begin{bmatrix} 0 & 1 & 0 \\ -\omega_j^2 & 0 & \omega_j g_j \\ 0 & -\omega_j g_j & 0 \end{bmatrix}, \ \mathbf{a}_j = \begin{bmatrix} 0 \\ 1 \\ 0 \end{bmatrix}, \ \mathbf{b}_j = \begin{bmatrix} 0 \\ 0 \\ 1 \end{bmatrix}, \quad j = 1,2,\dots n \tag{I.49}$$

are coefficient matrices. In feedback control, it is customary to consider even the relationship between the state vector, $\boldsymbol{w}_j(t)$, and the considered output, $v_j(t)$, defined as

$$v_j(t) = \mathbf{c}_j^{\mathrm{T}} \boldsymbol{w}_j(t), \qquad j = 1,2,\dots n \tag{I.50}$$

in which assuming each variable $\dot{\chi}_j$ as system output

$$\mathbf{c}_j^{\mathrm{T}} = [0\ 0\ 1], \qquad j = 1,2,\dots n \tag{I.51}$$

At this point, it is worthy to recall the relation between the output v_j and the actual electric output $\dot{\boldsymbol{\psi}}$, or in detail

$$v_j(t) = \dot{\chi}_j(t) = \boldsymbol{u}_j \cdot \dot{\boldsymbol{\psi}}\,(t), \qquad j = 1,2,\dots n \tag{I.52}$$

where $\boldsymbol{u}_j$ is the j-th unit length column of the transformation matrix U.

I.4 Controllability and Observability

In order to consider the controllability of the n systems (I.48) in need to control, let us examine the *controllability matrices*

$$\mathfrak{C}_j = \left[\mathbf{b}_j \vdots \Lambda_j \mathbf{b}_j \vdots \Lambda_j^2 \mathbf{b}_j\right] = \begin{bmatrix} 0 & 0 & \omega_j g_j \\ 0 & \omega_j g_j & 0 \\ 1 & 0 & -(\omega_j g_j)^2 \end{bmatrix}, \quad j = 1,2,\dots n \tag{I.53}$$

Equations (I.53) permit to state that the n reduced systems (I.48) are controllable if and only if each and every controllability matrix $\mathfrak{C}_j$ is of full rank 3; this is clearly the case because the matrix Γ is invertible and, thus, each element g_j is different from zero.
Next, let us consider the concept of observability introducing for the generalised voltage $\dot{\chi}_j$ the *observability matrices*

$$\mathcal{O}_j = \begin{bmatrix} \mathbf{c}_j^{\mathrm{T}} \\ \mathbf{c}_j^{\mathrm{T}} \Lambda_j \\ \mathbf{c}_j^{\mathrm{T}} \Lambda_j^2 \end{bmatrix} = \begin{bmatrix} 0 & 0 & 1 \\ 0 & -\omega_j g_j & 0 \\ \omega_j^3 g_j & 0 & -(\omega_j g_j)^2 \end{bmatrix}, \quad j = 1,2,\dots n \tag{I.54}$$

The n reduced systems (I.48) are observable if and only if each and every observability matrix $\mathcal{O}_j$ is of full rank 3. Thus, each system (I.48) is clearly observable.

I.5 Vibration Control with a Single Piezoelectric Transducer

Let us return to the problem design of the control law (I.47). Each of the systems (I.46) has the same form of the a single mechanical degree of freedom system with a single piezoelectric transducer having a unit inherent capacitance. The problem of vibration control of these systems has been under investigation for many years. The traditional approaches can be classify in two way: one a passive approach in which the piezoelectric element are integrated with an external shunt circuit, and the other an active approach based on measured feedback signal and control actions. It is important to note that shunting the piezoelectric in a passive way does not preclude the use of shunted piezoelectric materials as active actuators allowing hybrid solutions. This Section is dedicated to the available techniques for systems in study adjusting classical results to the considered configuration.

I.6 Generalised Passive Approach

The key idea of passive control is to shunt a piezoelectric transducer with an electrical impedance, or admittance. The last is more adequate for the planned beforehand purpose because, recalling the spirit of virtual passive approach, it is assumed to supply currents and to measure voltages. As the base structure vibrates, a voltage appears across the electrodes of the piezoelectric transducer, which causes the flow of electric current through the admittance. For a strictly passive admittance, it involves a loss of vibration energy. Hence, the electric admittance can be interpreted as a means of extracting mechanical energy from the host structure thanks to the piezoelectric transducer. The passive shunt circuit realised with a resistor and an inductor connected in series or in parallel were firstly proposed in [Hagood and Flotow, 1991] and in [Wu, 1996], respectively. It has been shown that with proper design of these components, one can obtain an electrical damper.

I.6.1 Parallel Configuration

In the case of a shunt circuit with a resistor, r_j, and an inductor, ℓ_j, connected in parallel, the control action (I.47) is given by

$$z_j = -\frac{1}{r_j}\dot{\chi}_j(t) - \frac{1}{\ell_j}\chi_j(t), \qquad j = 1,2,\dots n \tag{I.55}$$

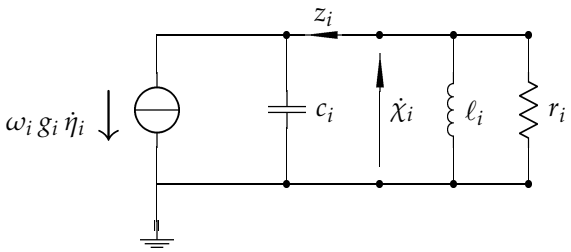


Figure I.2: Equivalent circuit for a virtual passive shunt circuit in parallel configuration.

Introducing the notation

$$\frac{1}{\ell_j} = \varpi_j^2, \quad \frac{1}{r_j} = 2\,\varpi_j\zeta_j \quad \text{and} \quad \beta_j = \frac{\varpi_j}{\omega_j} \tag{I.56}$$

the closed-loop equations are written as follows

$$\begin{cases} \ddot{\eta}_j(t) + \omega_j^2\,\eta_j(t) - \omega_j\, g_j\,\ddot{\chi}_j(t) = f_j(t) \\ \ddot{\chi}_j(t) + 2\,\varpi_j\zeta_j\dot{\chi}_j(t) + \varpi_j^2\chi_j(t) + \omega_j\, g_j\,\dot{\eta}_j(t) = 0 \end{cases} \tag{I.57}$$

In the second equation of (I.57), it can be recognised the electric subsystem constituted by the parallel of r_j, ℓ_j and a unit capacitance, whose eigenfrequency is ϖ_j, and loss factor is ζ_j.

Laplace transforming (I.57) and letting the initial condition be equal to zero, it possible computing the mechanical mobility, defined as the ratio between the transformed mode velocity, $L[\dot{\eta}_j]$, and the transformed disturbing modal force, $L[f_j]$, where the symbol L denotes the Laplace transform. Hence, the closed-loop transfer function from modal disturbing force f_j to mode velocity $\dot{\eta}_j$ is

$$M_j(s;\beta_j,\zeta_j) = \frac{s\,(s^2 + 2\,\beta_j\,\omega_j\,\zeta_j\,s + \beta_j^2\,\omega_j^2)}{s^4 + 2\,\beta_j\,\omega_j\,\zeta_j\,s^3 + \omega_j^2(1+\beta_j^2+g_j^2)s^2 + 2\,\beta_j\,\omega_j^3\,\zeta_j\,s + \beta_j^2\,\omega_j^4} \tag{I.58}$$

where the complex variable s defines the Laplace domain whilst β_j and ζ_j are the tuning parameters. To deal with the problem of control efforts and saturating actuators, it is opportune to introduce: the transfer function from modal disturbing force f_j to control action z_j, defined as the ratio between their Laplace transforms, that is

$$S_{z_j}(s) = \frac{\omega_j\, g_j s\,(2\,\beta_j\,\omega_j\,\zeta_j\,s + \beta_j^2\,\omega_j^2)}{s^4 + 2\,\beta_j\,\omega_j\,\zeta_j\,s^3 + \omega_j^2(1+\beta_j^2+g_j^2)s^2 + 2\,\beta_j\,\omega_j^3\,\zeta_j\,s + \beta_j^2\,\omega_j^4} \tag{I.59}$$

Herein two optimization way are showed. The former is based on the minimisation of the maximum value of the magnitude of the mobility. The latter minimises the decay time of free oscillations by the proper assignment of the closed-loop poles.

Optimal Control in the Frequency Domain: the Fixed Points Theory

The fixed points method was developed by Den Hartog in [Hartog, 1956] for mechanical vibration absorbers. The theory can be used to determine the optimal resonance circular frequency, ϖ_j, and damping ratio, ζ_j, of the electric subsystem, that reduces, without any increase, the modal velocity amplitudes of the mechanical structure in the neighbourhood of its natural frequency, ω_j. The underlying principle of the theory is that for a certain fixed value of ϖ_j in the mobility (I.58), of the composite system, primary structure and shunt circuit, there exist two points that are common to all curves of the mobility, regardless of the damping value in the shunt circuit. The locations of the invariant points depend only on the inductance tuning, *i.e.* β_j tuning. Thus, it is possible to determine the optimum values of β_j and ζ_j one by one. It is important to remark that, in general, such two fixed points exist for continuous structures with well separated natural frequencies; here, this is clearly the case thanks to the transformation U above specified. In order to calculate the locations of the fixed points, setting $s = ip$, the magnitudes of the mobility (I.58), are equated for two comfortable different values of ζ_j

$$\left.\frac{\beta_j^2\omega_j^2 p - p^3}{p^4 - \omega_j^2(1+\beta_j^2+g_j^2)\,p^2 + \beta_j^2\,\omega_j^4}\right|_{\zeta_j=0} = \left.-\frac{p}{\omega_j^2 - p^2}\right|_{\zeta_j\to\infty} \tag{I.60}$$

solving the (I.60) for the frequency p, the two fixed points are given by

$$p_{B,T\,j} = \frac{1}{2}\omega_j\sqrt{(2+2\beta_j^2+g_j^2) \pm \sqrt{(2+2\beta_j^2+g_j^2)^2 - 16\beta_j^2}} \tag{I.61}$$

where the subscript B is related to the minus and T to the plus. To calculate the optimal ratio β_j, letting ζ_j approach infinity, the magnitudes of the mobility (I.58) at these two fixed points are equated

$$\frac{p_{B_j}}{\omega_j^2 - p_{B_j}^2} = -\frac{p_{T_j}}{\omega_j^2 - p_{T_j}^2} \tag{I.62}$$

Hence, the optimal ratio β_j is

$$\beta_j^{opt} = 1 \tag{I.63}$$

Under the optimal ratio β_j, the aforementioned two fixed points are situated at

$$p_{B,T_j} = \frac{1}{2}\omega_j \sqrt{(4 + g_j^2) \pm g_j \sqrt{(8 + g_j^2)}} \tag{I.64}$$

Finally, the optimal damping can be computed by taking the derivative of the magnitude of the mobility with respect to the frequency p and equating such derivative at the fixed points to zero so that the magnitude of the mobility has the minimum possible value for its peak amplitudes. The optimal damping is

$$\zeta_j^{opt} = \frac{\sqrt{6}}{4} g_j \tag{I.65}$$

Obtained performances is characterised by small peak amplitudes; in particular, these peak amplitudes are the mobility magnitudes at fixed points, or

$$M_j^{opt} = \frac{p_{B_j}}{\omega_j^2 - p_{B_j}^2} = -\frac{p_{T_j}}{\omega_j^2 - p_{T_j}^2} \tag{I.66}$$

An important index to evaluate the performance of this method is linked to the relative distance between the fixed points. Indeed, as this distance increases, peak amplitudes decrease. In this case such index is

$$\frac{p_{T_j}^2 - p_{B_j}^2}{\omega_j^2} = \frac{1}{2} g_j \sqrt{(8 + g_j^2)} \tag{I.67}$$

Pole Allocation

The closed-loop pole locations have a direct impact on time response characteristics such as transient oscillations. In pole allocation method, these poles are selected in advance following the criterion of maximising all closed-loop pole distances from the imaginary axis, remaining on the left part of the

complex plane. This means to obtain on the one hand a large gain margin which guarantees asymptotic stability, on the other hand the largest decaying of free oscillations. Now, the optimal tuning parameters, β_j and ζ_j, allowing to reach the design specifications for making the closed-loop poles equal in pairs, as they are complex conjugates. A more extensive discussion is presented in [Hagood and Flotow, 1991]. Hence, denoting the closed-loop poles associated with the j-th system by

$$s_{j_{1,2}} = a_j + i\, b_j, \qquad s_{j_{3,4}} = a_j - i\, b_j \tag{I.68}$$

the related characteristic polynomial is

$$\begin{aligned}(s - s_{j_1})^2 (s - s_{j_3})^2 = \\ = s^4 - 4\, a_j\, s^3 + (6\, a_j^2 + 2\, b_j^2) s^2 - 4\, a_j (a_j^2 + b_j^2)\, s + (a_j^2 + b_j^2)^2\end{aligned} \tag{I.69}$$

Next, equating (I.69) to the denominator of the mobility (I.58) *i.e.* the characteristic polynomial in s of the system (I.57), the optimal tuning parameters can be found

$$\beta_j^{opt} = 1, \qquad \zeta_j^{opt} = g_j \tag{I.70}$$

and the optimal real and imaginary part of the closed-loop poles are

$$a_j^{opt} = -\frac{1}{2}\, \omega_j\, g_j, \qquad b_j^{opt} = \pm \frac{1}{2}\, \omega_j \sqrt{(4 - g_j^2)} \tag{I.71}$$

whilst the optimal damping factor, equal for the four poles, is

$$\varsigma_j^{opt} = \left| \frac{a_j}{\sqrt{a_j^2 + b_j^2}} \right| = \frac{g_j}{2} \tag{I.72}$$

On the Stability

At this point, it is possible to assemble the generalised control vector $\boldsymbol{z}$

$$\boldsymbol{z} = -\mathscr{R}\, \dot{\boldsymbol{\chi}} - \mathscr{L}\, \boldsymbol{\chi} \tag{I.73}$$

defining the diagonal matrices $\mathscr{R}_{hk} = (1/r_h)\delta_{hk}$ and $\mathscr{L}_{hk} = (1/\ell_h)\delta_{hk}$. Thus, the actual control law, $\boldsymbol{\imath}$, assumes the form

$$\boldsymbol{\imath} = -\mathcal{N}_R\, \dot{\boldsymbol{\psi}} - \mathcal{N}_L\, \boldsymbol{\psi} \tag{I.74}$$

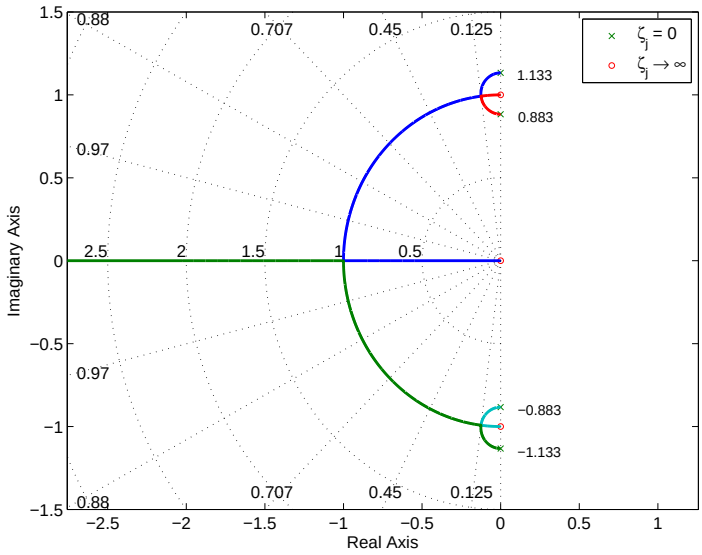


Figure I.3: The root locus diagram shows the trajectories of the closed-loop poles of the feedback system, with g_j equal to 0.25, as ζ_j varies over a continuous range of values, unchanging the optimal value of β_j. The frequency are normalised with respect to ω_j

utilising definitions (I.17) and (I.21) and setting

$$\mathcal{N}_R = U\mathscr{R}\,U^{\mathrm{T}} \quad \mathcal{N}_L = U\mathscr{L}\,U^{\mathrm{T}} \tag{I.75}$$

where $\mathcal{N}_R$ and $\mathcal{N}_L$ are control gain matrices. Because r_h and ℓ_h are strictly positive and the matrix U is orthogonal, it follows that the gain matrices $\mathcal{N}_R$ and $\mathcal{N}_L$ are *symmetric* and *positive definite*. These two $n \times n$ matrices can represent the inductive and the resistive part of a resistive-inductive network shunts to the piezoelectric terminals. The column vectors $\boldsymbol{u}_h$'s of the matrix U can be interpreted as their common eigenvectors, and $(1/r_h)$'s and $(1/\ell_h)$'s are the corresponding eigenvalues. Besides, to assure their realization with purely passive components, the control gain matrices should fulfil other conditions as well as being symmetric and positive definite. A sufficient further condition is the property to be diagonally dominant matrices, see *e.g.* [Weinberg, 1962]. In the preceding discussion, this additional condition has not been considered, therefore, obtained gain matrices can require active components for their actualization.

Now, inserting the control law (I.74) in the governing equations (I.16), it

can be written

$$\begin{cases} \ddot{\boldsymbol{\eta}} + \Omega^2 \boldsymbol{\eta} - \tilde{\Gamma} \dot{\boldsymbol{\psi}} = \boldsymbol{f} \\ \ddot{\boldsymbol{\psi}} + \mathcal{N}_R \dot{\boldsymbol{\psi}} + \mathcal{N}_L \boldsymbol{\psi} + \tilde{\Gamma}^{\mathrm{T}} \dot{\boldsymbol{\eta}} = \boldsymbol{0} \end{cases} \tag{I.76}$$

Next, multiplying on the left the first equation of the (I.76) by $\dot{\boldsymbol{\eta}}^{\mathrm{T}}$ and the second equation by $\dot{\boldsymbol{\psi}}^{\mathrm{T}}$ and rearranging, one obtains

$$\begin{cases} \dfrac{d}{dt}\left(\dfrac{1}{2}\dot{\boldsymbol{\eta}}^{\mathrm{T}}\dot{\boldsymbol{\eta}} + \dfrac{1}{2}\boldsymbol{\eta}^{\mathrm{T}}\Omega^2\boldsymbol{\eta}\right) = \dot{\boldsymbol{\eta}}^{\mathrm{T}}\tilde{\Gamma}\,\dot{\boldsymbol{\psi}} \\ \dfrac{d}{dt}\left(\dfrac{1}{2}\dot{\boldsymbol{\psi}}^{\mathrm{T}}\dot{\boldsymbol{\psi}} + \dfrac{1}{2}\boldsymbol{\psi}^{\mathrm{T}}\mathcal{N}_L\boldsymbol{\psi}\right) = -\dot{\boldsymbol{\psi}}^{\mathrm{T}}\mathcal{N}_R\,\dot{\boldsymbol{\psi}} - \dot{\boldsymbol{\psi}}^{\mathrm{T}}\tilde{\Gamma}^{\mathrm{T}}\dot{\boldsymbol{\eta}} \end{cases} \tag{I.77}$$

On the left hand side of the first equation it is possible identify the kinetic energy expressed in terms of modal velocities and the potential energy expressed in terms of modal displacements; on the left hand side of the second equation it is possible to recognise the electric energy stored in the piezoelectric inherent capacitances and the electric energy associated to the "inductive" gain matrix, $\mathcal{N}_L$. Last terms on the right hand side represent the power through the piezoelectric elements toward the mechanical subsystem in the first equation, and toward the electric subsystem in the second equation. Hence, the balance of power through the piezoelectric elements yields

$$\dot{\boldsymbol{\eta}}^{\mathrm{T}}\tilde{\Gamma}\,\dot{\boldsymbol{\psi}} - \dot{\boldsymbol{\psi}}^{\mathrm{T}}\tilde{\Gamma}^{\mathrm{T}}\dot{\boldsymbol{\eta}} = 0 \tag{I.78}$$

Next, exploiting the (I.78), Eqs. (I.77) can be rearranged as follows

$$\frac{d}{dt}\left(\frac{1}{2}\dot{\boldsymbol{\eta}}^{\mathrm{T}}\dot{\boldsymbol{\eta}} + \frac{1}{2}\boldsymbol{\eta}^{\mathrm{T}}\Omega^2\boldsymbol{\eta} + \frac{1}{2}\dot{\boldsymbol{\psi}}^{\mathrm{T}}\dot{\boldsymbol{\psi}} + \frac{1}{2}\boldsymbol{\psi}^{\mathrm{T}}\mathcal{N}_L\boldsymbol{\psi}\right) = -\dot{\boldsymbol{\psi}}^{\mathrm{T}}\mathcal{N}_R\,\dot{\boldsymbol{\psi}} \tag{I.79}$$

The expression inside the parentheses on the left hand side of Eqs. (I.79) can be identified as the total energy of the system, including the effect of the "inductive" matrix, $\mathcal{N}_L$. The objective of the feedback control is to drive the total energy to zero. Being the "resistive" matrix $\mathcal{N}_R$ positive definite, the right hand side of Eqs. (I.79) is sure negative, except when $\dot{\boldsymbol{\psi}}$ vanishes. Thus, the energy is being dissipated at all times until the whole structure is driven to rest. Hence, in this case the electro-mechanical structure is guaranteed to be asymptotically stable. Moreover, anyway being the gain matrices $\mathcal{N}_R$ and $\mathcal{N}_L$ *positive definite* even an unconditional stability is assured.

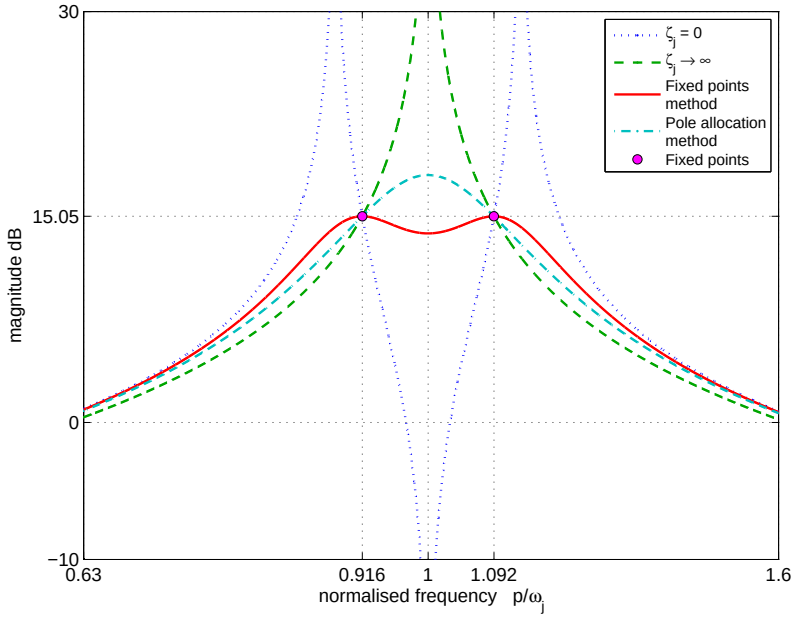


Figure I.4: Mobilities for a virtual passive shunt circuit realised with a resistor and an inductor connected in parallel and with a generalised coupling coefficient, g_j, equal to 0.25.

I.6.2 Series Configuration

Another possible kind of shunt circuit is constituted by a resistor, r_j, and an inductor, ℓ_j, connected in series, as displayed in Fig. I.5. It can be shown to have the governing equation

$$\dot{z}_j(t) + \frac{r_j}{\ell_j} z_j(t) = -\frac{1}{\ell_j}\dot{\chi}_j(t), \qquad j = 1,2,\dots n \tag{I.80}$$

consequently, the control action has the form

$$z_j = -\int_0^t \frac{1}{\ell_j} e^{-\frac{r_j}{\ell_j}(t-h)} \dot{\chi}_j(h)\, dh, \qquad j = 1,2,\dots n \tag{I.81}$$

Let us denote

$$\frac{1}{\ell_j} = \omega_j^2, \qquad \frac{r_j}{\ell_j} = 2\,\omega_j \zeta_j \quad \text{and} \quad \beta_j = \frac{\omega_j}{\omega_j} \tag{I.82}$$

Before continuing, it is convenient to introduce the natural frequency of the primary, mechanical structure under open circuit condition as

$$\tilde{\omega}_j = \omega_j \sqrt{(1 + g_j^2)} \tag{I.83}$$

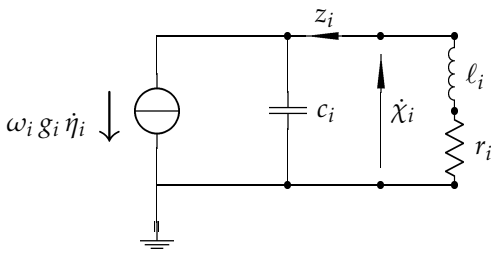


Figure I.5: Equivalent circuit for a virtual passive shunt circuit in series configuration.

This expression is computed by imposing z_j equal to zero in (I.46).

In this case, the closed-loop transfer functions of interest are given by

$$M_j(s;\beta_j,\zeta_j) = \frac{s\,(s^2 + 2\,\beta_j\,\omega_j\,\zeta_j\,s + \beta_j^2\,\omega_j^2)}{s^4 + 2\,\beta_j\,\omega_j\,\zeta_j\,s^3 + \omega_j^2(1+\beta_j^2+g_j^2)s^2 + 2\,\beta_j\,\omega_j\tilde{\omega}_j^2\,\zeta_j\,s + \beta_j^2\,\omega_j^4} \tag{I.84}$$

$$S_{z_j}(s) = \frac{\beta_j^2\,\omega_j^3\,g_j\,s}{s^4 + 2\,\beta_j\,\omega_j\,\zeta_j\,s^3 + \omega_j^2(1+\beta_j^2+g_j^2)s^2 + 2\,\beta_j\,\omega_j\tilde{\omega}_j^2\,\zeta_j\,s + \beta_j^2\,\omega_j^4} \tag{I.85}$$

Optimal Control in the Frequency Domain: the Fixed Points Theory

Going along the same procedure for the parallel connection again, the magnitudes of the mobility (I.84), are equated for two comfortable different values of ζ_j

$$\left.\frac{\beta_j^2\omega_j^2 p - p^3}{p^4 - \omega_j^2(1+\beta_j^2+g_j^2)\,p^2 + \beta_j^2\,\omega_j^4}\right|_{\zeta_j=0} = \left.-\frac{p}{\tilde{\omega}_j^2 - p^2}\right|_{\zeta_j\to\infty} \tag{I.86}$$

to obtain the locations of the fixed points

$$p_{B,T_j} = \frac{1}{2}\omega_j\sqrt{[2\beta_j^2 + 2(1+g_j^2)] \pm \sqrt{[2\beta_j^2 + 2(1+g_j^2)]^2 - 16\beta_j^2\left(1+\frac{g_j^2}{2}\right)}} \tag{I.87}$$

Next, letting ζ_j approach infinity and equating the magnitudes of the mobility (I.84) at these two fixed points

$$\frac{p_{B_j}}{\tilde{\omega}_j^2 - p_{B_j}^2} = -\frac{p_{T_j}}{\tilde{\omega}_j^2 - p_{T_j}^2} \tag{I.88}$$

the optimal ratio β_j is found to be

$$\beta_j^{opt} = \sqrt{2}\frac{(1+g_j^2)}{\sqrt{2+g_j^2}} \tag{I.89}$$

and the two optimal fixed points are placed at

$$p_{B,T\,j} = \frac{1}{2}\omega_j \sqrt{\frac{(2+2\,g_j^2)\left[(4+3\,g_j^2) \pm g_j\sqrt{8+5\,g_j^2}\right]}{2+g_j^2}} \tag{I.90}$$

On the contrary of the parallel connection, nevertheless, under the optimal ratio β_j, imposing that the magnitude of the mobility (I.84) has horizontal tangents at two fixed points, leads one to obtain two different values of the optimal damping factor ζ_j. This means that only one peak amplitude equates the value of mobility magnitude at one fixed point, whilst in the neighbourhood of the other fixed point the other peak amplitude is a little greater. Recalling it, the peak amplitudes of mobility (I.84) are about the mobility magnitudes at fixed points, or

$$M_j^{opt} \cong \frac{p_{B_j}}{\tilde{\omega}_j^2 - p_{B_j}^2} = -\frac{p_{T_j}}{\tilde{\omega}_j^2 - p_{T_j}^2} \tag{I.91}$$

and the before introduced performance index is

$$\frac{p_{T_j}^2 - p_{B_j}^2}{\omega_j^2} = \left(\frac{1+g_j^2}{2+g_j^2}\right) g_j\sqrt{(8+5\,g_j^2)} \tag{I.92}$$

Pole Allocation

The optimisation criterion used in the case of parallel connection is still valid for the present case as the mobility (I.84) has the same form of the (I.58). Hence, equating the characteristic polynomial (I.69) with the denominator of the new mobility (I.84), the optimal tuning parameters are

$$\beta_j^{opt} = 1+g_j^2, \qquad \zeta_j^{opt} = \frac{g_j}{\sqrt{(1+g_j^2)}} \tag{I.93}$$

and the optimal real and imaginary part of the closed-loop poles can be written as

$$a_j^{opt} = -\frac{1}{2}\,\tilde{\omega}_j\,g_j, \qquad b_j^{opt} = \pm\frac{1}{2}\,\tilde{\omega}_j\sqrt{(4-g_j^2)} \tag{I.94}$$

At the same time, the optimal damping factor, equal for the four poles, is

$$\varsigma_j^{opt} = \left| \frac{a_j}{\sqrt{a_j^2 + b_j^2}} \right| = \frac{g_j}{2} \tag{I.95}$$

On the Stability

In this case, the generalised control vector $\boldsymbol{z}$ satisfies the differential equation

$$\mathscr{L}\,\dot{\boldsymbol{z}} + \mathscr{R}\,\boldsymbol{z} = -\dot{\boldsymbol{\chi}} \tag{I.96}$$

defining the diagonal matrices $\mathscr{L}_{hk} = \ell_h \delta_{hk}$ and $\mathscr{R}_{hk} = r_h \delta_{hk}$. The actual control law, $\boldsymbol{\imath}$, fulfils

$$\mathcal{N}_L\,\dot{\boldsymbol{\imath}} + \mathcal{N}_R\,\boldsymbol{\imath} = -\dot{\boldsymbol{\psi}} \tag{I.97}$$

utilising definitions (I.17) and (I.21) and setting

$$\mathcal{N}_L = U \mathscr{L}\, U^{\mathrm{T}} \quad \mathcal{N}_R = U \mathscr{R}\, U^{\mathrm{T}} \tag{I.98}$$

where $\mathcal{N}_R$ and $\mathcal{N}_L$ are control gain matrices. Because ℓ_h and r_h are strictly positive and the matrix U is orthogonal, the gain matrices $\mathcal{N}_R$ and $\mathcal{N}_L$ are *symmetric* and *positive definite*. Similar considerations can be made even in this case for the network interpretation.

To examine the stability of the system, it is not adequate to work with the governing equations (I.16) that describe the system in terms of flux linkage but the equivalent governing equations in terms of electric charge are more easy. In these equations, each piezoelectric transducer is, according to Thevenin's theorem, electrically equivalent to a strain dependent voltage generator in series with a capacitance. Under these considerations, the governing equations are

$$\begin{cases} \ddot{\tilde{\boldsymbol{\eta}}} + \tilde{\Omega}^2\,\tilde{\boldsymbol{\eta}} - \Lambda\,\boldsymbol{q} = \tilde{\boldsymbol{f}} \\ \qquad\qquad \boldsymbol{q} - \Lambda^{\mathrm{T}}\,\tilde{\boldsymbol{\eta}} = \dot{\boldsymbol{\psi}} \end{cases} \tag{I.99}$$

where, denoting each natural frequency of undamped oscillation under open circuit condition with $\tilde{\omega}_j$ the matrix $\tilde{\Omega}$ is defined as $\tilde{\Omega}_{jh} = \tilde{\omega}_j\,\delta_{jh}$ and Λ is the $n \times n$ piezoelectric coupling matrix, $\boldsymbol{q}(t) = [\mathcal{Q}_1, \dots \mathcal{Q}_h, \dots \mathcal{Q}_n]^{\mathrm{T}}$ is the charge vector and $\tilde{\boldsymbol{\eta}}$ is the n-dimensional vector of generalised coordinates describing

the response of mechanical normal modes under open circuit condition, while the n-dimensional vector $\tilde{f}$, represents the corresponding mode forces. Now, considering the relation, $\dot{q} = \iota$, and inserting the control law (I.97) in the governing equations (I.99), it can be written

$$\begin{cases} \ddot{\tilde{\eta}} + \tilde{\Omega}^2 \tilde{\eta} - \Lambda q = \tilde{f} \\ \mathcal{N}_L \ddot{q} + \mathcal{N}_R \dot{q} + q - \Lambda^{\mathrm{T}} \tilde{\eta} = \mathbf{0} \end{cases} \tag{I.100}$$

Next, multiplying on the left the first equation of the (I.100) by $\dot{\tilde{\eta}}^{\mathrm{T}}$ and the second equation by $\dot{q}^{\mathrm{T}}$ and rearranging, one obtains

$$\begin{cases} \dfrac{d}{dt}\left(\dfrac{1}{2}\dot{\tilde{\eta}}^{\mathrm{T}}\dot{\tilde{\eta}} + \dfrac{1}{2}\tilde{\eta}^{\mathrm{T}}\tilde{\Omega}^2\tilde{\eta}\right) = \dot{\tilde{\eta}}^{\mathrm{T}}\Lambda q \\ \dfrac{d}{dt}\left(\dfrac{1}{2}\dot{q}^{\mathrm{T}}\mathcal{N}_L\dot{q} + \dfrac{1}{2}q^{\mathrm{T}}q\right) = -\dot{q}^{\mathrm{T}}\mathcal{N}_R\dot{q} + \dot{q}^{\mathrm{T}}\Lambda^{\mathrm{T}}\tilde{\eta} \end{cases} \tag{I.101}$$

Last terms on the right hand side represent the power through the piezoelectric elements toward the mechanical subsystem in the first equation, and toward the electric subsystem in the second equation. Hence, from the balance of power through the piezoelectric elements, one obtains

$$\dot{\tilde{\eta}}^{\mathrm{T}}\Lambda q + \dot{q}^{\mathrm{T}}\Lambda^{\mathrm{T}}\tilde{\eta} = 0 \tag{I.102}$$

using the (I.102), Eqs. (I.101) can be rearranged as follows

$$\frac{d}{dt}\left(\frac{1}{2}\dot{\tilde{\eta}}^{\mathrm{T}}\dot{\tilde{\eta}} + \frac{1}{2}\tilde{\eta}^{\mathrm{T}}\tilde{\Omega}^2\tilde{\eta} + \frac{1}{2}\dot{q}^{\mathrm{T}}\mathcal{N}_L\dot{q} + \frac{1}{2}q^{\mathrm{T}}q\right) = -\dot{q}^{\mathrm{T}}\mathcal{N}_R\dot{q} \tag{I.103}$$

Even in this case, the expression inside the parentheses on the left hand side of Eqs. (I.103) can be identified as the total energy of the system, including the effect of the positive definite "inductive" matrix, $\mathcal{N}_L$. Being the "resistive" matrix $\mathcal{N}_R$ positive definite, the right hand side of Eqs. (I.103) is sure negative, except when $\dot{q}$ vanishes. Thus, the whole structure dissipates energy continuously. In view of above discussion, it is clear that the electro-mechanical structure is asymptotically stable.

I.6.3 Comparisons

The effect of introduced shunt circuits is compared using two different judgement tools. On one hand the ratio between the maximum mobility magnitudes of the series and parallel connection, for the fixed points method; on

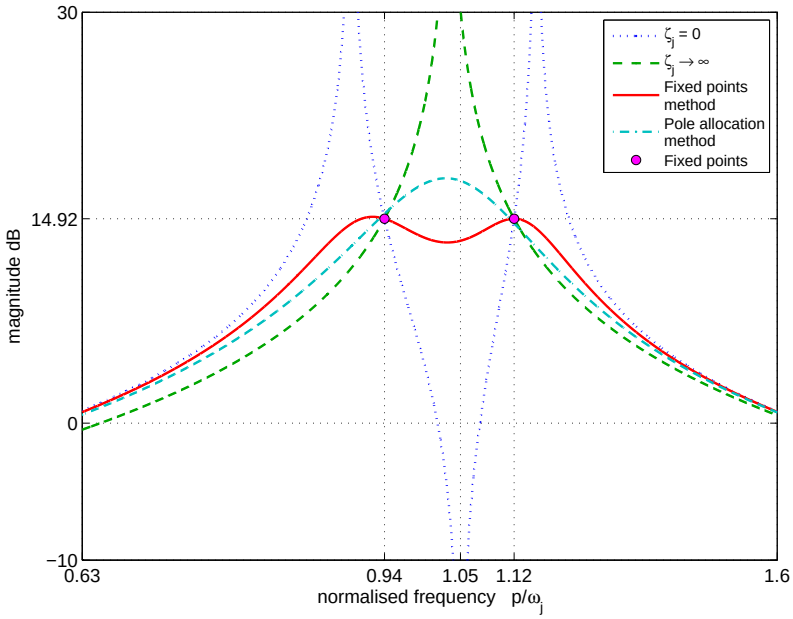


Figure I.6: Mobilities for a virtual passive shunt circuit realised with a resistor and an inductor connected in series and with a generalised coupling coefficient, g_j, equal to 0.25.

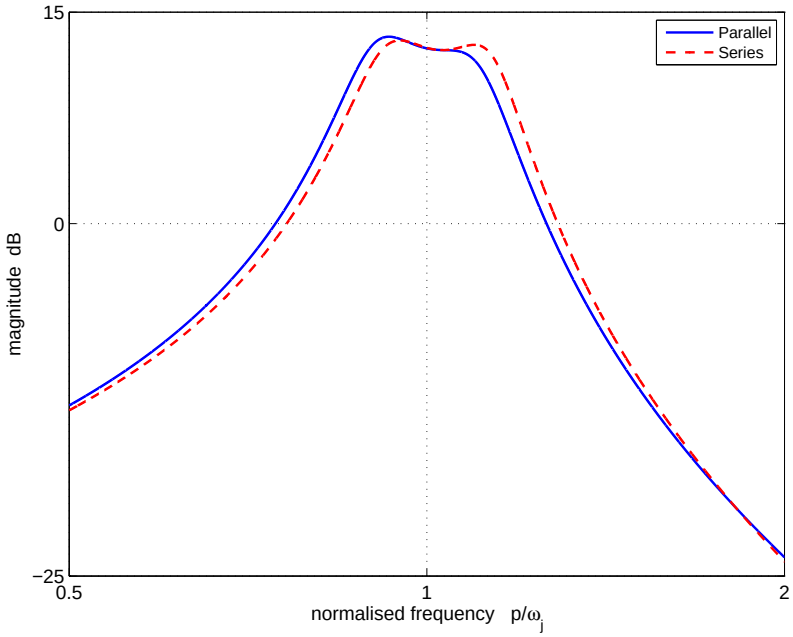


Figure I.7: Comparison between Sensitivity functions, S_{z_j}, for the fixed points method with g_j equal to 0.25.

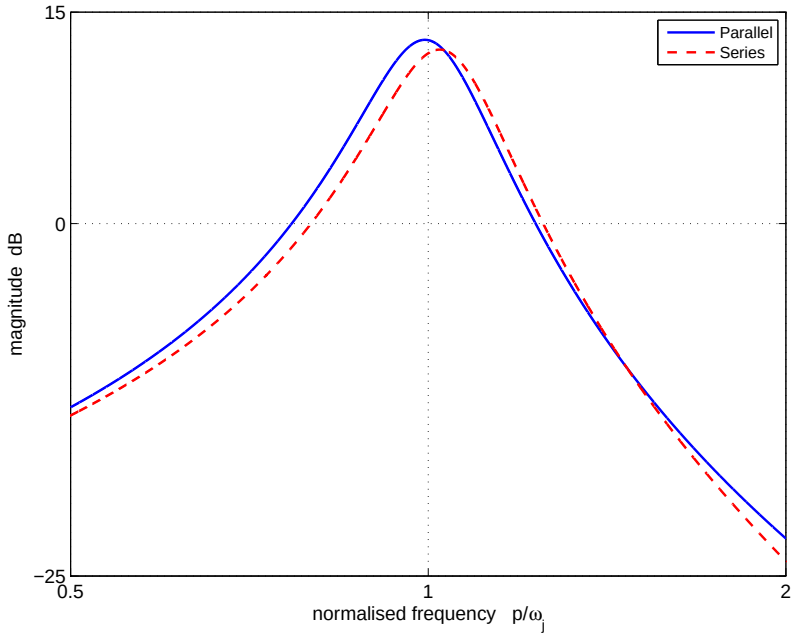


Figure I.8: Comparison between Sensitivity functions, S_{z_j}, for the pole allocation method with g_j equal to 0.25.

the other hand the real part of the closed-loop poles, for the pole allocation method.

The ratio between the optimal mobility peak amplitudes of the series and of the parallel connection depends only on the generalised electro-mechanical coupling coefficient g_j. The plot of such ratio versus g_j is shown in Fig. I.9. Clearly, the series connection provides a greater reduction in the mobility peak amplitude than the parallel one. Therefore, the performance of the series connection is better than the other connection, even though the difference is little.

Similar conclusions can be found comparing the aforementioned index associated to the relative distance between the fixed points, actuality

$$\left(\frac{1+g_j^2}{2+g_j^2}\right) g_j \sqrt{(8+5\,g_j^2)}\,\Big|_{\text{Series}} > \frac{1}{2}\, g_j \sqrt{(8+g_j^2)}\,\Big|_{\text{Parallel}} \tag{I.104}$$

The real part of the closed-loop poles promotes again the series connection

$$\frac{1}{2}\,\tilde{\omega}_j\, g_j\,\Big|_{\text{Series}} > \frac{1}{2}\,\omega_j\, g_j\,\Big|_{\text{Parallel}} \tag{I.105}$$

But, even in this case, the difference has a slight evidence.

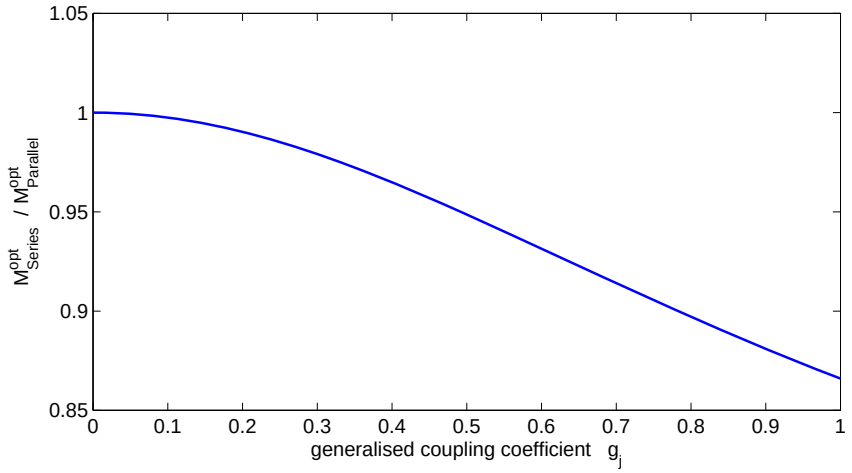


Figure I.9: Ratio between the optimal mobility peak amplitudes of the series and of the parallel connection, for the fixed points method.

In any case, it is impossible to change parameters so as to produce improvement in all performance indexes. Changes in parameters improving the performance as measured by one criterion degrade the performance as measured by another criterion. The figures I.4 and I.6 show that the mobilities obtained with the pole allocation method, in both cases, series and parallel connection, have peak amplitudes larger than those obtained with the fixed points method. Same result, but with roles reversed, occurs if the minimum decay time is compared for two methods. On contrary, as regards the control effort, there are not differences of great significance, see Figs. I.7 and I.8. Hence, there are limits to the performance improvement that can be achieved by modifying parameters for the given configuration. In order to improve further performances, it is advisable to redesign the control system.

I.7 Generalised Hybrid Approach

It is well known, in general, that the increase of the electro-mechanical coupling coefficient improves performances of the passive damping. The reason of it is clear, a larger electro-mechanical coupling allows a greater conversion between vibration and electrical energy that is stored and dissipated in the shunt circuit. Besides, a larger coupling coefficient implies a greater

distance between two fixed points, therefore, a larger vibration suppression can be achieved on a broader range of frequencies. Hence, it would be desirable to examine the possibility of enhancing the electro-mechanical coupling coefficient. As stated previously by several authors [Bondoux, 1996; Tang and Wang, 2001; Behrens et al., 2003], a compensation of the piezoelectric capacitive reactance in a piezoelectric shunt can increase the electro-mechanical coupling coefficient. The key idea, here, is to reduce as closely as possible the electric response of the piezoelectric transducer by means of a compensating current to obtain a greater weigh for the response related to the mechanical dynamic. This compensation is clearly active, therefore, adding it to passive shunt circuits before mentioned, a hybrid control is accomplished.

Let us return, now, to the reduced generalised systems (I.46) of second order. Denoting the ratio of the compensating action by κ_j with $\{j = 1,2,\dots n\}$ and adding the further feedback control generalised current, $\tilde{z}_j$, it can be written

$$\begin{cases} \ddot{\eta}_j(t) + \omega_j^2\,\eta_j(t) - \omega_j\,g_j\,\dot{\chi}_j(t) = f_j(t) \\ \qquad\qquad \ddot{\chi}_j(t) + \omega_j\,g_j\,\dot{\eta}_j(t) = \kappa_j\ddot{\chi}_j(t) + \tilde{z}_j(t) \end{cases} \tag{I.106}$$

in which the unit coefficient of $\ddot{\chi}_j$ on the left hand side of the second equation plays the role of a generalised piezoelectric capacitance. To evaluate the effect of a total or partial compensation of generalised piezoelectric capacitance, it is important to compute the change of the coupling coefficient as κ_j varies. To this end, it is possible to express, in general, the generalised electro-mechanical coupling g_j as function of natural frequencies of the mechanical structure under short and open circuit conditions. From Eq.(I.83), this function can be defined as

$$g_j = \sqrt{\frac{\tilde{\omega}_j^2 - \omega_j^2}{\omega_j^2}} \tag{I.107}$$

Next, setting $\tilde{z}_j$ equal to zero in the second equation of the (I.106) to calculate the natural frequency of the mechanical structure under open circuit condition with the compensation, integrating respect to t and solving for $\dot{\chi}_j$, one obtains

$$\dot{\chi}_j(t) = -\frac{\omega_j\,g_j}{(1-\kappa_j)}\,\eta_j(t) \tag{I.108}$$

Substituting in the first equation of the (I.106), it can write

$$\ddot{\eta}_j(t) + \omega_j^2 \left[1 + \frac{g_j^2}{(1-\kappa_j)} \right] \eta_j(t) = f_j(t) \tag{I.109}$$

Thus, the natural frequency of the mechanical structure under open circuit condition in presence of compensating action is

$$(\tilde{\omega}_j^{\kappa_j})^2 = \omega_j^2 \left[1 + \frac{g_j^2}{(1-\kappa_j)} \right] \tag{I.110}$$

In the end, observing that the natural frequency of the mechanical structure under short circuit condition remains the same, the apparent coupling coefficient is

$$\tilde{g}_j = \sqrt{\frac{(\tilde{\omega}_j^{\kappa_j})^2 - \omega_j^2}{\omega_j^2}} = \frac{g_j}{\sqrt{1-\kappa_j}}, \tag{I.111}$$

Hence, with κ_j over the interval (0, 1), the apparent coupling coefficient is more than when the compensation there is not. It should be remarked that if κ_j is less than zero the coupling $\tilde{g}_j$ is still defined but smaller than before; however, in this case instead to compensate the capacitive reactance, a further generalised capacitance is added. On the other hand, κ_j must not be greater than one because the compensation makes the system unstable. In addition, it is worthy of consideration that the further control action $\tilde{z}_j$ does not need to be a passive law.

Remark I.2. The capacitance compensation can be interpreted, roughly speaking, as a "negative" capacitance that is added in parallel to the generalised piezoelectric element. In [Tang and Wang, 2001] analogous considerations are made with a "negative" capacitance connects in series, but with the difference that the "negative" capacitance increases the overall capacitance of the shunt circuit. On contrary of the parallel connection, the compensation action can not be totally because of a stability issue. Thus the apparent coupling coefficient has an upper bound. In view of these considerations, then, it is preferable to add "negative" capacitances in parallel, since the limitations for the growth of the apparent coupling coefficient are less restrictive.

◇ ◇ ◇

I.7.1 A Passive Shunt Circuit with Compensating Action

To test the effectiveness of the compensation of the generalised piezoelectric capacitance, it is used together with a shunt circuit constituted by a resistor, r_j, and an inductor, ℓ_j, connected in parallel. Similar discussion can be made for the series connection.

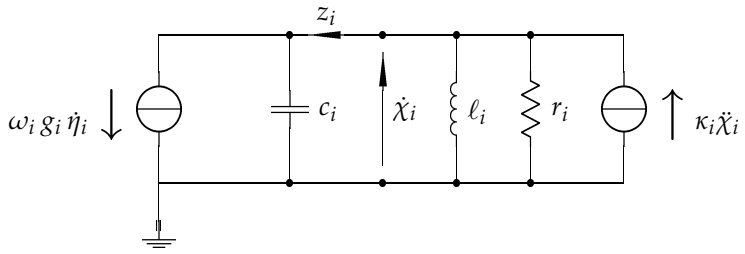


Figure I.10: Equivalent circuit for a virtual hybrid shunt circuit with compensating action.

The further control action, therefore, is given by

$$\tilde{z}_j = -\frac{1}{r_j}\dot{\chi}_j(t) - \frac{1}{\ell_j}\chi_j(t) \tag{I.112}$$

Replacing the control law (I.112) and the definition (I.111) in (I.106), one obtains the closed-loop equations

$$\begin{cases} \ddot{\eta}_j + \omega_j^2 \eta_j - \omega_j \tilde{g}_j \sqrt{1-\kappa_j}\,\dot{\chi}_j = f_j \\ (1-\kappa_j)\ddot{\chi}_j + \dfrac{1}{r_j}\dot{\chi}_j + \dfrac{1}{\ell_j}\chi_j + \omega_j \tilde{g}_j \sqrt{1-\kappa_j}\,\dot{\eta}_j = 0 \end{cases} \tag{I.113}$$

In this case, it is better to work with the auxiliary variable, v_j, defined as

$$v_j = \sqrt{1-\kappa_j}\,\chi_j \tag{I.114}$$

and substituting in (I.113), it is possible to write

$$\begin{cases} \ddot{\eta}_j(t) + \omega_j^2 \eta_j(t) - \omega_j \tilde{g}_j \dot{v}_j(t) = f_j(t) \\ \ddot{v}_j(t) + 2\varpi_j\zeta_j\dot{v}_j(t) + \varpi_j^2 v_j(t) + \omega_j \tilde{g}_j \dot{\eta}_j(t) = 0 \end{cases} \tag{I.115}$$

where

$$\varpi_j^2 = \frac{1}{\ell_j(1-\kappa_j)}, \quad 2\varpi_j\zeta_j = \frac{1}{r_j(1-\kappa_j)} \tag{I.116}$$

Comparing the equations (I.115) with the (I.57), it is clear that the application of the fixed points theory or pole allocation method yields similar results but with a coupling coefficient greater. The figure I.11 shows the mechanical mobility with different values of κ_j.

On the Stability

Following the approach of section I.6.1, the generalised control vector $\boldsymbol{z}$ can be shown to have the form

$$\boldsymbol{z} = \mathscr{K}\,\ddot{\boldsymbol{\chi}} - \mathscr{R}\,\dot{\boldsymbol{\chi}} - \mathscr{L}\,\boldsymbol{\chi} \tag{I.117}$$

in which the matrices $\mathscr{K}$, $\mathscr{R}$ and $\mathscr{L}$ are defined by $\mathscr{K}_{hk} = \kappa_h \delta_{hk}$, $\mathscr{R}_{hk} = (1/r_h)\delta_{hk}$ and $\mathscr{L}_{hk} = (1/\ell_h)\delta_{hk}$. Thus, the actual control law, $\boldsymbol{\imath}$, can be specified as

$$\boldsymbol{\imath} = \mathcal{N}_C\,\ddot{\boldsymbol{\psi}} - \mathcal{N}_R\,\dot{\boldsymbol{\psi}} - \mathcal{N}_L\,\boldsymbol{\psi} \tag{I.118}$$

where the control gain matrices, using definitions (I.17) and (I.21), are

$$\mathcal{N}_C = U\mathscr{K}\,U^{\mathrm{T}} \quad \mathcal{N}_R = U\mathscr{R}\,U^{\mathrm{T}} \quad \mathcal{N}_L = U\mathscr{L}\,U^{\mathrm{T}} \tag{I.119}$$

Because κ_h, r_h and ℓ_h are strictly positive and U is orthogonal, the gain matrices are all *symmetric* and *positive definite*.
Next, the power balance of the whole system whit the capacitance compensation can be written as follows

$$\frac{d}{dt}\left[\frac{1}{2}\dot{\boldsymbol{\eta}}^{\mathrm{T}}\dot{\boldsymbol{\eta}} + \frac{1}{2}\boldsymbol{\eta}^{\mathrm{T}}\Omega^2\boldsymbol{\eta} + \frac{1}{2}\dot{\boldsymbol{\psi}}^{\mathrm{T}}(I - \mathcal{N}_C)\,\dot{\boldsymbol{\psi}} + \frac{1}{2}\boldsymbol{\psi}^{\mathrm{T}}\mathcal{N}_L\boldsymbol{\psi}\right] = -\dot{\boldsymbol{\psi}}^{\mathrm{T}}\mathcal{N}_R\,\dot{\boldsymbol{\psi}} \tag{I.120}$$

The expression inside the parentheses on the left hand side of Eqs. (I.120) can be recognised as the total energy of the system, including the effect of the compensating matrix, $\mathcal{N}_C$ and of the "inductive" matrix, $\mathcal{N}_L$. Hence, in the case of compensating action, considering I as the identity matrix of order n, the matrix $(I - \mathcal{N}_C)$ must be positive definite to assure the asymptotic stability as well as matrices $\mathcal{N}_L$ and $\mathcal{N}_R$. Recalling the definition of $\mathcal{N}_C$, it is possible to write

$$(I - \mathcal{N}_C) = U(I - \mathscr{K})\,U^{\mathrm{T}} \tag{I.121}$$

From which, it is clear that all diagonal elements of $\mathscr{K}$ must be less than one to have the matrix $(I - \mathcal{N}_C)$ positive definite, *i.e.* all its eigenvalues strictly positive and so to ensure the stability of the whole system.

I.8 Generalised Active Control

In Section I.3, the state equations (I.48) for generalised reduced systems have been introduced as

$$\dot{\boldsymbol{w}}_j(t) = \Lambda_j \boldsymbol{w}_j(t) + \mathbf{a}_j f_j(t) + \mathbf{b}_j z_j(t), \quad j = 1,2,\dots n \tag{I.122}$$

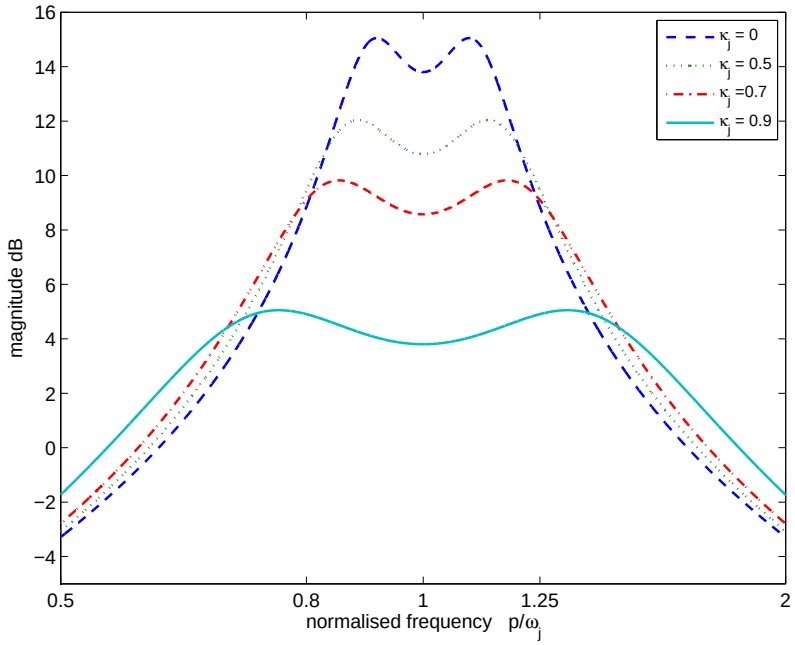


Figure I.11: Mobilities for a virtual hybrid shunt circuit with different compensating actions and g_j equal to 0.25 for κ_j null.

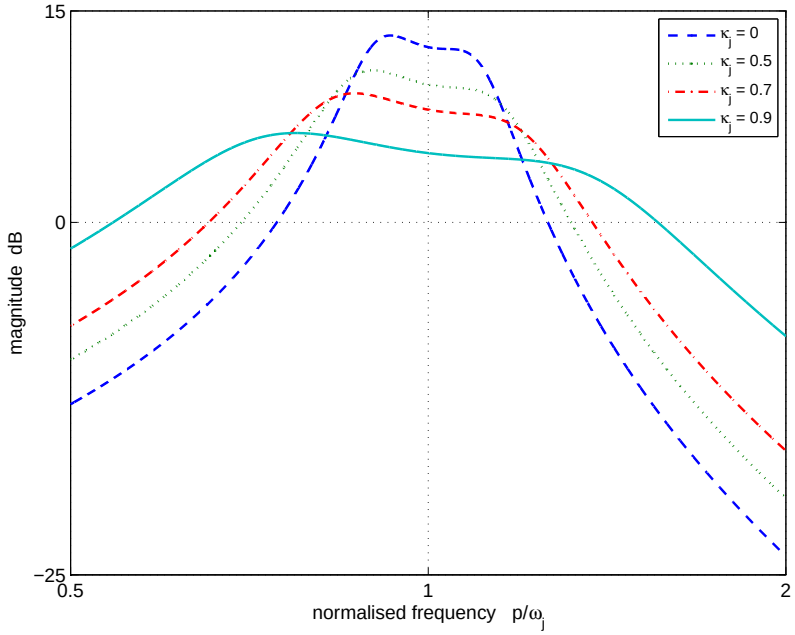


Figure I.12: Sensitivity functions, S_{z_j} with different compensating actions and g_j equal to 0.25 for κ_j null.

where $\boldsymbol{w}_j(t) = [\eta_j(t),\ \dot{\eta}_j(t),\ \dot{\chi}_j(t)]^{\mathrm{T}}$ is the state vector. The system is subject to the mechanical disturbance, $f_j(t)$, and is driven by the control generalised current, $z_j(t)$. Now, let us consider the case in which the control action depends on the state $\boldsymbol{w}_j$. Therefore, denoting the 3-dimensional feedback gain vector with $\mathbf{d}_j$, the state-feedback law is of type

$$z_j(t) = -\mathbf{d}_j^{\mathrm{T}}\, \boldsymbol{w}_j(t) \tag{I.123}$$

Introducing Eq. (I.123) into (I.122), it is possible to write for state feedback control

$$\dot{\boldsymbol{w}}_j(t) = \left(\Lambda_j - \mathbf{b}_j \mathbf{d}_j^{\mathrm{T}}\right) \boldsymbol{w}_j(t) + \mathbf{a}_j f_j(t) \tag{I.124}$$

From these equations it follows that the closed-loop poles depend on the control gain vector $\mathbf{d}_j^{\mathrm{T}}$ whose entries are indicated by $[d_{\eta_j}\, d_{\dot{\eta}_j}\, d_{\dot{\chi}_j}]$. The closed-loop poles, in fact, are the eigenvalues of $(\Lambda_j - \mathbf{b}_j \mathbf{d}_j^{\mathrm{T}})$. On the other hand, they also are poles of the closed-loop mobility from modal disturbing force f_j to modal velocity $\dot{\eta}_j$, or

$$M_j(s) = \frac{s\,(s + d_{\dot{\chi}_j})}{s^3 + d_{\dot{\chi}_j}\, s^2 + (\omega_j^2 + \omega_j\, g_j\, d_{\dot{\eta}_j} + \omega_j^2\, g_j^2) s + \omega_j^2\, d_{\dot{\chi}_j} + \omega_j\, g_j\, d_{\eta_j}} \tag{I.125}$$

and of the closed-loop transfer function from modal disturbing force f_j to control action z_j, or

$$S_{z_j}(s) = -\frac{s\,(d_{\dot{\eta}_j}\, s + d_{\eta_j} - \omega_j\, g_j\, d_{\dot{\chi}_j})}{s^3 + d_{\dot{\chi}_j}\, s^2 + (\omega_j^2 + \omega_j\, g_j\, d_{\dot{\eta}_j} + \omega_j^2\, g_j^2) s + \omega_j^2\, d_{\dot{\chi}_j} + \omega_j\, g_j\, d_{\eta_j}} \tag{I.126}$$

One of the most important objects of the control is to ensure the asymptotic stability, *i.e.* that the closed-loop poles lie in the left half of the complex plane. Applying the *Routh-Hurwitz* criterion on the *characteristic equation* of the closed-loop system (I.124), the asymptotic stability is guaranteed by the conditions

$$\begin{cases} d_{\dot{\chi}_j} > 0 \\ d_{\dot{\eta}_j}\, d_{\dot{\chi}_j} + \omega_j\, g_j\, d_{\dot{\chi}_j} - d_{\eta_j} > 0 \\ \omega_j^2\, d_{\dot{\chi}_j} + \omega_j\, g_j\, d_{\eta_j} > 0 \end{cases} \tag{I.127}$$

Two of the most widely used methods for calculating control gains are optimal control and pole allocation. These methods are discussed in the following sections.

I.8.1 Optimal Control in the Time Domain

The optimal control problem can be defined as follows:

> Determine an admissible control $z_j(t)$ causing the system to go to rest, as close as possible, in accordance with an admissible trajectory in the state space that minimises the cost function
>
> $$J(z_j) = \int_{t_0}^{t_f} h\left[\boldsymbol{w}_j(t), z_j(t), t\right]\, dt \tag{I.128}$$
>
> in which h is a given function, t_0 is the *initial time* and t_f is the *final time*. An optimal control can not exist, and if it exists there is no guarantee that it is unique. However, it is possible to define a variety of cost functions for a given system by choosing different function h in order to obtain a suited result.

The Linear Regulator Problem

The linear regulator problem is an optimal control in which the control action is a linear function of the state. So, the state-feedback law is of type (I.123) and minimises the quadratic cost function

$$J(z_j) = \frac{1}{2}\int_{t_0}^{t_f} \left[\boldsymbol{w}_j^{\mathrm{T}}(t) H_j\, \boldsymbol{w}_j(t) + z_j(t)\, \epsilon_j\, z_j(t)\right]\, dt \tag{I.129}$$

subject to the system dynamics (I.122). The weight matrix H_j is real symmetric positive semi-definite and ϵ_j is a strictly positive scalar. The optimal control problem characterised by the (I.129) can be interpreted as the problem of driven the initial state as close as possible to zero and at the same time inserting a penalty on the control effort. A suited choice for H_j is

$$H_j = \begin{bmatrix} \omega_j^2 & 0 & 0 \\ 0 & 1 & 0 \\ 0 & 0 & 1 \end{bmatrix} \tag{I.130}$$

It should be noted that the first term of the integrand in the quadratic cost function (I.129) represents, with the assumption (I.130), the total generalised energy of the reduced system, as a matter of fact

$$\frac{1}{2}\, \boldsymbol{w}_j^{\mathrm{T}}(t) H_j\, \boldsymbol{w}_j(t) = \frac{1}{2}\, \omega_j^2\, \eta_j^2 + \frac{1}{2}\, \dot{\eta}_j^2 + \frac{1}{2}\, \dot{\chi}_j^2 \tag{I.131}$$

The optimal feedback control gain vector has the form

$$\mathbf{d}_j^{\mathrm{T}} = \epsilon_j^{-1} \mathbf{b}_j^{\mathrm{T}} K_j \tag{I.132}$$

where K_j is a 3×3 symmetric matrix that solves the *Riccati equation*. Being each system (I.122) controllable and Λ_j, $\mathbf{b}_j$, H_j and e_j constant, the Riccati equation has a solution that approaches a constant value as the final time increases. In this case the Riccati equation becomes

$$\Lambda^{\mathrm{T}} K_j + K_j \Lambda - K_j \mathbf{b}_j \epsilon_j^{-1} \mathbf{b}_j^{\mathrm{T}} K_j + H_j = O \tag{I.133}$$

which is an algebraic equation, also called *steady-state matrix Riccati equation*.

I.8.2 Pole Allocation with State Feedback Control

In pole allocation method, the closed-loop poles are chosen in advance and the gains, $[d_{\eta_j}\, d_{\dot{\eta}_j}\, d_{\dot{\chi}_j}]$, are computed so as to produce these poles. In the addressed case the characteristic polynomial is of third order, thus, it admits of a real root and a pair of complex conjugate roots. Therefore, denoting the closed-loop eigenvalues associated with the j-th system (I.124) by

$$s_{j_{1,2}} = a_j \pm i\, b_j, \qquad s_{j_3} = c_j \tag{I.134}$$

the related characteristic polynomial is

$$\begin{aligned}(s - s_{j_1})(s - s_{j_2})(s - s_{j_3}) &= \\ &= s^3 - (2\,a_j + c_j)\, s^2 + (a_j^2 + b_j^2 + 2\,a_j\, c_j)\, s - c_j\, (a_j^2 + b_j^2)\end{aligned} \tag{I.135}$$

Next, equating (I.135) to the denominator of the mobility (I.125), *i.e.* the characteristic polynomial of the system (I.124), the control gains can be calculated. To this end, it is worth assuming

$$a_j = -\beta_j\, \omega_j\, \varsigma_j \tag{I.136}$$

$$a_j^2 + b_j^2 = \beta_j^2\, \omega_j^2 \tag{I.137}$$

$$c_j = -\alpha_j\, \omega_j \tag{I.138}$$

where α_j, β_j and ς_j are strictly positive. These assumptions emphasise the natural frequency of conjugate complex poles, $\beta_j\, \omega_j$, and their damping factor

ς_j. The real part of all poles are imposed to be strictly negative to guarantee asymptotic stability. Finally, the control gains are

$$d_{\eta_j} = \frac{\omega_j^2}{g_j}\left[\alpha_j\,(\beta_j^2 - 1) - 2\,\beta_j\,\varsigma_j\right] \tag{I.139}$$

$$d_{\dot{\eta}_j} = \frac{\omega_j}{g_j}\left[\beta_j^2 + 2\,\alpha_j\,\beta_j\,\varsigma_j - (1 + g_j^2)\right] \tag{I.140}$$

$$d_{\dot{\chi}_j} = 2\,\beta_j\,\omega_j\,\varsigma_j + \alpha_j\,\omega_j \tag{I.141}$$

In the way indicated, by tuning of the parameters β_j, α_j and ς_j, it is possible, on the basis of several criteria, to obtain a different performance of the control system. For instance, a good choice for β_j is 1 because it is not necessary to alter the open-loop frequency ω_j.

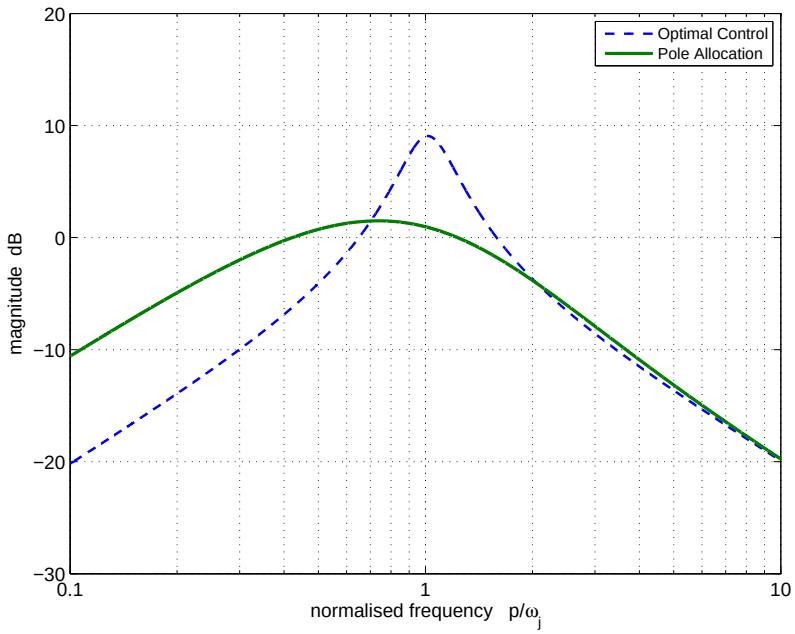


Figure I.13: Mobilities for active control and with g_j equal to 0.25. In pole allocation method, parameters β_j, α_j and ς_j are fixed equal to one.

I.8.3 State Estimation

In this section, the feedback controls discussed until now are based on the assumption that the full state vector, $\boldsymbol{w}_j(t)$, is available for measurement. But under normal conditions, it is not practical to measure the full state vector.

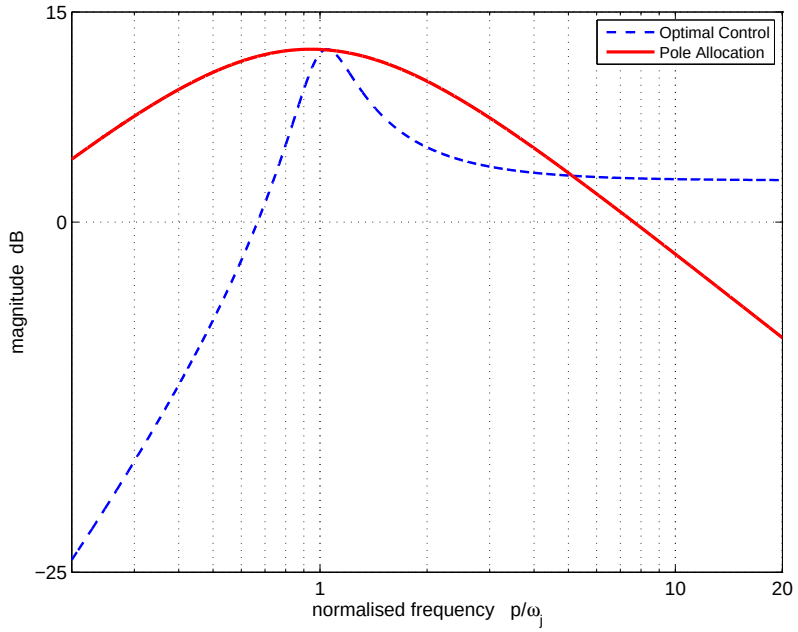


Figure I.14: Sensitivity functions, S_{z_j} for active control and with g_j equal to 0.25 and β_j, α_j and ς_j equalt to one in pole allocation method.

In order to provide more flexibility and advantage, an estimated state is used instead of the actual state. This estimate is obtained by means of a state estimator, also known as *observer*. A state estimate, $\hat{\boldsymbol{w}}_j(t)$, can be provided by the observer with equations

$$\dot{\hat{\boldsymbol{w}}}_j(t) = \Lambda_j \hat{\boldsymbol{w}}_j(t) + \mathbf{b}_j z_j(t) + \mathbf{k}_j \left[\dot{\chi}_j - \mathbf{c}_j^{\mathrm{T}} \hat{\boldsymbol{w}}_j(t) \right] \tag{I.142}$$

where the 3-dimensional vector $\mathbf{k}_j$ is the *observer gain*. The observer (I.142) uses the known input, $z_j(t)$, and the measurement $\dot{\chi}_j(t) = \boldsymbol{u}_j \cdot \dot{\boldsymbol{\psi}}(t)$ to generate the state estimate $\hat{\boldsymbol{w}}_j(t)$. A block diagram of the observer is depicted in Figure I.15. The use of an observer is possible thanks to the *separation principle*. It implies that the observer eigenvalues can be chosen independently of the closed-loop poles of the system (I.124).

A deterministic approach allows to assign the observer poles. The observer obtained in this way is usually known as a *Luenberger observer*. In order to compute a Luenberger observer, the characteristic polynomial associated

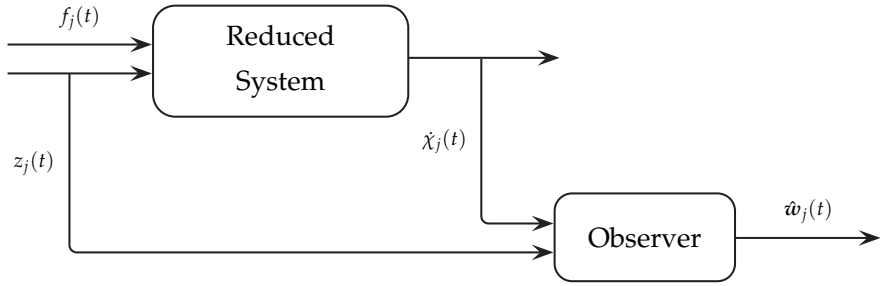


Figure I.15: Block diagram of the observer estimate.

with the matrix $(\Lambda_j - \mathbf{k}_j \mathbf{c}_j^{\mathrm{T}})$ of the observer can be written in the form

$$\begin{aligned} &\det[sI - \Lambda_j + \mathbf{k}_j \mathbf{c}_j^{\mathrm{T}}] = \\ &\qquad = s^3 + k_{3j}\, s^2 + (\omega_j^2 + \omega_j^2\, g_j^2 - \omega_j\, g_j\, k_{2j}) s + \omega_j^3\, g_j\, k_{1j} + \omega_j^2\, k_{3j} \end{aligned} \tag{I.143}$$

where k_{1j}, k_{2j} and k_{3j} are the components of the observer gain vector $\mathbf{k}_j$. Because the observer (I.142) is a 3-dimensional system, it is suited setting the observer poles in this parametric way

$$s_{j_{1,2}} = -\mu_j\, \omega_j\, \sigma_j \pm i\, \mu_j\, \omega_j \sqrt{1 - \sigma_j^2}, \qquad s_{j_3} = -\nu_j\, \omega_j \tag{I.144}$$

in which μ_j, ν_j and σ_j are designing parameters real and positive. Hence, imposing that the (I.144) are roots of the polynomial (I.143) and solving for k_{1j}, k_{2j} and k_{3j}, one obtains

$$k_{1j} = \frac{1}{g_j} \left[\nu_j\, (\mu_j^2 - 1) - 2\, \mu_j\, \sigma_j \right] \tag{I.145}$$

$$k_{2j} = \frac{\omega_j}{g_j} \left[(1 + g_j^2) - \mu_j^2 - 2\, \mu_j\, \nu_j\, \sigma_j \right] \tag{I.146}$$

$$k_{3j} = 2\, \mu_j\, \omega_j\, \sigma_j + \nu_j\, \omega_j \tag{I.147}$$

I.9 Control and Observer Spillover

It is well known that a combination of control and observation spillover due to the uncontrolled modes in a distributed parameter systems controlled by a finite number of actuators and sensors can be cause of instability. In order

to consider the effect of the control actions on the uncontrolled modes, referring to them as residual, they are denoted by the subscript R differently from the controlled modes denoted by the subscript C. By separating the residual modes from the controlled modes, the equations for the electro-mechanical system has the matrix form

$$\begin{cases} \ddot{\boldsymbol{\eta}}_C + \Omega_C^2 \boldsymbol{\eta}_C - \tilde{\Gamma}_C \dot{\boldsymbol{\psi}} = \boldsymbol{f}_C \\ \ddot{\boldsymbol{\eta}}_R + \Omega_R^2 \boldsymbol{\eta}_R - \tilde{\Gamma}_R \dot{\boldsymbol{\psi}} = \boldsymbol{f}_R \\ \ddot{\boldsymbol{\psi}} + \tilde{\Gamma}_C^{\mathrm{T}} \dot{\boldsymbol{\eta}}_C + \tilde{\Gamma}_R^{\mathrm{T}} \dot{\boldsymbol{\eta}}_R = \boldsymbol{\imath} \end{cases} \tag{I.148}$$

Next, it is possible to examine how the transformation U that solves the problem (I.32) affects the spillover. To this end, introducing U, the equations (I.148) can be rearranged as

$$\ddot{\boldsymbol{\eta}}_C + \Omega_C^2 \boldsymbol{\eta}_C - \tilde{\Gamma}_C U \dot{\boldsymbol{\chi}} = \boldsymbol{f}_C \tag{I.149a}$$

$$\ddot{\boldsymbol{\eta}}_R + \Omega_R^2 \boldsymbol{\eta}_R - \tilde{\Gamma}_R U \dot{\boldsymbol{\chi}} = \boldsymbol{f}_R \tag{I.149b}$$

$$\ddot{\boldsymbol{\chi}} + U^{\mathrm{T}} \tilde{\Gamma}_C^{\mathrm{T}} \dot{\boldsymbol{\eta}}_C + U^T \tilde{\Gamma}_R^{\mathrm{T}} \dot{\boldsymbol{\eta}}_R = \boldsymbol{z} \tag{I.149c}$$

It is clear from (I.149b) that there is control spillover in the residual modes due to the matrix product $\tilde{\Gamma}_R U$. The residual modes, usually at high frequencies, are more difficult to excite and therefore they generally can be ignored. In the (I.149c) the term $U^T \tilde{\Gamma}_R^{\mathrm{T}} \dot{\boldsymbol{\eta}}_R$ is responsible for the observation spillover which clearly causes same performance degradation. In any case, observation spillover can be greatly reduced by a proper design of control laws. Indeed, if the control law affects only the frequency range in the neighbourhood of the natural frequencies of controlled modes, as in the generalised passive approach thanks to the tuning procedure, the spillover due to the residual modes can be neglected. In the case of active control with state observer, this last can be used as a filter in order to exclude the contribution of the residual modes. It is for this reason that the Luenberger observer has been used instead of the more usual Kalman filter. Moreover, distributed sensors, like piezoelectric patches, have a natural cutoff wavelength due to their finite surface, therefore, there is a finite and limited number of modes that are actually measured. Besides, any structure has a small amount of mechanical damping that increases the stability margin to be often sufficient to overcome the observation spillover.

CHAPTER II

Physical System Models

> Everything should be made as simple as possible, but not simpler.
>
> ALBERT EINSTEIN (1879–1955)
> *German physicist*

A review is presented here of the physical systems that are pertinent to material in later chapters. In this chapter it is explained and discussed the model of a full clamped rectangular thin plate. In order to provide the necessary elements to develop the proposed subject, first the model of thin plate is introduced and soon afterward piezoelectric transducers employed for control purposes are taken in consideration with the involving electromechanical coupling with the plate.

II.1 First Order Theory of Thin Plates

II.1.1 Introduction

This section is dedicated to provide the governing equation of a thin plate with small deflections [Timoshenko and Woinowsky-Krieger, 1959]. A very satisfactory approximate theory of plate bending can be developed by neglecting the *shear energy* with respect to the *bending energy*.

Let the no-strain configuration be the reference one for a rectangular plate with boundary conditions completely clamped, see figure II.1. All introduced vector valued functions or tensors, unless otherwise noted, are defined into

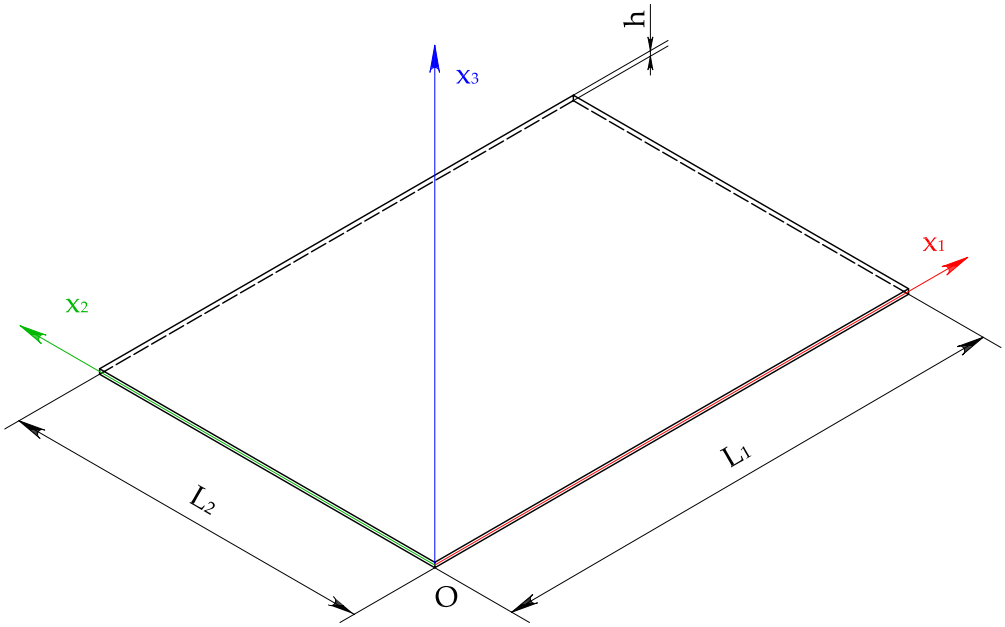


Figure II.1: Reference configuration and reference frame.

domain $\mathscr{P} = [0, L_1] \times [0, L_2] \times [-h/2, h/2]$ and into $C^2(\mathscr{P})$ that is the class of continuous functions in $\mathscr{P}$ together with their derivatives up to order 2. It is worth identifying between two sub-problems which are uncoupled each other, when the deformation motion of a plate is examined: one the in-plane problem and the other the out-of-plane problem. The former is regarded as a stretching problem; the latter is regarded as a bending problem. Herein, the bending problem will be dealt for its importance with regard to vibrations. In order to write the plate equation, it is assumed all points constituting the plate configuration have a perpendicular motion with respect to the plane x_1x_2. This displacement is called $w(x_1, x_2, t)$, considering it as the restriction of the total displacement field to the middle surface. The dependence by the variable x_3, that is to say the coordinate representing the distance with sign between a certain point of the plate and the middle surface, is neglected because one can assume the deflection w reasonable constant along x_3, in the theory takes in account. Let the displacement w be much smaller than the uniform thickness, h, and let us assume that points of the plate lying initially on a normal-to-the-middle plane of the plate remain on the normal-to-the-middle surface of the plate after bending. In addition, it is assumed negligible

the rotational inertia. This is justifiable, as to neglect the shear energy, only at opportune low frequencies. That is to say an upper limit exists for the range of interesting frequencies beyond that it is necessary to introduce into model corrective contributions for both phenomena here neglected. These assumptions are characteristic of the *Kirchhoff model*. As for the external loads, they are assumed uniformly distribute.

It is reasonable admit the following components of stress tensor, T, are zero because of the plane-stress hypothesis for the external faces[1]

$$\begin{cases} T_{33} = 0 & \forall\ x_1, x_2, x_3 \in \mathscr{P} \\ T_{13} = T_{23} = 0 & \forall\ x_1, x_2 \in \overline{\mathscr{A}} \text{ and } x_3 = \pm\, h/2 \end{cases} \tag{II.1}$$

where $\mathscr{A} = (0, L_1) \times (0, L_2)$.

Taking in account these assumptions, by easy geometric argumentations, one finds

$$\begin{aligned} u(x_1, x_2, x_3, t) &= -x_3\, \frac{\partial w}{\partial x_1} \\ v(x_1, x_2, x_3, t) &= -x_3\, \frac{\partial w}{\partial x_2} \end{aligned} \tag{II.2}$$

where u and v are the displacement coordinates along x_1 and x_2 axes, respectively. Made hypotheses for components of the small strain tensor, S, which is symmetric, lead to

$$\begin{aligned} S_{11} &\triangleq \frac{\partial u}{\partial x_1} = -x_3\, \frac{\partial^2 w}{\partial x_1^2} \\ S_{22} &\triangleq \frac{\partial v}{\partial x_2} = -x_3\, \frac{\partial^2 w}{\partial x_2^2} \\ S_{12} &\triangleq \frac{1}{2}\left(\frac{\partial v}{\partial x_1} + \frac{\partial u}{\partial x_2}\right) = -x_3\, \frac{\partial^2 w}{\partial x_1 \partial x_2} \\ S_{33} &\triangleq \frac{\partial w}{\partial x_3} = x_3\, \frac{\nu}{1-\nu}\left(\frac{\partial^2 w}{\partial x_1^2} + \frac{\partial^2 w}{\partial x_2^2}\right) \\ S_{13} &\triangleq \frac{1}{2}\left(\frac{\partial w}{\partial x_1} + \frac{\partial u}{\partial x_3}\right) = 0 \\ S_{23} &\triangleq \frac{1}{2}\left(\frac{\partial w}{\partial x_2} + \frac{\partial v}{\partial x_3}\right) = 0 \end{aligned} \tag{II.3}$$

where ν is the Poisson ratio. The component S_{33} has been calculated utilising the Hook's laws

$$S_{ij} = \frac{1+\nu}{Y}\, T_{ij} - \frac{\nu}{Y}\, T_{kk}\delta_{ij} \tag{II.4}$$

[1] See the observation at page 117 of the appendix A.1.

where Y indicates the Young's modulus and δ_{ij} is the Kronecker symbol. The repeated indexes, according to Einstein's convention, imply the sum.

Remark II.1. It could seem contradictory to consider the dependence of S_{33} by x_3 differently from w, recalling that this strain component is defined as the derivative of such displacement relative to x_3. This apparent discrepancy can be removed keeping in mind that the S_{33} series expansion has a zero constant term and thus, it is not at all allowed to neglect the linear term, although it is very small, with respect to zero. It is worth noting, on the other hand, that S_{33} is of the same order of magnitude as the S_{11} and S_{22}. If one assumes it zero, besides, a plane-strain hypothesis is made having yet considered a plane-stress hypothesis. The two assumptions coexist if and only if the Poisson ratio is zero.

◇ ◇ ◇

II.1.2 Hamiltonian Formulation

Analytical Considerations

After removed all doubts on the hypotheses and on the restrictions of the used model to describe the plate by means of the strong formulation[2], the governing equation of the plate will be derived by the Hamiltonian formulation in view to add the piezoelectric transducers, that introduce discontinuities in the stiffness and in the inertial term for which it is hard to consider a law that describes appropriately the loads applied by them.

It is worth, however, before to go ahead recalling briefly some overture elements. Assuming a motion M, known as *true path*, then, *synchronous varied paths*, X, are all fictitious motions belong to the set of possible motions, $\mathcal{F}$, having a small variation with respect to M and coinciding with it at the limits of an arbitrary, but given, range of time $\mathcal{I} = [t_0, t_1]$. In other words for any generic instant $t \in \mathcal{I}$ the assuming configuration of the system during the true path is extremely close to that one of varied paths having introduced in $\mathcal{F}$ an adapted metric. This small variation can be arbitrarily chosen, provided

[2]See appendix A.1.

it is compatible with the constraints. Defining on $\mathcal{F}$ the functional $\mathcal{S}$

$$\mathcal{S}(X) \;=\; \int_{t_0}^{t_1} (K - \Pi + \mathcal{W})\, dt \tag{II.5}$$

where K represents the kinetic energy, Π the elastic strain energy, and $\mathcal{W}$ the work done by the not conservative external forces, one is able to state the Hamilton's principle in the following form

$$\delta\mathcal{S} = 0 \tag{II.6}$$

It is significant to remark that the integral $\mathcal{S}$ calculated between the initial instant, t_0, and the final one, t_1, assumes a certain value for all the possible motions, true or varied. The equation (II.6) expresses the circumstance that the variation in path $\delta\mathcal{S}$, passing from a generic true path to any synchronous varied path between the same initial and final configurations, is zero, that is to say X is a stationary point in $\mathcal{F}$ of the functional $\mathcal{S}$ if and only if coincide with M.

Mechanical Energy of the Plate

In order to apply the Hamilton's principle, it is necessary the computation of the mechanical energy for the system taken in account. The kinetic energy of the plate occupying the domain $\mathscr{P}$ is given by

$$K = \frac{1}{2} \iint_{\mathscr{A}} \rho\, h \Big(\frac{\partial w}{\partial t}\Big)^2 d\mathscr{A} \tag{II.7}$$

where ρ is the mass density and $d\mathscr{A}$ is the element of measure in $\mathscr{A} \subset \mathbb{R}^2$. The elastic strain potential is

$$\Phi = \frac{1}{2} T_{ij}\, S_{ij} \tag{II.8}$$

Using the (II.4), it can be written in this fashion

$$\Phi = \frac{Y}{2(1-\nu^2)} \Big[{S_{11}}^2 \,+\, 2\nu\, S_{11}\, S_{22} \,+\, {S_{22}}^2 + 2\,(1-\nu)\, {S_{12}}^2 \Big] \tag{II.9}$$

considering the (II.3) and integrating along x_3 from $-h/2$ to $h/2$, one obtains the two-dimensional elastic potential

$$\varphi = \frac{B}{2} \Big[\Big(\frac{\partial^2 w}{\partial x_1^2}\Big)^2 + \Big(\frac{\partial^2 w}{\partial x_2^2}\Big)^2 + 2\,\nu\, \frac{\partial^2 w}{\partial x_1^2}\, \frac{\partial^2 w}{\partial x_2^2} + 2\,(1-\nu) \Big(\frac{\partial^2 w}{\partial x_2 \partial x_1}\Big)^2 \Big] \tag{II.10}$$

where B is the flexural modulus. Finally, the integration on the open set $\mathscr{A}$ of φ yields the strain energy of the plate

$$\Pi = \iint_{\mathscr{A}} \varphi \, d\mathscr{A} \tag{II.11}$$

Remark II.2. Note that into (II.8) the components of stress tensor T_{13} and T_{23} are different from zero as said in the remark A.1 at page 117. In order to obtain the (II.9), however, the terms corresponding to such components have been neglected because, in spite of the fact that they are different from zero, representing the effect of the shear energy, they are smaller than terms corresponding to the bending energy, provided that the frequency range taken into account has not an upper limit too high.

◇ ◇ ◇

The work of external forces, p, acting on $\mathscr{A}$ is given by

$$\mathcal{W} = \iint_{\mathscr{A}} p \, w \, d\mathscr{A} \tag{II.12}$$

Calculating variations of these terms and introducing them into (II.6), the equation of the plate is obtained with the boundary conditions[3]. Summarising, the governing equation of the plate has the form

$$B \, \nabla^4 w(x_1, x_2, t) \; + \; \rho \, h \frac{\partial^2 w}{\partial t^2}(x_1, x_2, t) \; = \; p(x_1, x_2, t) \quad \forall \, x_1, x_2 \in \mathscr{A} \tag{II.13}$$

II.2 Piezoelectric Transducers

II.2.1 General Notices

The word *transducer*, in this circumstance, is used with the meaning of a device that can transfer energy between one system and another. In case that such a flow of energy is turned towards the system to control and the purpose is to make work on this, the transducer behaves as actuator; on contrary, if the energy moves in opposite direction and the purpose is to bring information, then it has a behaviour of a sensor.

[3] See the appendix A.2.

Piezoelectric materials can be used both as actuators and as sensors because of reversibility of the piezoelectric effect. Thanks to the direct effect a piezoelectric patch is a sensor of strain, in a similar manner of a strain gauge, or of a strain rate; for the converse effect it is able to impose local deformation by the application of suitable voltage or charge, that is to say it is an actuator. Moreover, the piezoelectric element can be utilised even at the same time in both the way, making it particularly attractive for many applications. Here, piezoelectric transducers placed on the host plate in an antisymmetric arrangement are employed as showed in figure II.2, in order to measure and to induce only bending deformation. This arrangement is to avoid measuring and exciting the in-plane motion, in order to reduce the observer or control spillover.

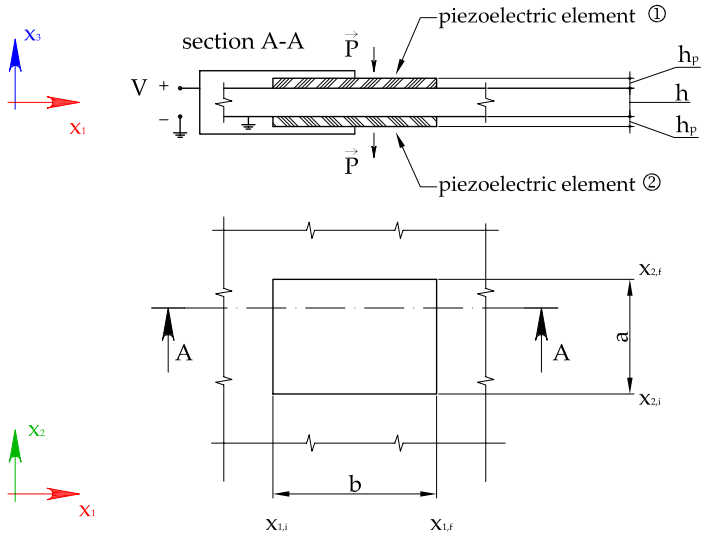


Figure II.2: Piezoelectric transducers in bending configuration.

Hypotheses made with regard to these transducers for the nature of piezoelectric material involve two different points of view: the mechanical and the electrical one. The mechanical assumptions are similar to these made for the thin plate and they are summarised by the following hypotheses:

a) the piezoelectric patches are perfectly bonded on the upper and lower surfaces of plate with an antisymmetric arrangement;

b) the "fibres" of the piezoelectric items that are orthogonal to the middle

surface of the plate in the no-strain reference configuration, keep remaining orthogonal also in any other configuration, *i.e.* even for them are neglected the shear deformations;

c) the thickness of piezoelectric transducers, h_p, is assumed much less large than the one of plate, h;

d) it is adopted a plane-stress hypothesis;

e) it is neglected rotational inertia.

As regards electrical assumptions, the full electromagnetic equations are not needed under ordinary conditions. The quasi-electrostatic approximation is adequate because the phase velocities of vibration waves are approximately five orders of magnitude less than the velocities of electromagnetic waves. Under these circumstances, magnetic effects can be shown to be negligible compared to electrical effects. The electric field vector, $\vec{E}$, is considered constant along the x_3 axis and only its Cartesian component on such axis, E_3, is supposed significant on basis of geometric considerations.

Constitutive relations of the piezoelectric continuous poled in the thickness direction according to the linear theory of piezoelectricity [ANSI/IEEE Std 176-1987] can be expressed, in agreement with summation convention, in this way

$$S_{ij} = \mathfrak{s}_{ijkl} T_{kl} + d_{rij} E_r \tag{II.14}$$

$\mathfrak{s}$ and d are the compliance tensor with constant electric field and the piezoelectric tensor, respectively. The (II.14) must be completed with the equation concerning the electric displacement, $\vec{D}$

$$D_i = d_{ikl} T_{kl} + \epsilon_{ij} E_j \tag{II.15}$$

where ϵ is the dielectric tensor with constant stress.

In order to write the elastic and piezoelectric tensors in the compressed matrix form, a different notation is introduced in place of the tensor one. This matrix notation, referred to as Voigt, consists of replacing a couple of indexes by one according to Table II.1. It should be remarked that when the Voigt notation is used, the transformation properties of the tensors become unclear. Hence, the tensor indexes must be employed when coordinate transformations have to be made.

Table II.1: Index correspondences between tensor and Voigt notation.

tensor notation	Voigt notation
11	1
22	2
33	3
23 or 32	4
31 or 13	5
12 or 21	6

Therefore, the constitutive relationships (II.14) and (II.15) in the new notation can be simplified as

$$S_p = \mathfrak{s}_{pq} T_q + d_{rp} E_r \tag{II.16a}$$

$$D_i = d_{ik} T_k + \epsilon_{ij} E_j \tag{II.16b}$$

Using this notation, thanks to the symmetry of tensors due to the transverse isotropy of piezoelectric material[4], the second order tensors of stress, T, and of small strain, S, become 6-dimensional column arrays, the fourth order tensor of compliance $\mathfrak{s}$ a square matrix 6×6, and the three order piezoelectric tensor a matrix 3×6. Besides, these matrices are not full, and can be typified in the following way

$$\mathfrak{s} = \begin{bmatrix} \mathfrak{s}_{11} & \mathfrak{s}_{12} & \mathfrak{s}_{13} & 0 & 0 & 0 \\ \mathfrak{s}_{12} & \mathfrak{s}_{22} & \mathfrak{s}_{23} & 0 & 0 & 0 \\ \mathfrak{s}_{13} & \mathfrak{s}_{23} & \mathfrak{s}_{33} & 0 & 0 & 0 \\ 0 & 0 & 0 & \mathfrak{s}_{44} & 0 & 0 \\ 0 & 0 & 0 & 0 & \mathfrak{s}_{55} & 0 \\ 0 & 0 & 0 & 0 & 0 & (\mathfrak{s}_{11} - \mathfrak{s}_{12}) \end{bmatrix} \tag{II.17}$$

$$d = \begin{bmatrix} 0 & 0 & 0 & 0 & d_{15} & 0 \\ 0 & 0 & 0 & d_{24} & 0 & 0 \\ d_{31} & d_{32} & d_{33} & 0 & 0 & 0 \end{bmatrix} \tag{II.18}$$

[4]The piezoelectric material undergone the poling process, as this usually used, indeed, is orthotropic.

$$\epsilon = \begin{bmatrix} \epsilon_{11} & 0 & 0 \\ 0 & \epsilon_{22} & 0 \\ 0 & 0 & \epsilon_{33} \end{bmatrix} \tag{II.19}$$

In order to derive a two dimensional theory from the three dimensional one described above, the significant equations of the (II.16a), expressing the components of $\mathfrak{s}$ and recalling that $T_3 = 0$ for the plane-stress hypothesis[5], it can be written

$$\begin{cases} S_1 &= \dfrac{1}{Y_p}(T_1 - \nu_p T_2) + d_{31} E_3 \\ S_2 &= \dfrac{1}{Y_p}(T_2 - \nu_p T_1) + d_{32} E_3 \\ S_6 &= \dfrac{(1+\nu_p)}{Y_p} T_6 \end{cases} \tag{II.20}$$

where Y_p is the in-plane Young's modulus at constant electric field and ν_p equal to $-\mathfrak{s}_{12}/\mathfrak{s}_{11}$ is the Poisson ratio of piezoelectric material; d_{31} supposed identical to d_{32} is the piezoelectric strain constant with electric field along x_3 axis and strain along x_1 or x_2 axes in the order given. Resolving the equations (II.20) for the variables T_j, one finds

$$\begin{cases} T_1 &= K_{mm}(S_1 + \nu_p S_2) - K_{me} E_3 \\ T_2 &= K_{mm}(S_2 + \nu_p S_1) - K_{me} E_3 \\ T_6 &= K_{mm}(1 - \nu_p) S_6 \end{cases} \tag{II.21}$$

The material constants K_{mm} and K_{me} into (II.21) are given by

$$\begin{aligned} K_{mm} &= \frac{Y_p}{1 - {\nu_p}^2} \\ K_{me} &= d_{31} \frac{Y_p}{1 - \nu_p} \end{aligned} \tag{II.22}$$

The only significant component of the electric displacement, $\vec{D}$, it yields

$$D_3 = d_{31} T_1 + d_{32} T_2 + \epsilon_{33} E_3 \tag{II.23}$$

using the (II.21) the equation (II.23) can be rewritten as

$$D_3 = K_{me}(S_1 + S_2) + K_{ee} E_3 \tag{II.24}$$

[5]It should be noted that the same considerations made on T_4 and T_5 for the plate, are still valid.

where

$$K_{ee} = \left(\epsilon_{33} - 2\,{d_{31}}^2\,\frac{Y_p}{1-\nu_p}\right) \tag{II.25}$$

For more details the reader is referred to [Mitchell and Reddy, 1995; Alessandroni et al., 2004; Gopinathan et al., 2000; Fernandes and Pouget, 2002].

II.2.2 Equations of Plate with Transducers

The Hamilton's principle, used to obtain governing equations of plates with the piezoelectric transducers in bending configuration, can be expressed in the form

$$\delta \int_{t_0}^{t_1} (K - \Pi + \mathcal{L}_p + \mathcal{W})\, dt = 0 \tag{II.26}$$

The kinetic energy of the plate, K, and the strain energy, Π, have been computed above in section II.1.2. The modified Lagrangian function, $\mathcal{L}_p$, is defined as the difference between the kinetic energy of piezoelectric patches, K_p, and their electric enthalpy, H. The kinetic energy of a piezoelectric pair is

$$K_p = \iint_{\mathscr{A}} \rho_p\, h_p \left(\frac{\partial w}{\partial t}\right)^2 \wp\; d\mathscr{A} \tag{II.27}$$

where $d\mathscr{A}$ is the element of measure on open set, $\mathscr{A} = (0, L_1) \times (0, L_2)$, the constant ρ_p is the mass density of the piezoelectric material and w has the same meaning of above, *i.e.* the transverse displacement of the middle surface of the plate. The function $\wp(x_1, x_2)$ defined by

$$\wp = [H_1(x_1 - x_{1,i}) - H_1(x_1 - x_{1,f})][H_2(x_2 - x_{2,i}) - H_2(x_2 - x_{2,f})]$$

being $H_1(x_1)$ and $H_2(x_2)$ the Heaviside or unitary step functions, selects the area, $\mathscr{A}_p = (x_{1,i}, x_{1,f}) \times (x_{2,i}, x_{2,f})$, occupied by the pair of the patches.

The density of electric enthalpy, returning to the tensor notation and taking the Einstein's convention in account, was defined by Maugin in 1985 as follows

$$\mathscr{H}(S_{ij}, E_i) = \frac{1}{2}\, T_{ij}\, S_{ij} - \frac{1}{2}\, D_i E_i \tag{II.28}$$

Next, neglecting the shear energy compared to the bending energy and substituting into (II.28) constitutive relations (II.21) and (II.24), the density of electric enthalpy becomes

$$\begin{aligned}\mathscr{H} =& \frac{1}{2} K_{mm} \left[{S_{11}}^2 + 2\,\nu_p\, S_{11}\, S_{22} + {S_{22}}^2 + 2\,(1-\nu_p)\,{S_{12}}^2\right] + \\ & - K_{me}(S_{11} + S_{22})\, E_3 - \frac{1}{2} K_{ee}\,{E_3}^2\end{aligned} \tag{II.29}$$

On the basis of a geometric analysis about transducers, the significant components of the small strain tensor can be made explicit only inside of the area delineated by the patches

$$S_{11} = -x_3 \frac{\partial^2 w}{\partial x_1^2} \qquad S_{22} = -x_3 \frac{\partial^2 w}{\partial x_2^2} \qquad S_{12} = -x_3 \frac{\partial^2 w}{\partial x_2 \partial x_1} \tag{II.30}$$

recollecting that the electric field vector, $\vec{E}$, is conservative, it is possible to describe it in terms of its potential, $\mathscr{V}(x_1, x_2, x_3)$, obtaining $\vec{E} = -\nabla\mathscr{V}$. Besides, the voltage imposed at the electrodes of transducers is specified by $V = -(\mathscr{V}|_{x_3=h_p+h/2} - \mathscr{V}|_{x_3=h/2})$ and, in agreement with made hypotheses, the only significant component of the electric field is

$$E_3 = \pm\frac{V}{h_p}\,\wp$$

where the plus sign corresponds to the upper patch and the minus sign to the lower one. Carrying out the due substitutions in the (II.29), it has

$$\begin{aligned}\mathscr{H} = &\frac{1}{2}K_{mm}\Big[\Big(\frac{\partial^2 w}{\partial x_1^2}\Big)^2 + \Big(\frac{\partial^2 w}{\partial x_2^2}\Big)^2 + 2\nu_p \frac{\partial^2 w}{\partial x_1^2}\frac{\partial^2 w}{\partial x_2^2} + 2(1-\nu_p)\Big(\frac{\partial^2 w}{\partial x_2 \partial x_1}\Big)^2\Big]x_3^2 + \\ &+ \left\{\pm K_{me}\Big(\frac{\partial^2 w}{\partial x_1^2} + \frac{\partial^2 w}{\partial x_2^2}\Big)\frac{V}{h_p}x_3 - \frac{1}{2}K_{ee}\frac{V^2}{{h_p}^2}\right\}\wp\end{aligned} \tag{II.31}$$

Finally, integrating $\mathscr{H}$ on $\mathscr{I}_{x_3} = [-h/2 - h_p, -h/2] \cup [h/2, h/2 + h_p]$ with respect to the variable x_3, the electric enthalpy can be written as

$$\begin{aligned}H(w,V) = \iint_{\mathscr{A}} \Bigg\{ &K_{mm}\Big[\Big(\frac{\partial^2 w}{\partial x_1^2}\Big)^2 + \Big(\frac{\partial^2 w}{\partial x_2^2}\Big)^2 + 2\nu_p \frac{\partial^2 w}{\partial x_1^2}\frac{\partial^2 w}{\partial x_2^2} + \\ &+ 2(1-\nu_p)\Big(\frac{\partial^2 w}{\partial x_2 \partial x_1}\Big)^2\Big]\left(\frac{h^2 h_p}{4} + \frac{h\,h_p^2}{2} + \frac{h_p^3}{3}\right) + \\ &+ K_{me}\Big(\frac{\partial^2 w}{\partial x_1^2} + \frac{\partial^2 w}{\partial x_2^2}\Big)(h + h_p)\,V - K_{ee}\frac{V^2}{h_p}\Bigg\}\,\wp\, d\mathscr{A}\end{aligned} \tag{II.32}$$

The last term of the (II.26), $\delta\mathcal{W}$, represents the sum of the virtual external mechanical work, $\delta\mathcal{W}_m$, and the virtual external electrical work, $\delta\mathcal{W}_e$. The former is

$$\delta\mathcal{W}_m = \iint_{\mathscr{A}} p\,\delta w\; d\mathscr{A} \tag{II.33}$$

whilst the latter is

$$\delta\mathcal{W}_e = \iint_{\mathscr{A}} 2q^+\,\delta V\;\wp\, d\mathscr{A} \tag{II.34}$$

where q is the density of the free electrical charge per unit of surface on the electrodes of each patch. It should be noted that q is not the polarisation charge showing on the opposite faces in the thickness direction of the piezoelectric material. The superscripts "+" indicates the external electrodes of the piezoelectric elements connected in parallel.

Elaborating the (II.26), the two governing equations for the plate equipped with a double wafer transducer in bending configuration is given by

$$\begin{cases} \tilde{B}\nabla^4 w + \tilde{m}\dfrac{\partial^2 w}{\partial t^2} &= p + K_{me}\,(h+h_p)\,V\nabla^2\wp \\ 2\,q^+ &= 2C_{ee}V + K_{me}\,(h+h_p)\Big(\dfrac{\partial^2 w}{\partial x_1^2}+\dfrac{\partial^2 w}{\partial x_2^2}\Big) \end{cases} \tag{II.35}$$

The first equation is defined in $\mathscr{A}$, whilst the second is defined only on the area covered by the pair of patches, in $\mathscr{A}_p$, and both equations are valid for all t in $\mathbb{R}_0^+$. The constants appearing in the (II.35) are the capacitance per unit of surface at null strain, $C_{ee} = K_{ee}/h_p$. The total bending stiffness $\tilde{B}$ is the sum of the plate bending stiffness B and the term due to the piezoelectric material $K_{mm}\left(\frac{h^2\,h_p}{2} + h\,h_p^2 + \frac{2}{3}h_p^3\right)\wp$, similarly the total mass per unit of surface $\tilde{m}$ is the sum of $\rho\,h$ and $2\rho_p\,h_p\wp$. In addition to the boundary conditions already seen for the fully clamped plate (A.13), the further conditions are to be taken into account for the transducers

$$2K_{mm}\Delta H_2\Big[\frac{\partial^3 w}{\partial x_1^3} + (2-\nu_p)\frac{\partial^3 w}{\partial x_1\partial x_2^2}\Big]_{x_1=x_{1,i}}^{x_1=x_{1,f}} = 0 \tag{II.36a}$$

$$2K_{mm}\Delta H_1\Big[\frac{\partial^3 w}{\partial x_2^3} + (2-\nu_p)\frac{\partial^3 w}{\partial x_2\partial x_1^2}\Big]_{x_2=x_{2,i}}^{x_2=x_{2,f}} = 0 \tag{II.36b}$$

$$\Big[\Big[4K_{mm}(1-\nu_p)\frac{\partial^2 w}{\partial x_1\partial x_2}\Big]_{x_1=x_{1,i}}^{x_1=x_{1,f}}\Big]_{x_2=x_{2,i}}^{x_2=x_{2,f}} = 0 \tag{II.36c}$$

Herein the notation $[f(x_1)]_{x_{1,i}}^{x_{1,f}} = f(x_{1,f}) - f(x_{1,i})$ has been used. As for ΔH_1 and ΔH_2, they are $[H_1(x_1 - x_{1,i}) - H_1(x_1 - x_{1,f})]$ and $[H_2(x_2 - x_{2,i}) - H_2(x_2 - x_{2,f})]$, respectively. The first two boundary conditions indicate a generalised force along the x_3 axis that is zero on all the perimeter of each transducer; whilst the last correspond to a twisting moment null on the corners.

The first equation of the (II.35) evidences the effect of piezoelectric transducers, *i.e.* an increase of the mass and of the bending stiffness placed on the area covered by them, $\mathscr{A}_p$, as well as a bending moment acting on the perimeter of the same area $\mathscr{A}_p$ and proportional to the voltage, V, imposed to the

pair of patches connected in parallel. The second equation of the (II.35) represents the Coulomb's theorem at a dielectric-conductor interface, $q_{free} = \vec{D} \cdot \hat{n}$, where $\hat{n}$ is the outward unit normal to the conductor surface. The free charge per unit of surface on each external electrode is given by

$$q^{+} = -D_3|_{x_3=h_p+h/2} = D_3|_{x_3=-h_p-h/2} \tag{II.37}$$

thus, summing the second and the third term of the (II.37) the result is exactly the second equation of the (II.35), neglecting h_p with respect to $h/2$.

Remark II.3. The electric displacement vector $\vec{D}$ satisfies the Maxwell's equation for an insulator, assuming zero the components D_1 and D_2

$$\frac{\partial D_3}{\partial x_3} = 0 \tag{II.38}$$

By the analysis of the constitutive relation (II.24), being the electric field constant, it is clear that the Maxwell's equation (II.38) can not be satisfied owing to the linear dependence of the small strain tensor on x_3. The equation (II.38) is valid if the electric potential, $\mathscr{V}$, has a quadratic dependence on x_3. Hence, it should be written

$$\mathscr{V} = a_0(x_1, x_2) + a_1(x_1, x_2)\, x_3 + a_2(x_1, x_2)\, x_3^2 \tag{II.39}$$

where the relevant coefficients, a_1 and a_2, can be estimated by the satisfaction of the (II.38) imposing the boundary condition given by the voltage, V. Thus, it has

$$\begin{aligned} a_2 &= -\frac{1}{2}\frac{K_{me}}{K_{ee}}\left(\frac{\partial^2 w}{\partial x_1^2} + \frac{\partial^2 w}{\partial x_2^2}\right) \\ a_1 &= \pm\frac{V}{h_p} \mp a_2(h + h_p) \end{aligned} \tag{II.40}$$

The double sign in this last equation is correlated to the antisymmetric configuration of the patches. That upper is referred to the transducer on top and that lower to the transducer on bottom. Moreover, in the usually applications the coefficient a_2 is negligible and thus $\mathscr{V}$ is considered linear in x_3, like above.

◇ ◇ ◇

Finally, it is possible to represent the dynamic of the plate with several

transducers attached with an appropriate pattern for the control of vibrations

$$\begin{cases} \tilde{B}\nabla^4 w + \tilde{m}\dfrac{\partial^2 w}{\partial t^2} = p + \displaystyle\sum_{r=1}^{n_p} K_{me}\,(h+h_p)\,\nabla^2 \wp_r \,\frac{d\phi_r}{dt} \\ Q_r \;\; = \;\; C_r \dfrac{d\phi_r}{dt} + \displaystyle\int_{\mathscr{A}_r} K_{me}\,(h+h_p)\Big(\frac{\partial^2 w}{\partial x_1^2} + \frac{\partial^2 w}{\partial x_2^2}\Big)\, d\mathscr{A}_r, \quad r = 1,2,\dots n_p \end{cases} \tag{II.41}$$

in which electric equations are integrated on the area occupied by each piezoelectric pair, n_p is the number of piezoelectric transducers bonded on the plate, Q_r is the induced charge on the r-th pair of patches and ϕ_r is the associated flux linkage. Besides, $C_r = 2C_{ee}\mathscr{A}_r$ is the overall inherent capacitance of the r-th piezoelectric pair. The total bending stiffness and the total mass per unit of surface are respectively

$$\tilde{B} = B + \sum_{r=1}^{n_p} K_{mm}\left(\frac{h^2 h_p}{2} + h\,h_p^2 + \frac{2}{3}h_p^3\right)\wp_r \tag{II.42}$$

$$\tilde{m} = \rho\,h + 2\sum_{r=1}^{n_p} \rho_p\, h_p \wp_r \tag{II.43}$$

II.3 Modal Analysis

Making the substitution (I.5), equations (II.41) can be rewritten as follows

$$\begin{cases} \tilde{B}\nabla^4 w + \tilde{m}\dfrac{\partial^2 w}{\partial t^2} = p + \displaystyle\sum_{r=1}^{n_p} \frac{K_{me}\,(h+h_p)}{\sqrt{C_r}}\,\nabla^2 \wp_r \,\frac{d\psi_r}{dt} \\ \mathcal{Q}_r \;\; = \;\; \dfrac{d\psi_r}{dt} + \displaystyle\int_{\mathscr{A}_r} \frac{K_{me}\,(h+h_p)}{\sqrt{C_r}}\Big(\frac{\partial^2 w}{\partial x_1^2} + \frac{\partial^2 w}{\partial x_2^2}\Big)\, d\mathscr{A}_r, \quad r = 1,2,\dots n_p \end{cases} \tag{II.44}$$

In order to consider the eigenvalue problem (I.9), assuming the boundary conditions of fully clamped edges for the transverse displacement, w, and the short circuit condition for normalised voltage, $\dot{\psi}_r$, it is possible to write

$$\begin{cases} w = 0 \quad \text{and} \quad \dfrac{\partial w}{\partial x_1} = 0 \quad \text{along } x_1 = \{0, L_1\} \\ w = 0 \quad \text{and} \quad \dfrac{\partial w}{\partial x_2} = 0 \quad \text{along } x_2 = \{0, L_2\} \\ \dot{\psi}_r = 0 \qquad r = 1,\dots n_p \end{cases} \tag{II.45}$$

Let us assume that the eigenfunctions $W(x_1, x_2)$ defined by the relation (I.8) are orthogonal and normalised to unit modal mass, thus they satisfy the relations

$$\int_{\mathscr{A}} \rho\, h\, W_i W_j \, d\mathscr{A} + 2 \sum_{r=1}^{n_p} \int_{\mathscr{A}_r} \rho_p\, h_p W_i W_j \, d\mathscr{A}_r = \delta_{ij} \tag{II.46a}$$

$$\begin{aligned} &\int_{\mathscr{A}} B \nabla^4[W_i] W_j \, d\mathscr{A} + \\ &+ \sum_{r=1}^{n_p} \int_{\mathscr{A}_r} K_{mm} \left(\frac{h^2\, h_p}{2} + h\, h_p^2 + \frac{2}{3} h_p^3 \right) \nabla^4[W_i] W_j \, d\mathscr{A}_r = \omega_i^2 \delta_{ij} \end{aligned} \tag{II.46b}$$

Substituting the expression (I.8) into the (II.44), the mode model of the smart plate can be obtained

$$\begin{cases} \ddot{\boldsymbol{\eta}} + \Omega^2\, \boldsymbol{\eta} - \tilde{\Gamma}\, \dot{\boldsymbol{\psi}} = \boldsymbol{f} \\ \qquad\quad \ddot{\boldsymbol{\psi}} + \tilde{\Gamma}^{\mathrm{T}}\, \dot{\boldsymbol{\eta}} = \boldsymbol{\imath} \end{cases} \tag{II.47}$$

where

$$\tilde{\Gamma}_{ir} = \frac{K_{me}\,(h + h_p)}{\sqrt{C_r}} \left(\int_{x_{2,i}^{(r)}}^{x_{2,f}^{(r)}} \left[\frac{\partial W_i}{\partial x_1} \right]_{x_{1,i}^{(r)}}^{x_{1,f}^{(r)}} dx_2 + \int_{x_{1,i}^{(r)}}^{x_{1,f}^{(r)}} \left[\frac{\partial W_i}{\partial x_2} \right]_{x_{2,i}^{(r)}}^{x_{2,f}^{(r)}} dx_1 \right) \tag{II.48}$$

are entries of the electro-mechanical coupling matrix $\tilde{\Gamma}$ and considering the unit-frequency normalised coupling matrix Γ

$$\Gamma_{ir} = \frac{1}{\omega_i}\, \tilde{\Gamma}_{ir} \tag{II.49}$$

whilst

$$f_i = \int_{\mathscr{A}} p(x_1, x_2, t) W_i \, d\mathscr{A} \quad i = 1, \ldots n_m \tag{II.50}$$

are generalised forces per unit of surface.

II.4 Finite Element Model

Once fixed the position of the piezoelectric elements, accurate estimate of the natural frequencies and corresponding plate mode shapes, including effects of the piezoelectric transducers under short circuit condition, is obtained by a finite element analysis. To this end, the commercial code **ANSYS**® is employed to perform this analysis. The finite element model, here elaborated, is based on the choice of brick elements for the discretization of piezoelectric patches and of quadrilateral shell elements for modelling the plate given that

they are designed to model efficiently thin structures. Indeed, Ansys includes 3D solid elements with piezoelectric capabilities, but not piezoelectric plate or shell elements. More in detail, the overall structure is modelled using elastic shell elements, shell93, for the plate and 3D solid elements, solid226, with piezoelectric capabilities for the transducers. The shell93 element is an eight node structural shell element with six degrees of freedom at each node, three for displacements and three for rotations. The solid226 element has twenty nodes with four degrees of freedom per node, three for displacements and one for the electric potential. It is clear that the connection between these two kind of elements is a crucial problem for modelling overall structure. The condition of bonding the piezoelectric material on the plate is realised in Ansys by constraint equations, where node displacements of piezoelectric element at the interface with the plate are imposed to make null the relative displacement between the two types of element according to the hypotheses of the Kirchhoff-Love model applied to the plate, as proposed in [Tliba and Abou-Kandil, 2005]. In order to use the Kirchhoff-Love hypotheses, the element mesh must ensure that each nodal point of the solid element for piezoelectric transducers matches the nodal point of the related shell element at the interface, see the figure II.3.

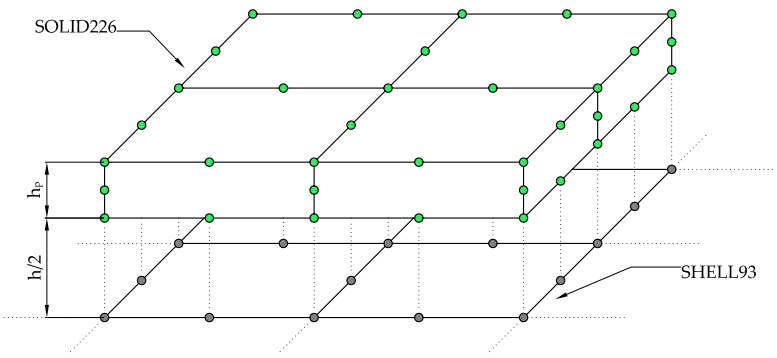


Figure II.3: A frame detail of a plate modelled as shell elements and a piezoelectric transducer modelled as solid elements.

The element mesh is sufficiently fine in order to have acceptable accuracy. To assess accuracy, the mesh is refined until the results shows little change. For higher accuracy, the aspect ratio of the elements is assigned as close to unity as possible. For this reason and to avoid excessively increasing the num-

ber of elements and the time of computation, piezoelectric transducers are modelled using solid elements with twenty nodes, specifically consisting of one element along the direction of minimum thickness.

The short circuit condition for the piezoelectric elements is modelled by imposing a null voltage on both electrodes of each patch.

CHAPTER III

Numerical Simulations

> For everything you have missed, you have gained something else, and for everything you gain, you lose something else.
>
> Ralph Waldo Emerson (1803–1882)
> *American Poet*

Numerical case studies are considered in this chapter to determine features of proposed vibration controls. At first a numerical analysis is performed on a thin beam with both ends clamped. To further illustrate characteristics of these controls a second case is considered involving a rectangular fully clamped plate. Herein, a most important assumption is to consider for each mechanical mode in need of control two identical thin slice of piezoelectric material bonded symmetrically onto either faces of the thin structures and connected in parallel. They are bonded with inverted polarization directions in order to produce opposite deformations and to induce pure bending. In this way each transducer pair is associated to one electric degree of freedom because of the parallel connection.

III.1 Clamped-Clamped Beam Case Study

The clamped-clamped beam is made of aluminium with a rectangular cross section of height h equal to 2.9×10^{-3} m and width 2×10^{-2} m and having length L equal to 0.45 m. Three pairs of piezoelectric elements are bonded on the beam to implement the proposed technique on three mechan-

ical modes. The modes of interest are the lowest because they are prominent in the dynamics of interest. The piezoelectric transducers are assumed to be of ceramic material with properties given in table III.1. The example results given below are for piezoelectric patches of width b_p equal to 1.8×10^{-2} m and thickness h_p equal to 2.67×10^{-4} m. Table III.2 displays lengths of the piezoelectric transducers and their positions defined as the distance of each piezoelectric pair from the left end of the beam.

Table III.1: Material characteristics of the piezoelectric transducers.

	symbol	value	unit
Permittivity at constant Stress	ε_{33}	$3800\ \varepsilon_0$	
Piezoelectric Strain Constant	d_{33}	650×10^{-12}	m V^{-1}
	d_{31}	-320×10^{-12}	m V^{-1}
Density Mass	ρ_{pe}	7800	kg m^{-3}
Young Modulus	Y_3	50×10^9	Pa
	Y_1	62×10^9	Pa
Poisson's Ratio	ν_{pe}	0.31	

The derivation of governing equations for the beam with piezoelectric patches involves more discussion than is worthwhile here [Maurini, 2005]. Indeed, a mode model of the beam with piezoelectric transducers has the same form presented in chapter I

$$\begin{cases} \ddot{\boldsymbol{\eta}} + \Omega^2 \boldsymbol{\eta} - \Omega\, \Gamma\, \dot{\boldsymbol{\psi}} = \boldsymbol{f} \\ \ddot{\boldsymbol{\psi}} + (\Omega\, \Gamma)^{\mathrm{T}}\, \dot{\boldsymbol{\eta}} = \boldsymbol{\imath} \end{cases} \tag{III.1}$$

In agreement with classical results [Park, 2003; Maurini et al., 2006], the expression for the entries of the normalised piezoelectric coupling matrix Γ are

$$\Gamma_{jr} = \frac{d_{31}\, Y_1\, (h + h_p)\, b_p}{\omega_j \sqrt{C_r}} \left[\frac{\partial W_j}{\partial x_1} \right]_{x_{1,i}^{(r)}}^{x_{1,f}^{(r)}} \tag{III.2}$$

where the notation $[f(x_1)]_{x_{1,i}}^{x_{1,f}} = f(x_{1,f}) - f(x_{1,i})$ has been used, $x_{1,i}^{(r)}$ and $x_{1,f}^{(r)}$ represent respectively the start and end of the r-th pair of transducers, $\partial W_j / \partial x_1$ is the mode rotation function of the beam for the j-th mechanical

mode under *short circuit condition* and ω_j is the natural frequency associated with it. These entries are also proportional to the average mode curvature of the region covered by the piezoelectric patches. The r-th capacitance of the two-element piezoelectric transducer, according to assumption of section II.2, is

$$C_r \;=\; 2\Big(\varepsilon_{33} - 2\,d_{31}^2\,Y_1\Big)\,\frac{a_r\,b_p}{h_p} \tag{III.3}$$

Locations of piezoelectric transducers are important to ensure an acceptable level of vibration reduction. This can be achieved by placing the two-element piezoelectric transducers in order to enhance the coupling between each transducer and the mechanical modes of interest. To this end, the expression (III.2) has been used to compute the piezoelectric coupling Γ_{ir} with the approximation to use the mode shapes of the Euler-beam without changes due to the piezoelectric mass and stiffness.

Table III.2: Specifications of the piezoelectric transducers.

piezo	length a_r (m)	location $x_{1,i}^{(r)}$ (m)
1	0.036	0.003
2	0.07	0.155
3	0.036	0.411

Given any piezoelectric transducer, it is possible to calculate the piezoelectric coupling with different modes and to display it as a function of the piezoelectric length and the piezoelectric position on the beam. The obtained graphs for each of the first three mechanical modes are showed in the left hand side of the figure III.1. Also the mode rotations and curvatures of these three modes, *i.e.* derivatives of mode shapes respectively of orders one and two, are displayed at right hand side for their significance. The analysis performed on these graphs justifies the chosen locations that are summarised in table III.2. Indeed two piezoelectric pairs are placed near to the clamps of the beam and one is located close to, but not exactly, the middle section to sense or excite even the second mode. The lengths are chosen to obtain coupling coefficients with comparable values of wavelengths of modes of interest.

In previous sections the assumption that the system possesses negligible

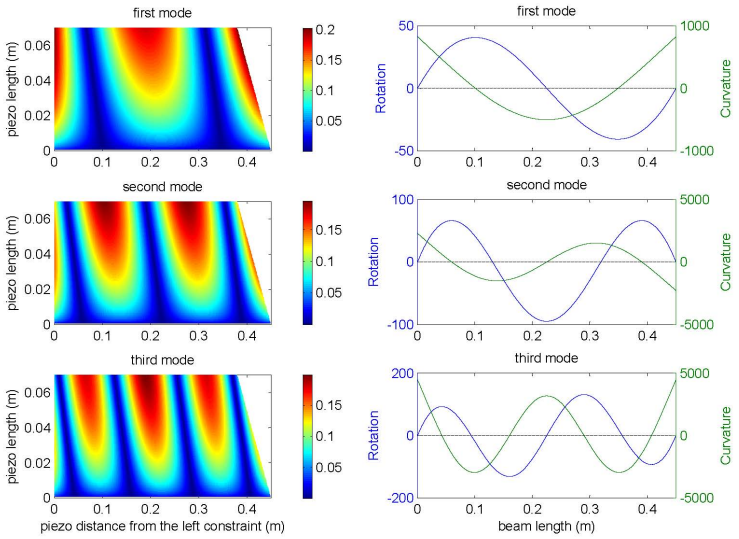


Figure III.1: On the left hand side are depicted the plots of piezoelectric coupling between one piezoelectric transducer and the first three mechanical modes, as the length of piezoelectric element and its position vary on the beam. On the right hand side are displayed rotations and curvatures for the first three modes.

mechanical damping is made. At this point the damping effect is included. Introducing this effect and recalling the relation (I.5) to make explicit the electric flux linkage $\boldsymbol{\phi}$, the governing equations for the whole system assume the form

$$\begin{cases} \ddot{\boldsymbol{\eta}} + D\,\dot{\boldsymbol{\eta}} + \Omega^2\,\boldsymbol{\eta} = P\,\dot{\boldsymbol{\phi}} + \boldsymbol{f} \\ C\,\ddot{\boldsymbol{\phi}} + \aleph_p\,\dot{\boldsymbol{\phi}} = -P^{\mathrm{T}}\,\dot{\boldsymbol{\eta}} + \tilde{\boldsymbol{\imath}} \end{cases} \tag{III.4}$$

in which Ω is the diagonal matrix of natural frequencies under the short-circuit condition, $\dot{\boldsymbol{\phi}} = \mathbf{0}$; the matrix P defined as

$$P = \Omega\,\Gamma\,\sqrt{C} \tag{III.5}$$

is the *piezoelectric coupling* matrix; $\boldsymbol{f}$ is the modal mechanical forcing vector. The vector $\boldsymbol{\eta}$ has as elements the modal coordinates. In this case the damping is assumed of the proportional type. This implies that the matrix D is diagonal and can be expressed as

$$D_{ij} = 2\xi_j\omega_j\delta_{ij} \tag{III.6}$$

where ξ_j is the damping ratio of the j-th mode assumed equal to 4×10^{-3} for all modes and δ_{ij} is the Kronecker symbol. The second equation is the

current balance at the electrodes of the piezoelectric elements. The matrix C is a diagonal positive definite matrix of piezoelectric capacitances, whose elements $C_h\delta_{hk}$ represent inherent capacitances of piezoelectric patches at blocked modal deflections, $\dot{\boldsymbol{\eta}} = \mathbf{0}$, the matrix $\aleph_p$ is a diagonal positive definite matrix , whose entries are $(1/R_h)\delta_{hk}$ being R_h the internal resistances assumed all equal to 10 MΩ; the term $\tilde{\boldsymbol{\imath}} = \sqrt{C}\,\boldsymbol{\imath}$ represents the currents flowing through the piezoelectric transducers. With the chosen electromechanical state variables, the conservative piezoelectric coupling appears in a gyroscopic form. In the mechanical equation, the term $P\,\dot{\boldsymbol{\phi}}$ represents the mechanical modal forces due to the piezoelectric voltages. In the electric equation, the term $P^{\mathrm{T}}\,\dot{\boldsymbol{\eta}}$ may be interpreted as a set of current generators in parallel connection with the inherent piezoelectric capacitances whose current intensities are proportional to the mechanical modal velocities.

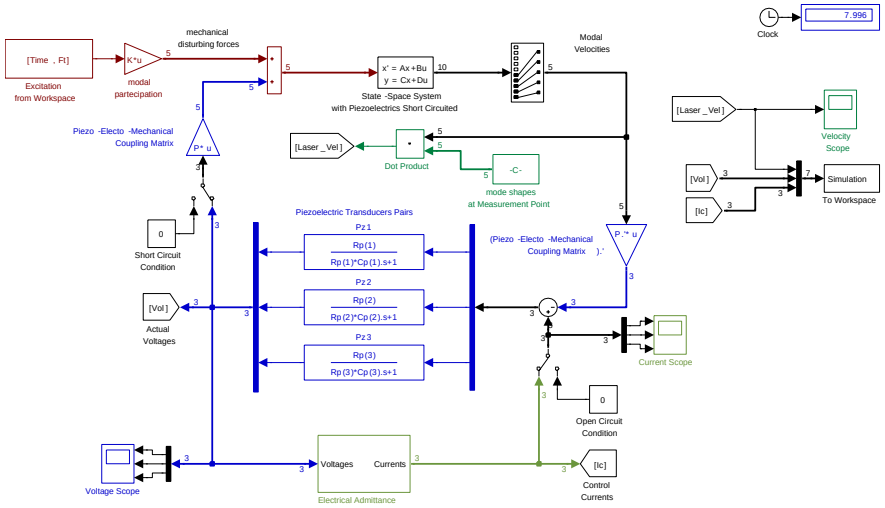


Figure III.2: Simulink diagram of the studied system.

The system (III.4) can be modelled in Simulink and the diagram III.2 shows this model. A great care has been devoted to set up the model in order to allow Simulink to execute it faster and more accurately. This numeric scheme is based on two feedback loops that simulate the interaction between the host mechanical system and the piezoelectric transducers and between these and the control device, *i.e.* an electric admittance. The forcing input to the mechanical system under short circuit condition is the sum of the me-

chanical disturbing forces and the piezoelectric coupling actions. The electric behaviour of each transducer is modelled by the inherent capacitance of the piezoelectric patch in parallel with the internal resistance. To take account of the spillover problem the system model is characterised by five mechanical modes instead of three. The Simulink model permits both to calculate all frequency response functions, FRF, of interest and to predict the output time history due to a known input like an impulse. The main objective in this analysis is to estimate input-output relationships. A dual channel FFT analysis of the input and output of a system is performed to calculate a function FRF which describes its dynamic behaviour, assuming the system is linear. Indeed, this function characterises the system independent of the input signal. The locations used to excite the beam and to compute its response have been chosen to avoid the nodes appearing for low frequency bending modes. In the simulation the beam is exited by an impulse with a frequency spectrum covering a frequency range from near zero to f_{max} that is 1200 Hz at 8×10^{-2} m from one end of the beam. To model the impulse, the disturbance force is a half sine. This force is characterised by its peak value F_0 and time duration τ. The peak value is assumed equal to 1 N and the time duration τ is equal to 2.78×10^{-4} s so that $1/\tau = 1.5\, f_{max}$. The time of simulation T is equal to 10.49 s, thus the frequency analysis has a frequency resolution Δf equal to 0.1 Hz. A fixed-step solver is considered because requires less memory to implement and is faster than the variable-step solver. The simulation step size equal to the discrete sample time is $1/12500$ s to avoid computation errors. The output is the velocity at the point x_1 equal to 0.333 m.

III.1.1 Numerical Results

The unit-frequency normalised coupling matrix Γ has been computed, according to the formula (III.2), using the mode shapes and natural frequencies of the double clamped beam provided by a finite element model realised with Ansis. The same assumptions of the plate in section II.4 are used for the Ansis model of the beam. The frame of the system is modelled with a uniform mesh consisting in 153×7 shell elements for the beam, $12 \times 7 \times 1$ solid elements for each piezoelectric patch at the beam ends and $24 \times 7 \times 1$ elements for the

central piezoelectric patches. Therefore, the matrix Γ is

$$\Gamma = \begin{bmatrix} -0.111 & 0.133 & -0.111 \\ 0.096 & -0.097 & -0.099 \\ -0.081 & -0.102 & -0.083 \end{bmatrix} \tag{III.7}$$

Solving the equation set (I.40) using the matrix (III.7), it obtains a transformation matrix

$$U = \begin{bmatrix} -0.404 & 0.642 & -0.652 \\ 0.656 & -0.293 & -0.696 \\ -0.638 & -0.709 & -0.302 \end{bmatrix} \tag{III.8}$$

that yields the new coupling matrix

$$\mathcal{G} = \begin{bmatrix} 0.202 & -0.032 & 0.013 \\ -0.040 & 0.160 & 0.035 \\ 0.018 & 0.037 & 0.149 \end{bmatrix} \tag{III.9}$$

Here, the second step of optimisation introduced in section I.2.2 has not been performed and the rows of Γ are not mutually perpendicular. In fact, the angles ϑ_{ij} between the i-th row and the j-th row of Γ are

$$\begin{aligned} \vartheta_{12} &= 0.619\,\pi \\ \vartheta_{13} &= 0.455\,\pi \\ \vartheta_{23} &= 0.369\,\pi \end{aligned} \tag{III.10}$$

For this reason, the entries below and above the main diagonal of $\mathcal{G}$ are only an order of magnitude less than the diagonal entries, so the undesired piezoelectric cross actions decrease but do not vanish. In this case, the proposed method exploits the fact that in vicinity of a natural frequency, the behaviour of the beam is dominated by a single mode, as for most mechanical systems. The piezoelectric shunting controller acts almost independently on the various modes in part by the effect of the transformation U and in part by a proper designing that introduces damping in the near of the resonances of interest without cross actions. Therefore, the controller is designed to affect only those frequency ranges close to the resonances of mechanical modes in need of control. Hence, even though it is impractical to make the rows of Γ mutually perpendicular, a useful performance can be obtained for a most part of mechanical systems whose poles are well spaced in frequency domain. On

the contrary, this last feature is unnecessary if the rows of Γ can be made mutually perpendicular.

Figures from III.3 to III.6 display the transfer mobilities of the uncontrolled beam with short-circuited piezoelectric elements and the beam with the optimal shunts outlined in sections I.6, I.7 and I.8. It is shown that at the first, second and third eigenfrequencies the controlled beam mobility decreases of about 20 dB for the passive controllers and even 30 dB for active controllers. Figures III.7-III.9 shows the comparison between impulse response of the controlled and uncontrolled beam. The controlled response decreases faster than the uncontrolled one. In fact, at 0.15 s the controlled response reduces of about 99% for all cases, instead of the uncontrolled one that decreases of 98% at 1 s.

The active controllers reach better performance than the passive controllers but with a greater control effort. In other respect, the passive controllers are unconditionally stable.

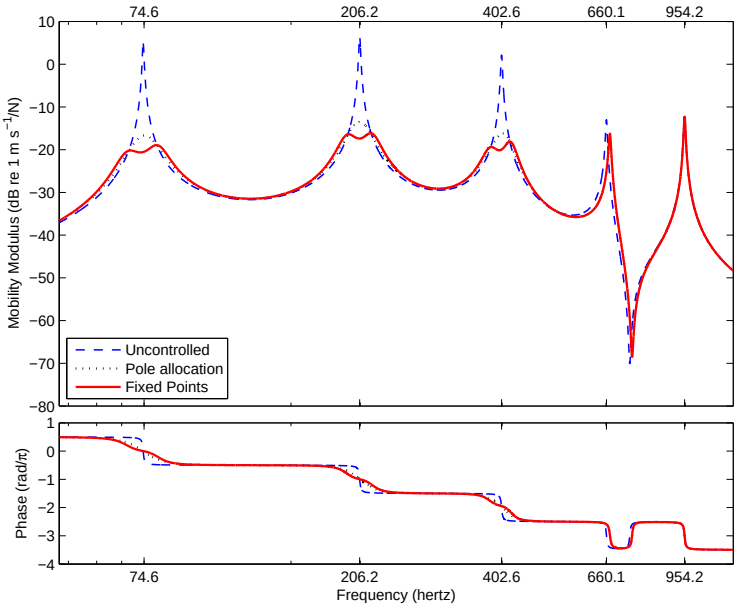


Figure III.3: Mobility of the uncontrolled beam and the comparison with proposed control for the passive approach in parallel configuration implemented on the first three modes.

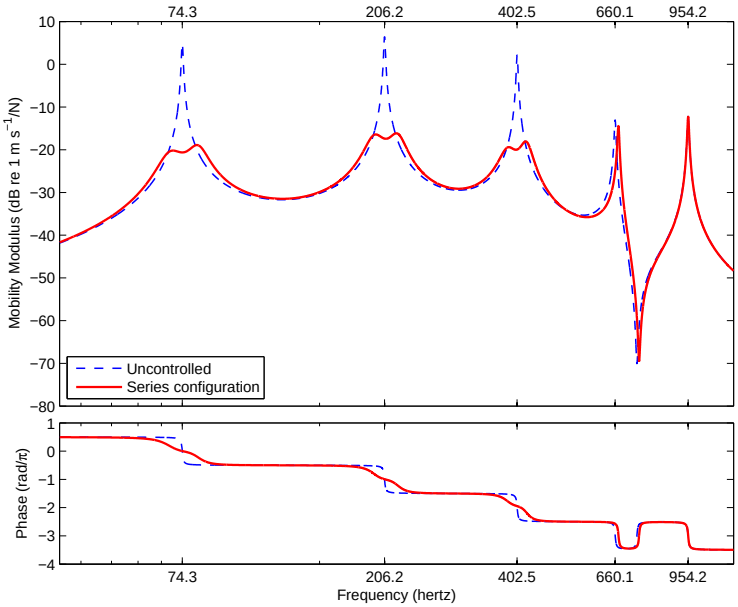


Figure III.4: Mobility of the uncontrolled beam and the comparison with proposed control for the passive approach in series configuration implemented on the first three modes.

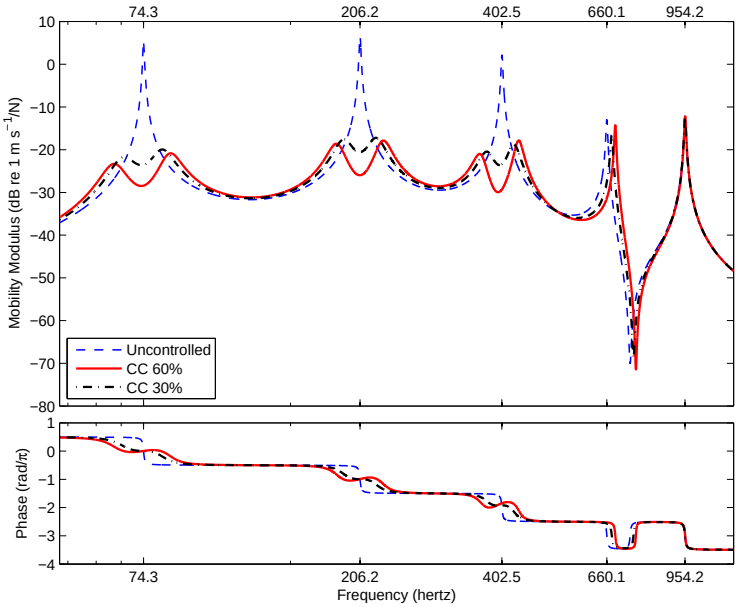


Figure III.5: Mobility of the uncontrolled beam and the comparison with proposed control for the hybrid approach with capacitance compensation (CC) of 30% and 60% applied on the first three modes.

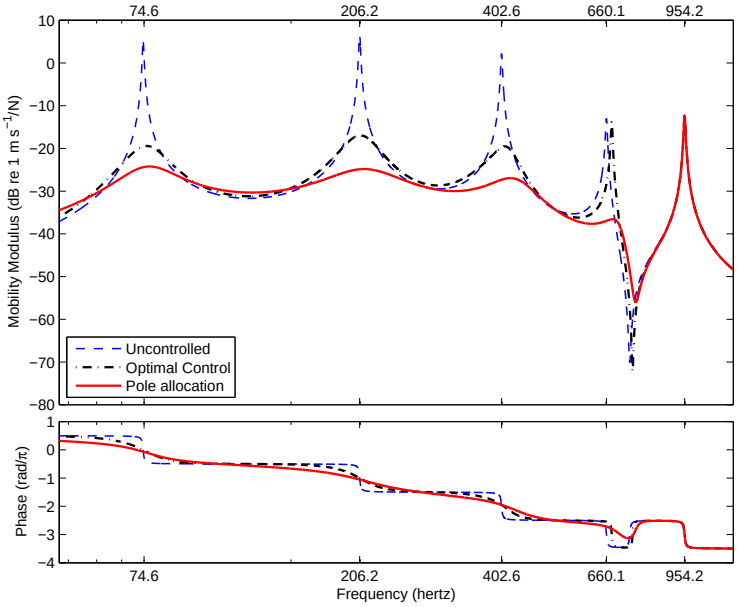


Figure III.6: Mobility of the uncontrolled beam and the comparison with proposed control for the active approach implemented on the first three modes.

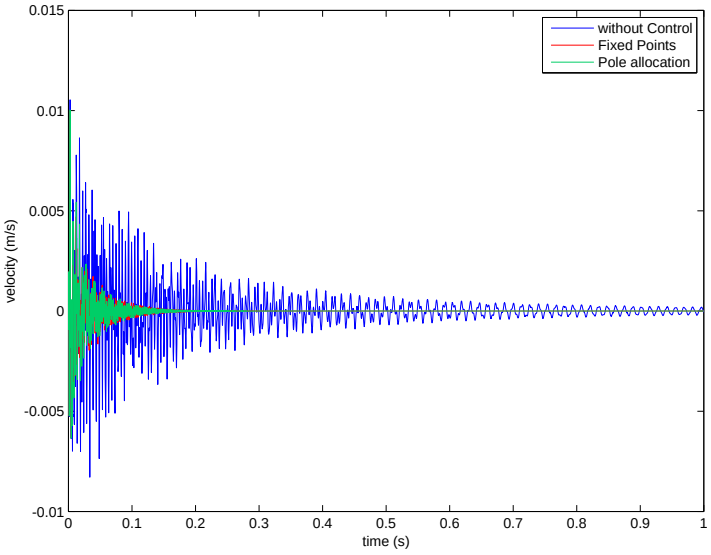


Figure III.7: Impulse response of the uncontrolled beam and the comparison with proposed control for the passive approach in parallel configuration.

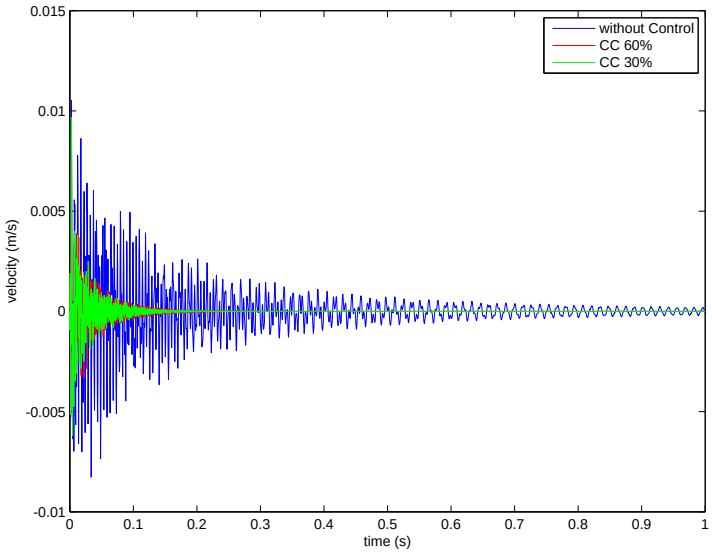


Figure III.8: Impulse response of the uncontrolled beam and the comparison with proposed control for the hybrid approach with capacitance compensation (CC) of 30% and 60%.

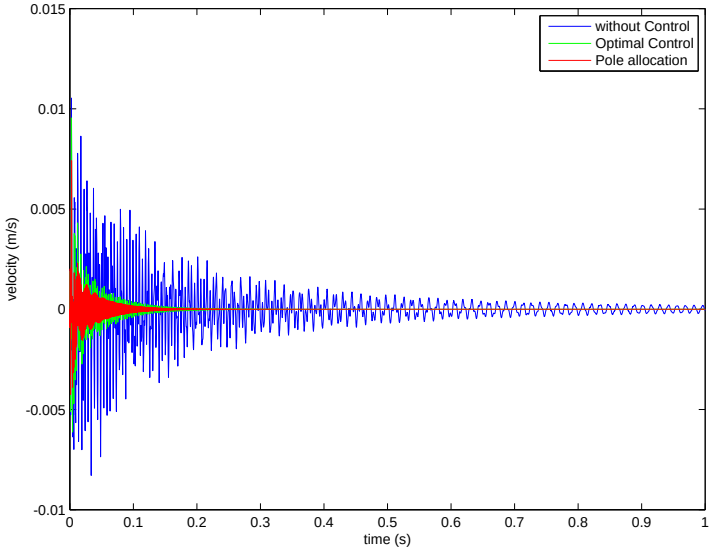


Figure III.9: Impulse response of the uncontrolled beam and the comparison with proposed control for the active approach.

III.2 Fully Clamped Plate Case Study

The plate investigated in this case study is a rectangular fully clamped aluminium plate with multiple piezoelectric transducer pairs in bending configuration according to figure III.10. In order to control five mechanical modes, the proposed control uses five piezoelectric transducer pairs. Let the five transducer pairs be identical, consisting of thin rectangular laminae thickness polarised, piezoelectric ceramic, covered by metal electrodes with negligible mechanical properties. The model used below is based on that developed in chapter II. The domain $\mathscr{A} = [0, L_1] \times [0, L_2]$ denotes the region occupied by the plate and $\mathscr{A}_k = [x_{1,i}^{(k)}, x_{1,f}^{(k)}] \times [x_{2,i}^{(k)}, x_{2,f}^{(k)}]$ is the region occupied by the k-th transducer pair. Tables III.3 and III.1 report the material and geometric characteristics of the plate and of the piezoelectric elements.

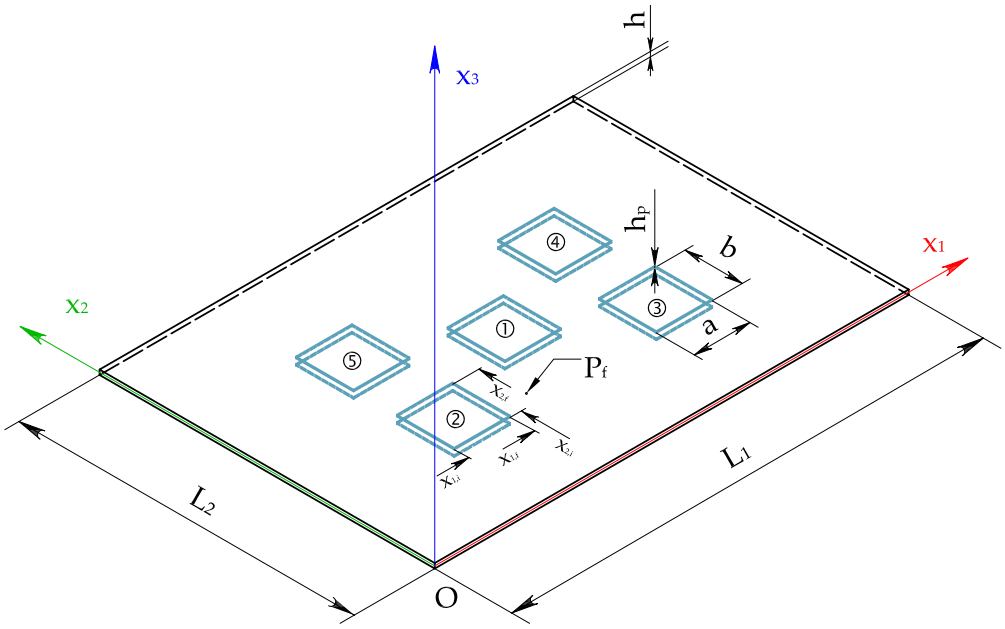


Figure III.10: Plate with five piezoelectric transducer pairs in bending configuration.

III.2.1 Piezoelectric Transducer Allocation

This section presents an example that illustrates the optimisation problem of the transducer allocation on the plate using the procedure outlined in section I.2.2 based on the index (I.44), which reduces the error ϵ of a $\mathscr{G}$

Table III.3: Geometric and material characteristics of the plate.

	symbol	value	unit
Length	L_1	0.297	m
Width	L_2	0.210	m
Thickness	h	0.001	m
Density mass	ρ	2700	kg m^{-3}
Young modulus	Y	69×10^9	Pa
Poisson's ratio	ν	0.33	

non-diagonal. To set up the problem, one piezoelectric pair out of five, $\mathscr{A}_1$, is placed right in the middle of the plate a priori. The other four piezoelectric pairs are located to form a symmetric pattern as shown in figure III.10. Lengths, a, and widths, b, of the piezoelectric laminae are fixed equal and comparable with wave lengths of the modes of interest. Thus, the edges of the piezoelectric elements are 3.6×10^{-2} m, whilst the thickness h_p is equal to 2.67×10^{-4} m. These choices allow to make a parameterisation of the transducer arrangement by means of two scalar parameters $[\alpha_1,\ \alpha_2]$ which represent the coordinates of left lower corner, $[x_{1,i}^{(2)},\ x_{2,i}^{(2)}]$, of the piezoelectric pair $\mathscr{A}_2$. Holding their symmetry the positions of piezoelectric pairs from $\mathscr{A}_2$ to $\mathscr{A}_5$ are dependent only on the position of $\mathscr{A}_2$. Thus, the goal in this example is to find a set of values $[\tilde{\alpha}_1, \tilde{\alpha}_2]$ that maximise the index (I.44), that is

$$\mu(\Gamma) = \|D_{\Gamma\Gamma^{\mathrm{T}}}\| - \frac{1}{2}\|N_{\Gamma\Gamma^{\mathrm{T}}}\| \tag{III.11}$$

as parameters $[\alpha_1,\ \alpha_2]$, subject to the constraint to avoid overlap between transducers, vary in a quarter of the plate. Remind that the matrix Γ is related to the distribution of the piezoelectric transducer pairs, indeed, it can write $\Gamma = \Gamma(\alpha_1,\ \alpha_2)$.

To solve this two-dimensional problem, it is necessary to calculate the coupling matrix, Γ, which requires the computation of the mode shapes and the natural frequencies of the plate under short circuit condition. The considered case study has not an eigenvalue problem that leads to closed-form solutions, owing to boundary conditions as well as mass and stiffness distributions that are non-uniform and non-linear for piezoelectric pairs. Thus, it

is opportune to seek approximate solutions as for mode shapes and natural frequencies. For this reason, the entries of Γ have been computed, according to the formula (II.49), using the mode shapes and natural frequencies of the plate provided by finite element model realised with Ansis. The frame of the system is modelled with a uniform mesh consisting in 75×53 shell elements for the plate and $9\times9\times1$ solid elements for each piezoelectric patch. The plate is constrained at its border where displacements and rotations are zero, and the piezoelectric electrodes are short-circuited that is their reference potential is imposed equal to zero.

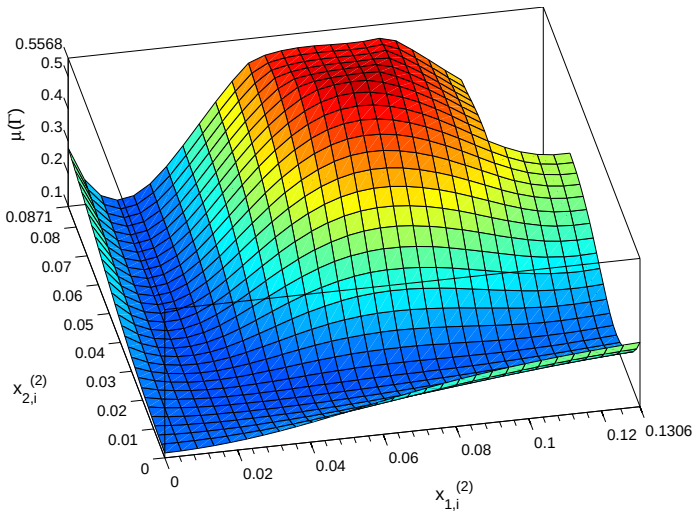


Figure III.11: Piezoelectric placement objective function $\mu(\Gamma)$ for a quarter of plate.

This optimisation is iterative and requires the computation of the whole finite element model at each step, thus it is very expensive. For this reason, a roughly analysis is previously performed using mode shapes and natural frequencies of the plate without transducers. This analysis based on the procedure described in appendix A.3, permits to make faster the following finite element analysis using as initial guess for the parameter vector $[\alpha_1,\ \alpha_2]$ the optimal parameter vector obtained in this preceding step, see figure III.11. Thus, the starting guess is initialised to $[6.22,\ 5.50]\times10^{-2}$ and the optimal parameter vector obtained with the finite element model is

$$[\tilde{\alpha}_1,\ \tilde{\alpha}_2] = [6.76,\ 5.54]\times10^{-2} \tag{III.12}$$

which corresponds to the position of the piezoelectric elements represented in figure III.10. Note that the finite element analysis yields little different result from the preliminary one, so it could be safely ignored.

III.2.2 Numerical Results and Comparisons

The unit-frequency normalised coupling matrix Γ for the plate is given by

$$\Gamma = \begin{bmatrix} 0.196 & 0.0849 & 0.0849 & 0.0849 & 0.0849 \\ 0 & 0.151 & -0.151 & -0.151 & 0.151 \\ 0 & 0.149 & 0.149 & -0.149 & -0.149 \\ 0.212 & -0.121 & -0.121 & -0.121 & -0.121 \\ 0 & 0.198 & -0.198 & 0.198 & -0.198 \end{bmatrix} \tag{III.13}$$

the transformation matrix U is

$$U = \begin{bmatrix} 0.754 & 0 & 0 & 0.657 & 0 \\ 0.328 & 0.5 & 0.5 & -0.377 & 0.5 \\ 0.328 & -0.5 & 0.5 & -0.377 & -0.5 \\ 0.328 & -0.5 & -0.5 & -0.377 & 0.5 \\ 0.328 & 0.5 & -0.5 & -0.377 & -0.5 \end{bmatrix} \tag{III.14}$$

and the coupling matrix in the coordinates $\chi_k(t)$ becomes

$$\mathcal{G} = \begin{bmatrix} 0.250 & 0 & 0 & 9.75 \times 10^{-4} & 0 \\ 0 & 0.302 & 0 & 0 & 0 \\ 0 & 0 & 0.297 & 0 & 0 \\ 7.84 \times 10^{-4} & 0 & 0 & 0.323 & 0 \\ 0 & 0 & 0 & 0 & 0.396 \end{bmatrix} \tag{III.15}$$

In this case the second step of optimisation introduced in section I.2.2 has been performed and the rows of Γ are all mutually perpendicular, although the angle ϑ_{14} between the first row and the fourth row of Γ is a slightly different, it is in fact 0.498π.

To validate damping performances of the proposed control, a Simulink model with the same layout used for the beam is employed. In detail, the plate is excited by an impulse with a frequency spectrum over a frequency range from near zero to f_{max} that is 1000 Hz. The mobility is considered between the transversal force applied at the point P_f shown in figure III.10, and

the transversal velocity calculated at the same point. The position of the point P_f is chosen to excite and observe all modes in the frequency range of interest by avoiding nodal lines as more as possible. The impulse has a peak value F_0 of 1 N and a time duration τ of 3.33×10^{-4} s so that $1/\tau = 1.5\ f_{max}$. The time of simulation T is equal to 10.49 s, thus the frequency resolution Δf is 0.1 Hz. The simulation step size is set equal to $1/12500$ s to avoid computation errors. To take into account the spillover problem the system model consists of ten mechanical modes instead of five. Figures from III.12 to III.14 display the point mobilities of the uncontrolled plate with short-circuited piezoelectric elements and the controlled plate with the optimal shunting networks outlined in sections I.6, I.7 and I.8. It is shown that at the first five eigenfrequencies the controlled plate mobility decreases of about 25 dB for the passive controllers and even 26 dB for active controllers. The proposed control is equally effective on all modes acting simultaneously on five picks. Similar considerations to the ones presented for the beam can be made about the plate.

◇ ◇ ◇

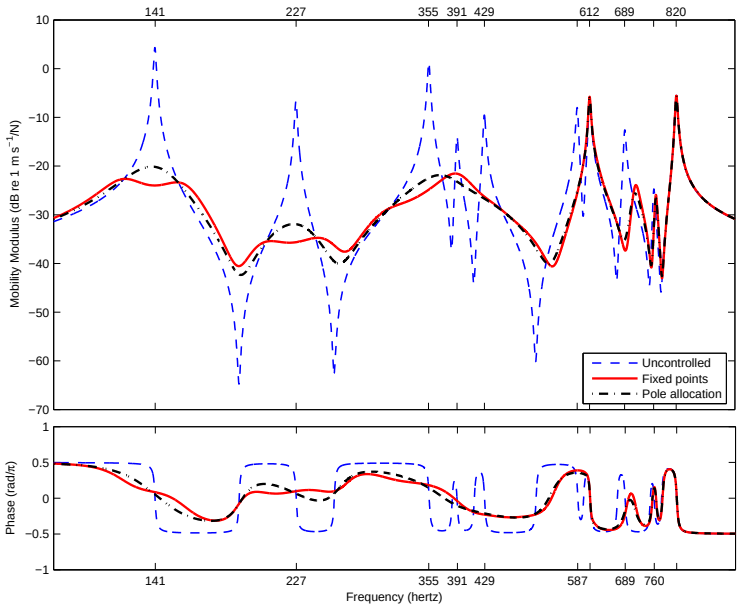


Figure III.12: Mobility of the uncontrolled plate and the comparison with proposed control for the passive approach in parallel configuration implemented on the first five modes.

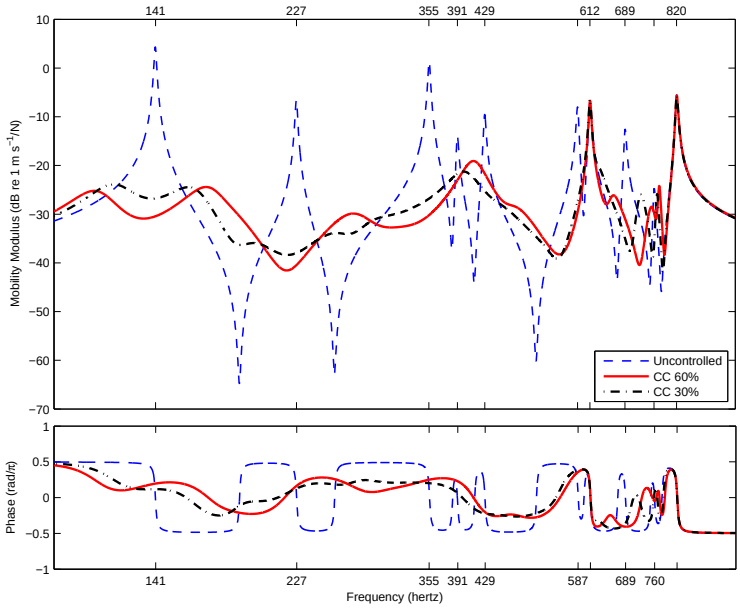


Figure III.13: Mobility of the uncontrolled plate and the comparison with proposed control for the hybrid approach with capacitance compensation (CC) of 30% and 60% applied on the first five modes.

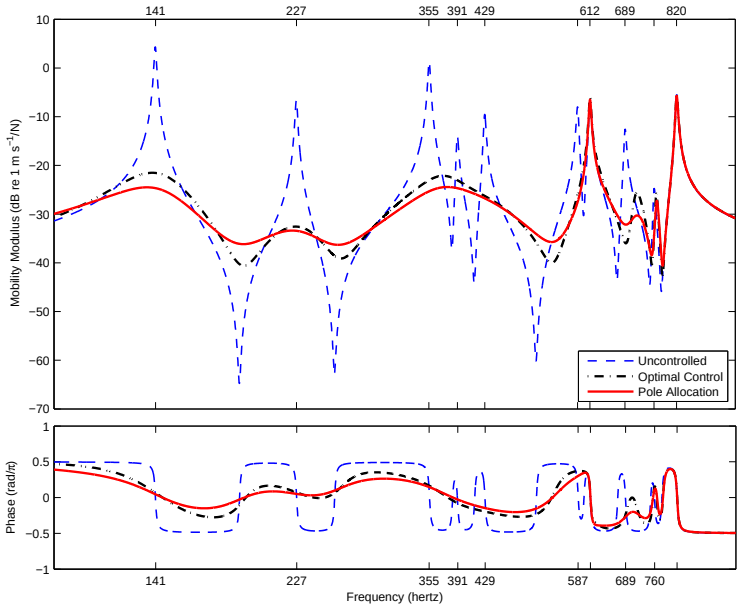


Figure III.14: Mobility of the uncontrolled plate and the comparison with proposed control for the active approach implemented on the first five modes.

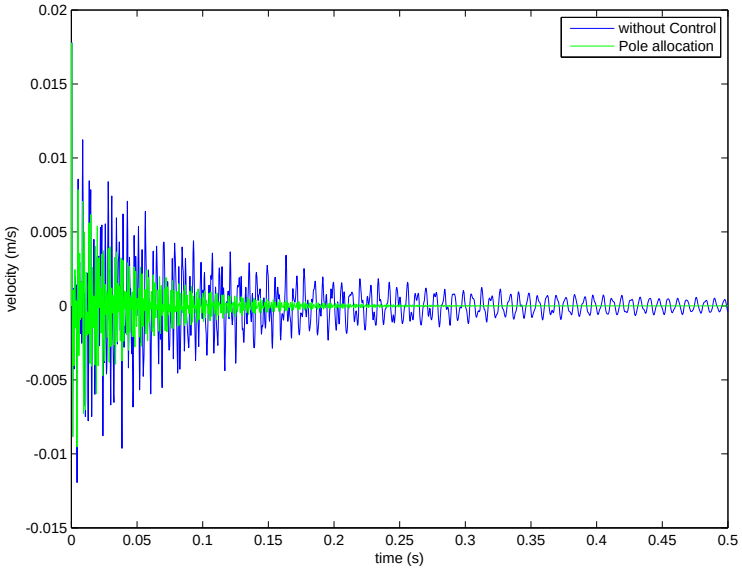


Figure III.15: Impulse response of the uncontrolled plate and the comparison with proposed control for the passive approach in parallel configuration.

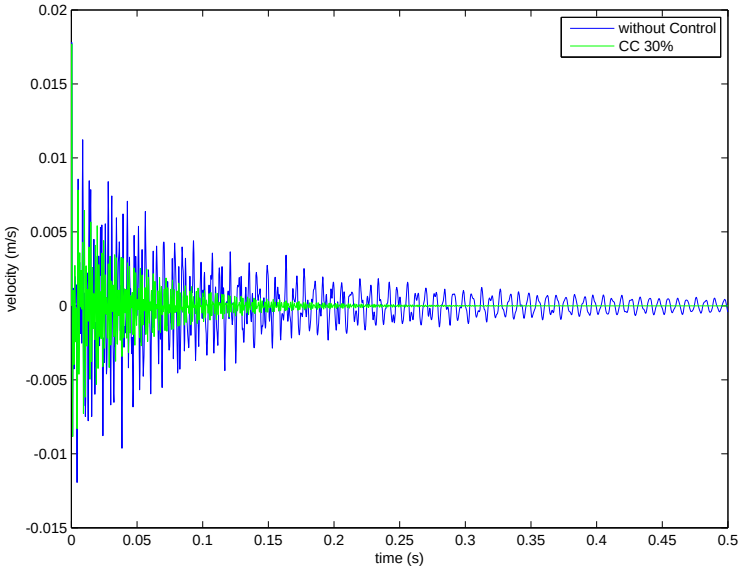


Figure III.16: Impulse response of the uncontrolled plate and the comparison with proposed control for the hybrid approach with capacitance compensation (CC) of 30% and 60%.

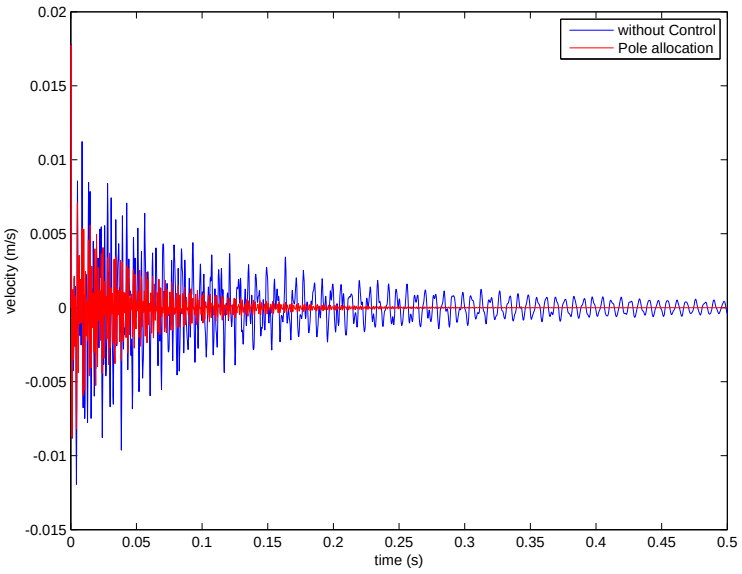


Figure III.17: Impulse response of the uncontrolled plate and the comparison with proposed control for the active approach.

Several authors extended the technique of the single shunt to damp multiple mechanical modes [Hollkamp, 1994; Wu, 1998; Behrens et al., 2003]. They shunt a single piezoelectric element with a circuit including several resistors, capacitors, and inductors, to obtain a multi-resonant behaviour.

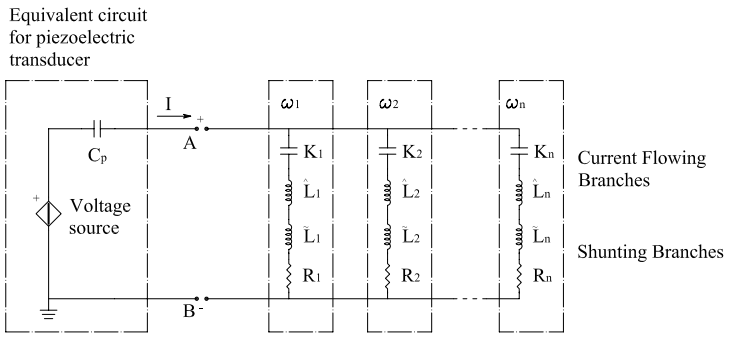


Figure III.18: A single shunt for multi-modal current flowing control.

Among the different solutions, the current flowing shunt circuit proposed in [Behrens et al., 2003] seems the most efficient thanks to the modular cir-

cuital pattern and the reduced number of elements. The shunt has as many parallel branches as the number of mechanical modes to be damped. Each branch is a series composed of two inductors $\hat{L}_i$, $\tilde{L}_i$, a capacitor K_i and a resistor R_i. The series $\hat{L}_i K_i$ behaves as a passband filter centred at the eigenfrequency ω_i of the i-th mechanical mode; in that frequency interval, the series $\tilde{L}_i R_i$ operates in a similar way as in a resistive-inductive single resonant circuit. Ideally, with this configuration each branch controls a single mechanical mode, without affecting the others. With this assumption, the optimal inductance for i-th mode would have the following expression

$$L_i = \hat{L}_i + \tilde{L}_i = \frac{1}{{\omega_i}^2}\left(\frac{1}{K_i} + \frac{1}{C_h}\right) \tag{III.16}$$

where C_h is the capacitance of the piezoelectric transducer. To account for the undesired cross influence of the branches on the mechanical modes to be controlled, a further numerical fine-tuning is applied. Also, the additional capacitances K_i's are set approximately to 10% of the piezoelectric capacitance C_h, considering that additional capacitances worsen the electro-mechanical coupling and smaller capacitances requires larger inductances. Finally, the

Table III.4: Parameters of the five current flowing circuits identical used for comparison.

		I branch	II branch	III branch	IV branch	V branch
L_i	H	89.61	33.98	13.97	11.14	8.84
R_i	kΩ	4.5	3.5	1.7	1.5	1.5
K_i	nF	14.6	14.6	14.6	14.6	14.6

performance of the proposed shunting controls is compared with this multimodal shunting technique. To make this method comparable with the proposed shunting technique, the single-shunt approach is generalised for the use of multiple piezoelectric patches. Consequently, the five piezoelectric elements are shunted with five identical multi-resonant current flowing circuits. Table III.4 reports the corresponding numerical values for the circuital components in figure III.18. The inductances of each shunt are chosen according to (III.16), with a further numerical fine-tuning. The resistances R_i's are opti-

mised numerically to minimise the maximum amplitude of the plate mobility function around each natural frequency.

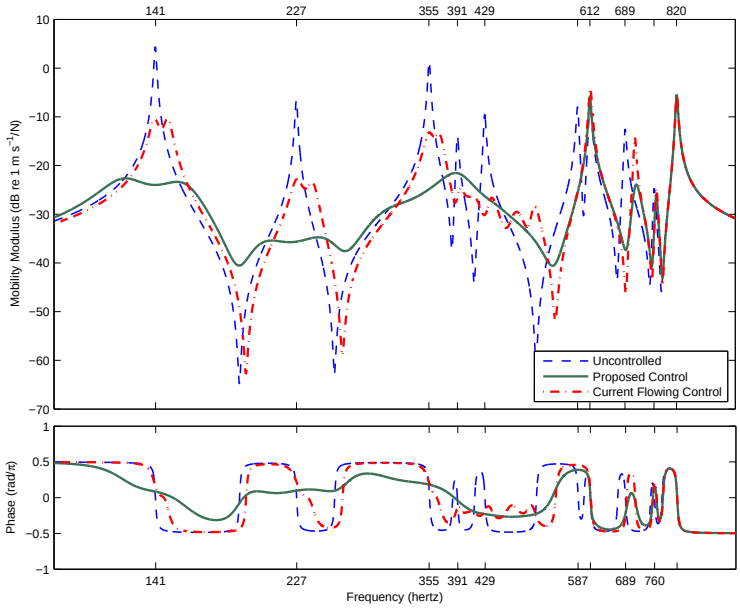


Figure III.19: Mobility of the uncontrolled plate and the comparison between the proposed control for passive approach in parallel configuration and the current flowing control on the first five modes.

Figure III.19 shows that with this approach the maximum reduction in the magnitude of mobility is of about 15 dB instead of 25 dB. The main feature of the proposed technique is to exploit the coupling of the different piezoelectric transducers in an optimal way, by the maximisation of the transfer power and improvement of the energy flux efficiency between the mechanical and electrical system. Furthermore, the proposed approach does not employ additional capacitances which reduce the efficiency of electromechanical coupling.

CHAPTER IV

Laboratory Experiments

> If we were not ignorant there would be no probability, there could only be certainty. But our ignorance cannot be absolute, for then there would be no longer any probability at all. Thus the problems of probability may be classed according to the greater or less depth of our ignorance.
>
> HENRI POINCARÉ (1854–1912)
> *French physicist*

EXPERIMENTAL results are presented in this chapter for a thin beam with both ends clamped to illustrate the effectiveness of proposed controls. First, a system parameter identification is accomplished for obtaining an adequate understanding —both mechanical and electrical— of the laboratory prototype through a multi-degree-of-freedom curve-fitting. Comparison between numerical simulations and experimental measurements is shown. Finally, the proposed control is tested and proved to be reliable.

IV.1 Experimental Set Up

The test system is a uniform aluminium beam with rectangular cross section and experimentally clamped boundary conditions at both ends. Great attention has been devoted to fix end points of the beam to ground, in order to ensure that the whole assembly gives repeatable results. One of the tackled

problems is the change in stiffness due to axial load caused by environment temperature variations. To avoid this problem the axial displacement at one end is allowed. Three pairs of piezoelectric ceramic rectangular patches are bonded symmetrically to either side of the beam surface. Each pair is connected in parallel. They are used as actuator to provide disturbing force, as sensor and also as shunting layer. Experimental structure is displayed in figure IV.1 and is the same described in chapter III.

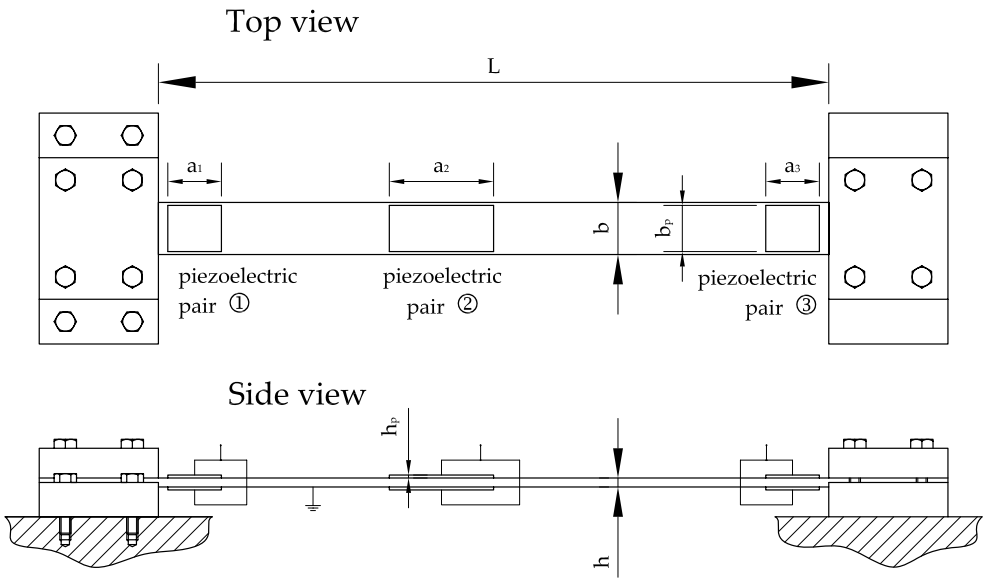


Figure IV.1: Experimental beam.

IV.1.1 Mobility Estimations

To estimate mobilities of interest, the beam is excited by one piezoelectric actuator with a random band-limited signal so as to excite four bending modes with a frequency spectrum covering a range from near zero to 700 Hz. A power amplifier to drive the piezoelectric actuator with voltage is used. The National Instruments PCI-6711 board is used as an arbitrary waveform generator. The analog outputs of this board have a resolution of 12 bits with an update rate of 1 megasample per second, a maximum voltage range of $\pm 10\,\mathrm{V}$ and a range accuracy of 8.62 mV. It is well known that the piezoelectric material presents a non-linear behaviour when the level of excitation is very high. To check for non-linearity a particular mobility measurement has

been repeated a number of times using different levels and types of excitation. Thus, a level of excitation equal to 1 V has been chosen to avoid nonlinearity. A Polytec scanning laser vibrometer PSV-400 provides the output at the point with a distance 0.33 m from the left end of the beam. The National Instruments PCI-4552 board is the data acquisition device that have a resolution of 16 bits with a frequency accuracy of ± 25 ppm and sampling rates from 5 to 204.8 kilosample per second in increments of 190.735 microsample per second. The analysis is performed with a frequency resolution of about 195 mHz and 64 averages. The sample frequency is 3.2 kHz to avoid aliasing. The nominal estimate of the mobility function magnitudes, $\left|\hat{H}(f)\right|$, and phases, $\hat{\alpha}(f)$, are shown in figures IV.2-IV.4 using each of the three piezoelectric transducers as actuator. The coherence data advise that the estimate mobility magnitudes and phases involves random or bias errors. However, it should be noted that the coherence is near unity at most frequencies and there are significant notches also at frequencies that coincide with notches in mobility magnitudes as it is expected.

In the figures, it is shown also the uncertainty regions at all frequencies. Assuming 3 standard deviations of the normal distribution, there is a 99.6% probability that the true response is within the uncertainty band. The random error is directly related to the coherence function $\hat{\gamma}^2_{xy}(f)$ and the number of averages n_d used in calculations of the spectral density estimates. The normalised random error of the mobility magnitude $\left|\hat{H}(f)\right|$ and the standard deviation of the mobility phase $\hat{\alpha}(f)$, in accordance with [Bendat and Piersol, 1980], are given by

$$\varepsilon\left[\left|\hat{H}(f)\right|\right] = \frac{\sqrt{1-\hat{\gamma}^2_{xy}(f)}}{\left|\hat{\gamma}_{xy}(f)\right|\sqrt{2n_d}} \qquad \sigma[\hat{\alpha}(f)] = \arcsin\{\varepsilon\left[\left|\hat{H}(f)\right|\right]\} \tag{IV.1}$$

Specifically, the magnitude $|H(f)|$ and the phase $\alpha(f)$ can be expressed with the 99.6% confidence interval by

$$\begin{aligned} |H(f)| &= \left|\hat{H}(f)\right|\left(1 \pm 3\,\varepsilon\left[\left|\hat{H}(f)\right|\right]\right) \\ \alpha(f) &= \hat{\alpha}(f) \pm 3\,\sigma[\hat{\alpha}(f)] \end{aligned} \tag{IV.2}$$

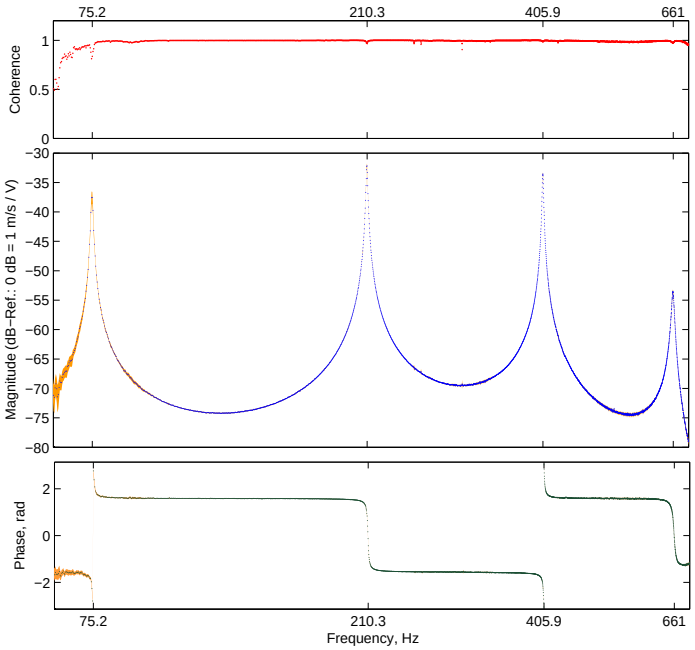


Figure IV.2: Mobility function for beam experiment using as actuator the first piezoelectric double element.

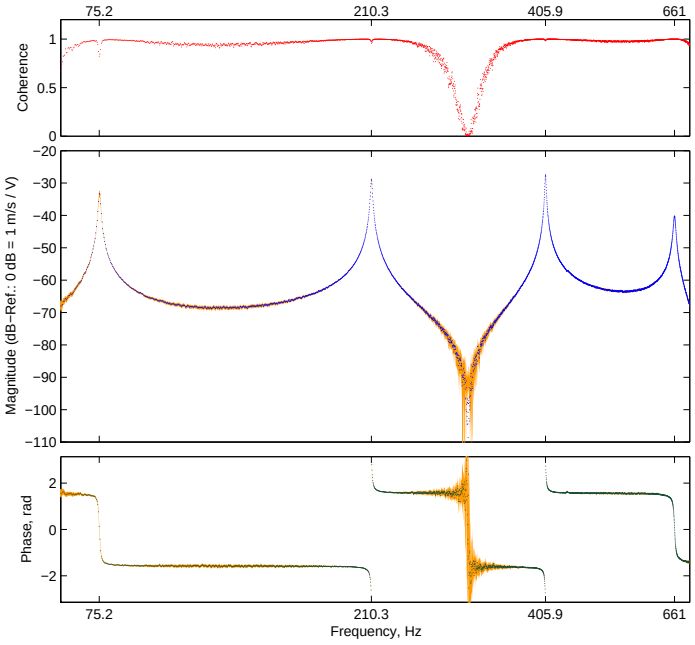


Figure IV.3: Mobility function for beam experiment using as actuator the second piezoelectric double element.

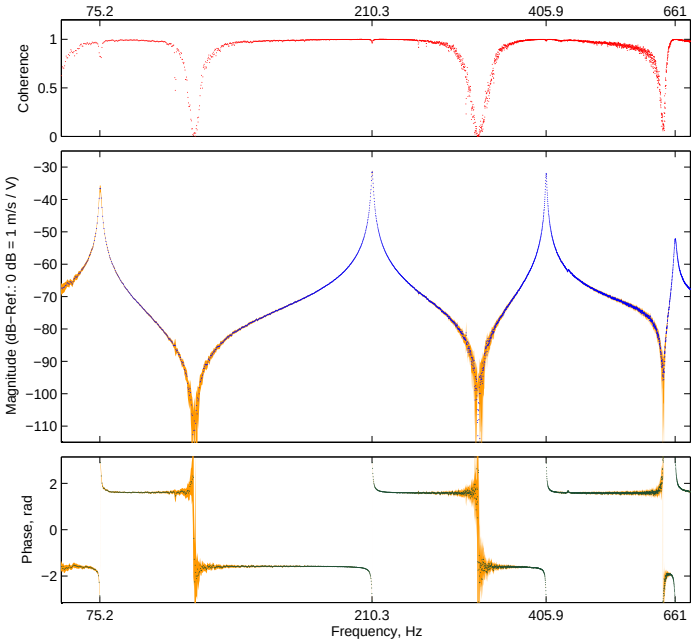


Figure IV.4: Mobility function for beam experiment using as actuator the third piezoelectric double element.

IV.2 System Identification

IV.2.1 Mechanical Parameters

The mobility functions estimated are collected as magnitude and phase vectors depending on the frequency. Denoting the generic mobility measured data with a complex vector $\hat{H}(\Omega_l)$ at each circular frequency Ω_l of the measure, modal parameters, that is resonance frequencies, damping ratios and modal constants, are extracted from the actual measured data by performing multi-degree of freedom curve fits. To this end, consider the following mobility evaluated at the same frequencies

$$H(\Omega_l) = \sum_{r=1}^{4} \frac{i\,\Omega_l\, P_{rh} W_r(x_{1,m})}{\omega_r^2 - \Omega_l^2 + 2\,\xi_r \omega_r i\,\Omega_l} + \frac{i\,\Omega_l}{K_{Res}} \tag{IV.3}$$

where the quantity K_{Res} is the residual stiffness due to the high frequency modes, see [Ewins, 1984]. The coefficients $P_{rh}W_r(x_{1,m})$, ω_r, ξ_r, K_{Res} are all to be determined as the index r varies over the modes of interest taking into account the h-th piezoelectric actuator. The modal constant $P_{rh}W_r(x_{1,m})$ is the product of the coupling matrix entry P_{rh} and the mode shape of the beam

evaluated at the measure point $x_{1,m}$. This non-linear curve-fitting problem is solved in least-squares sense defining the cost function

$$E = \sum_{l=1}^{N} w_l(\Omega_l) \left| \left(\hat{H}(\Omega_l) - H(\Omega_l) \right)^2 \right| \tag{IV.4}$$

in which $w_l(\Omega_l)$ is a weighting factor, and N is the number of the data points. The curve fit process has to determine the values of the unknown modal parameters such that the error E is minimised.

After performing the curve fits, to evaluate the goodness of fit the R^2 indicator has been examined separately for the magnitude and phase of mobility functions. Indeed, R^2 can take on any value less than or equal to one, with a value closer to one indicating a better fit. In particular, the R^2 is adjusted based on the residual degrees of freedom, V, defined as the number of data values N minus the number of fitted coefficients F. Therefore, the degrees of freedom adjusted R^2 is defined as

$$R^2 = 1 - \frac{SSE\,(N-1)}{SST\,(V)} \tag{IV.5}$$

in which SSE is the sum of squares due to error and represents the total deviation from the fit to the response values whilst SST is also called the sum of squares about the mean and represents the total deviation from the mean to the response values.

During the estimation process, uncertainty information is taken into account. The coherence function, $\hat{\gamma}^2_{xy}(\Omega_l)$, is chosen as weighting function w_l. In figures IV.5-IV.10, it is shown the comparison between the measured mobility functions and the regenerated curves obtained by the extracted modal parameters. The obtained modal parameters of interest are summarised in tables IV.2 and IV.1. In table IV.2 are presented also the resonance frequencies obtained by the finite element analysis for comparing experimental and numerical results.

Table IV.1: Damping ratio of the bending modes.

mode 1	mode 2	mode 3	mode 4
$(3.48 \pm 0.04)10^{-3}$	$(2.97 \pm 0.06)10^{-3}$	$(2.30 \pm 0.06)10^{-3}$	$(4.2 \pm 0.1)10^{-3}$

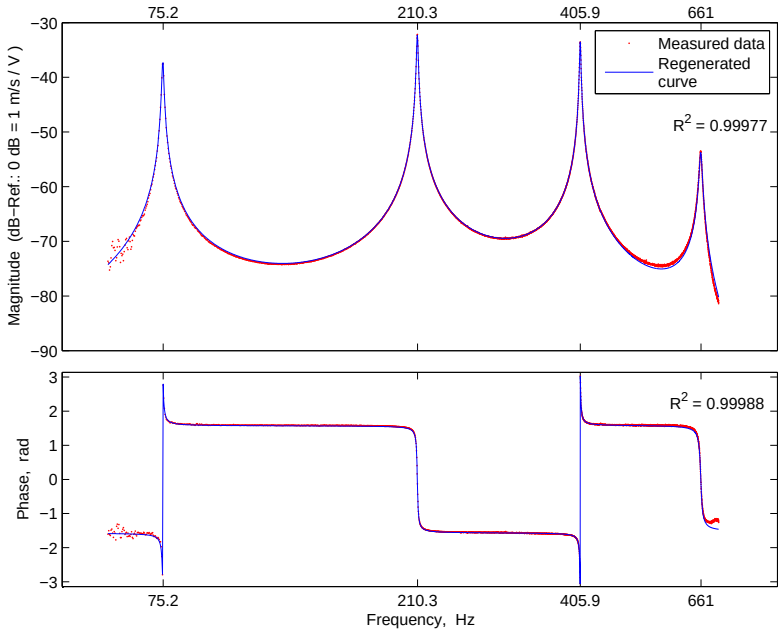


Figure IV.5: Comparison of measured mobility with the first piezoelectric actuator and curve fit.

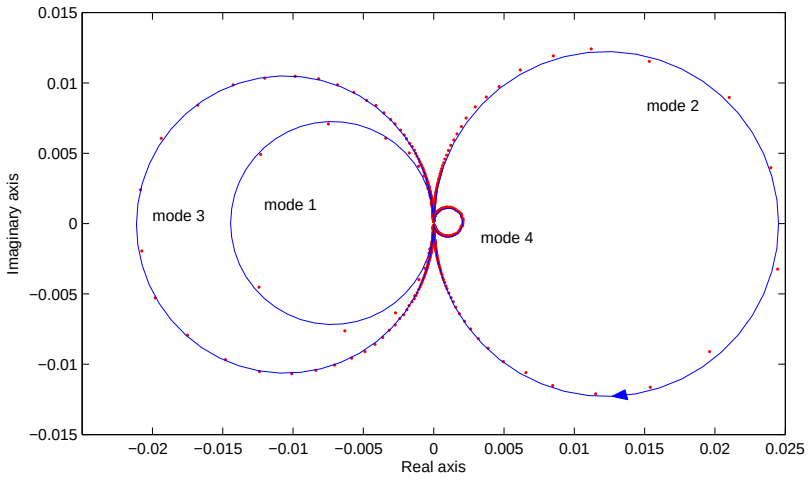


Figure IV.6: Nyquist plot of mobility with the first piezoelectric actuator and curve fit.

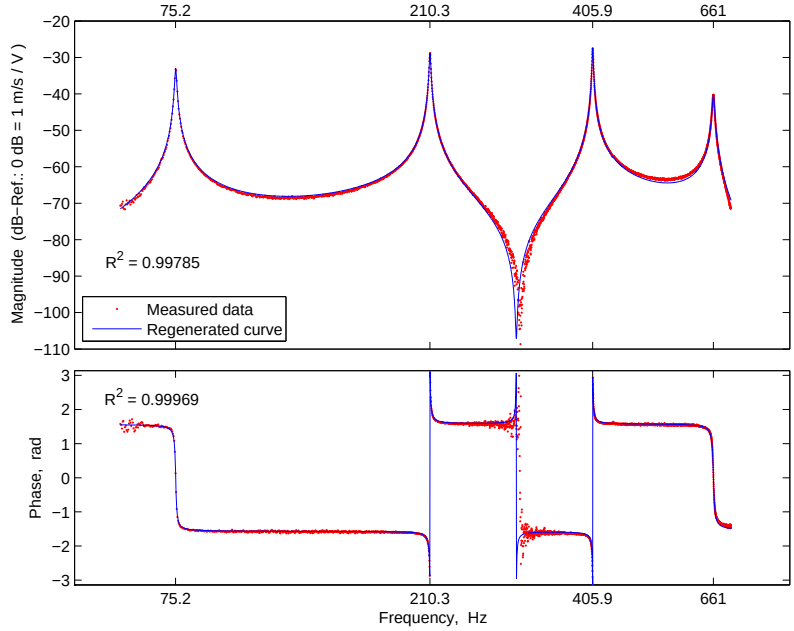


Figure IV.7: Comparison of measured mobility with the second piezoelectric actuator and curve fit.

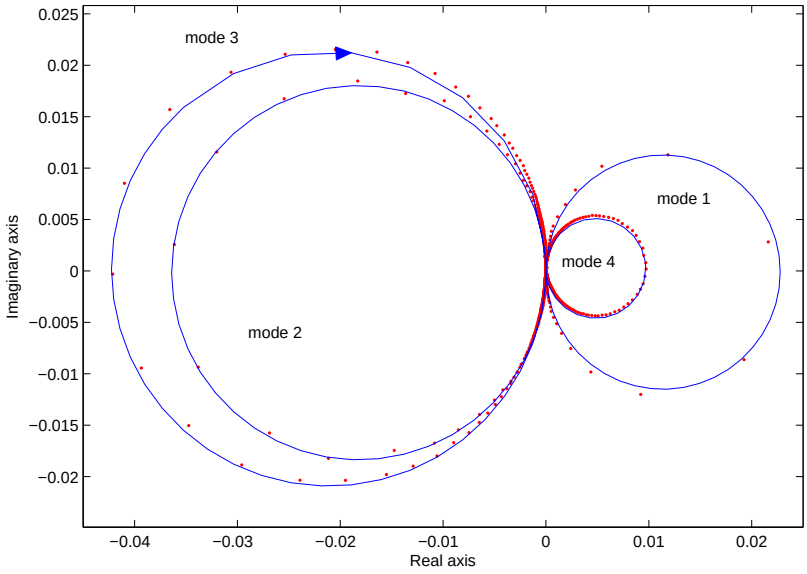


Figure IV.8: Nyquist plot of mobility with the second piezoelectric actuator and curve fit.

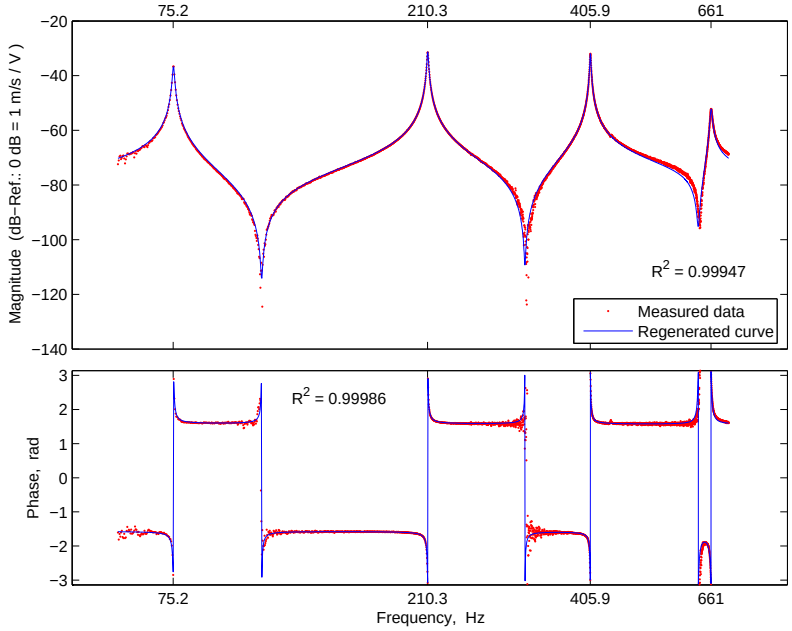


Figure IV.9: Comparison of measured mobility with the third piezoelectric actuator and curve fit.

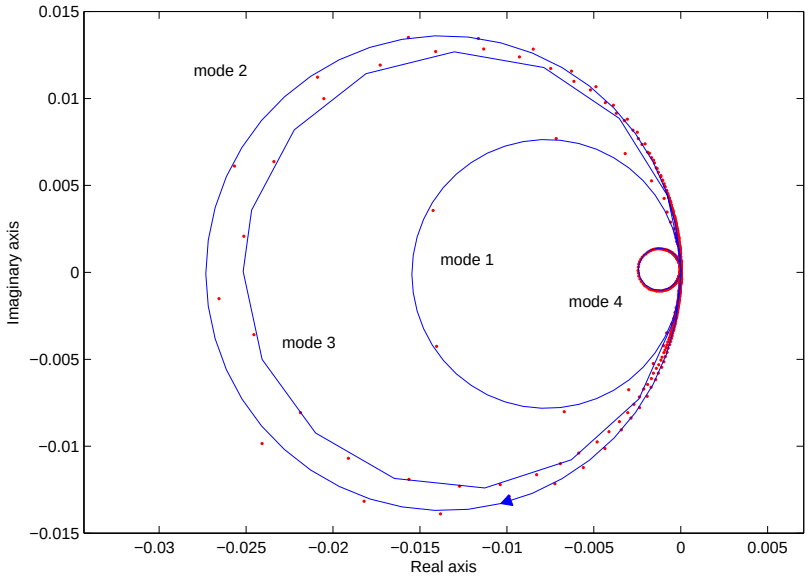


Figure IV.10: Nyquist plot of mobility with the third piezoelectric actuator and curve fit.

Table IV.2: Resonance frequencies of the beam.

	experimental (Hz)	numerical (Hz)	discrepancy (%)
mode 1	75.2 ± 0.2	74.6	0.8
mode 2	210.3 ± 0.3	209.6	0.3
mode 3	405.9 ± 0.2	405.6	0.08
mode 4	661.0 ± 0.7	662.4	0.2

IV.2.2 Piezoelectric Parameters

Piezoelectric parameters can be extracted from electric impedances of the piezoelectric transducers by performing multi-degree of freedom curve fits. The piezoelectric impedances to be measured is obtained by applying a broad-band random excitation current over a frequency range near zero to 700 Hz and then measuring the resulting voltage response on the same piezoelectric transducer. This type of test requires a current source which is voltage driven. By using a Fourier analysis, the electric impedance, $\hat{Z}_h(\Omega_l)$, can be estimated as a complex vector for the h-th piezoelectric transducer at each circular frequency Ω_l of the measure. The analysis is performed with a frequency resolution of 0.1 Hz and 15 averages. Piezoelectric parameters, that is capacitances and coupling coefficients, can be obtained directly by fitting the actual measured data with the following impedance

$$Z_h(\Omega_l) = \frac{G_m}{i\,\Omega_l}\left(C_h + \frac{1}{i\,\Omega_l\,R_N} + \sum_{r=1}^{4}\frac{P_{rh}^2}{\omega_r^2 - \Omega_l^2 + 2\,\xi_r\omega_r i\,\Omega_l}\right)^{-1} \tag{IV.6}$$

where G_m, equal to 0.0065 S, is the transconductance[1] of the voltage controlled current source and R_N is its Norton's equivalent resistance. The coefficients P_{rh}^2 and C_h are all to be determined. This non-linear curve-fitting problem is solved in least-squares sense as made for the mobility functions. The normalised piezoelectric coupling coefficients are computed by the following relationship

$$\Gamma_{jh} = \frac{P_{jh}}{\omega_j\sqrt{C_h}} \tag{IV.7}$$

[1]Transconductance, also known as mutual conductance, is the ratio of the current at the output port and the voltage at the input ports of certain electronic components.

The obtained piezoelectric parameters are summarised in tables IV.3 and IV.4. In figures IV.11-IV.16, it is shown the comparison between the measured piezoelectric impedances and the regenerated curves obtained by the extracted piezoelectric parameters.

Table IV.3: Curve-fitting estimated piezoelectric coupling coefficients.

	piezo 1	piezo 2	piezo 3
mode 1	-0.093 ± 0.005	0.111 ± 0.005	-0.100 ± 0.003
mode 2	0.075 ± 0.002	-0.084 ± 0.003	-0.090 ± 0.002
mode 3	-0.063 ± 0.001	-0.084 ± 0.002	-0.073 ± 0.002
mode 4	-0.042 ± 0.001	-0.123 ± 0.002	0.046 ± 0.001

Table IV.4: Curve-fitting estimated piezoelectric capacitances (nF).

pair 1	pair 2	pair 3
100.4 ± 0.5	204 ± 2	96.6 ± 0.4

◇ ◇ ◇

Alternatively it is possible to perform an identification procedure based on one-mode approximation to measure the piezoelectric coupling parameters exploiting the classical results based on the inductive-resistive single resonant piezoelectric shunt circuit and the fixed point theory. For further details the reader is referred to the paper [Porfiri et al., 2007]. The beam is excited through one piezoelectric transducer by a voltage source using a chirp signal of amplitude 1 V which rises linearly in frequency nearly to the mechanical eigenfrequency of interest for a time of 10 s. A second two-element piezoelectric transducer is used as sensor, to obtain the frequency response function of the system. The last piezoelectric transducer is shunted with a series RL tuned circuit where the inductor is a variable device op-amp based. According with the fixed point theory, the coupling parameters are calculated

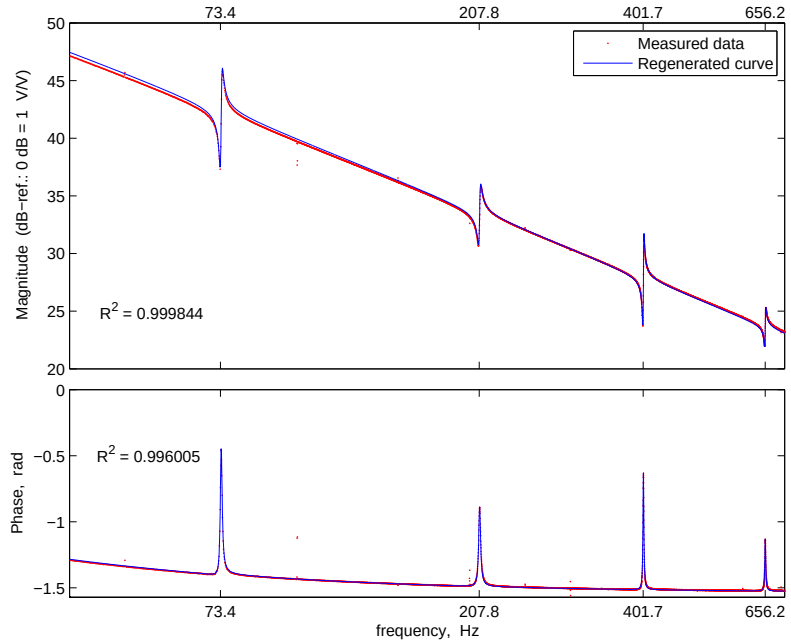


Figure IV.11: Comparison of measured electric impedance of the first piezoelectric transducer and curve fit.

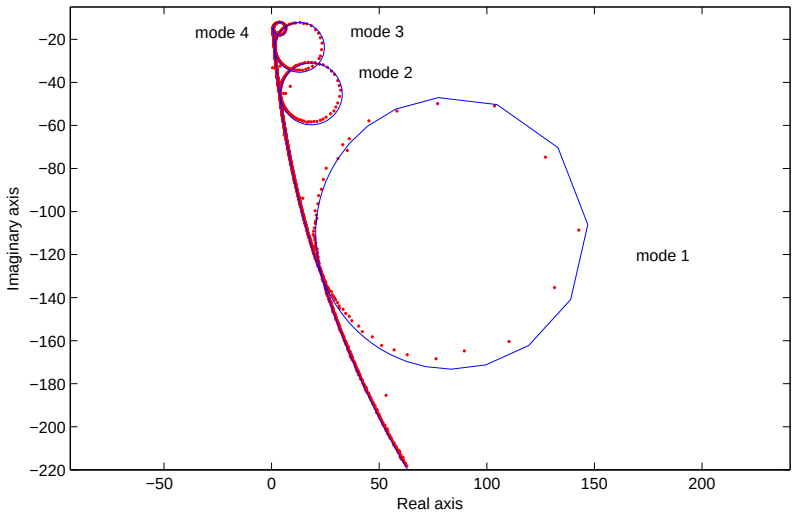


Figure IV.12: Nyquist plot of impedance of the first piezoelectric transducer and curve fit.

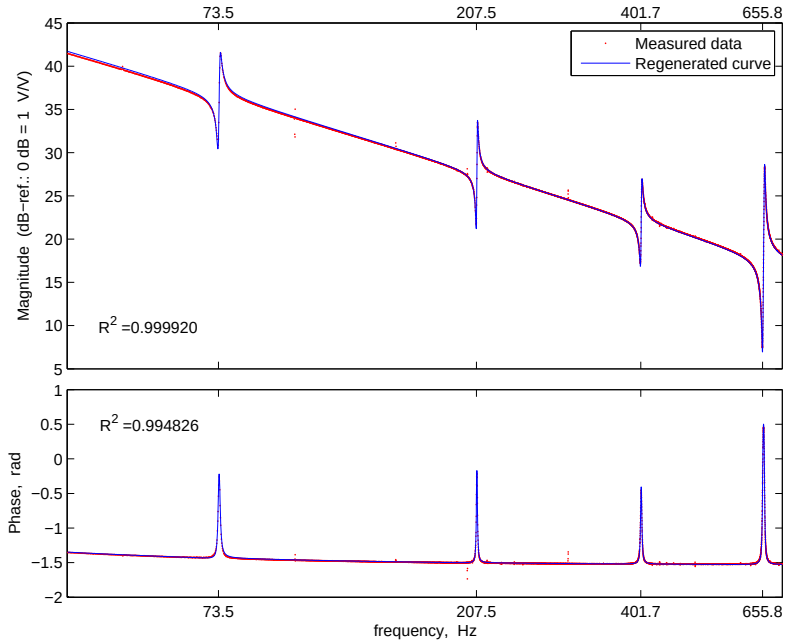


Figure IV.13: Comparison of measured electric impedance of the second piezoelectric transducer and curve fit.

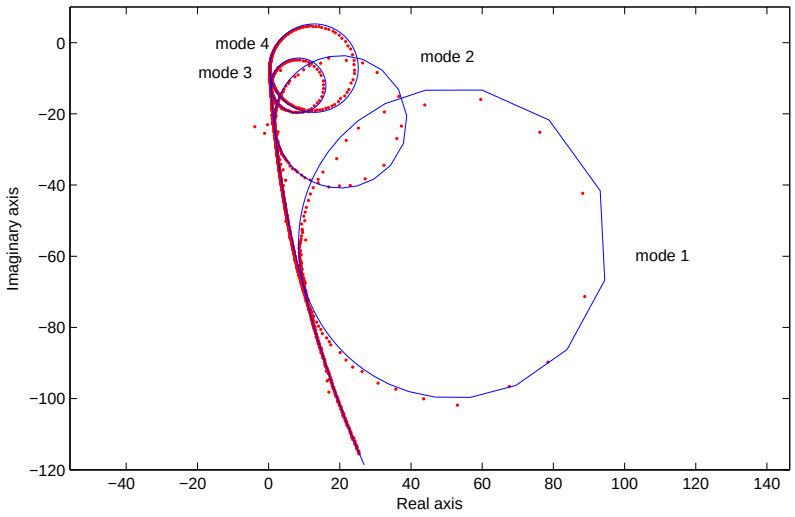


Figure IV.14: Nyquist plot of impedance of the second piezoelectric transducer and curve fit.

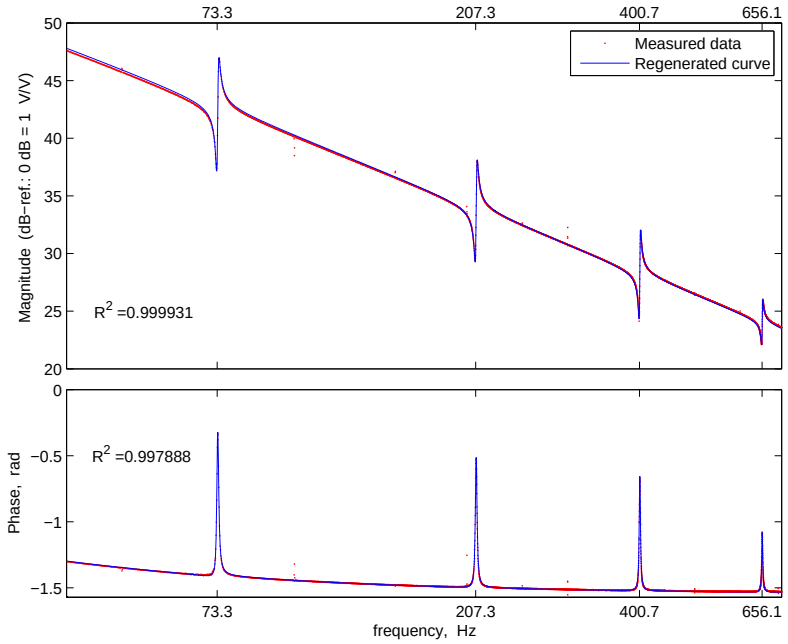


Figure IV.15: Comparison of measured electric impedance of the third piezoelectric transducer and curve fit.

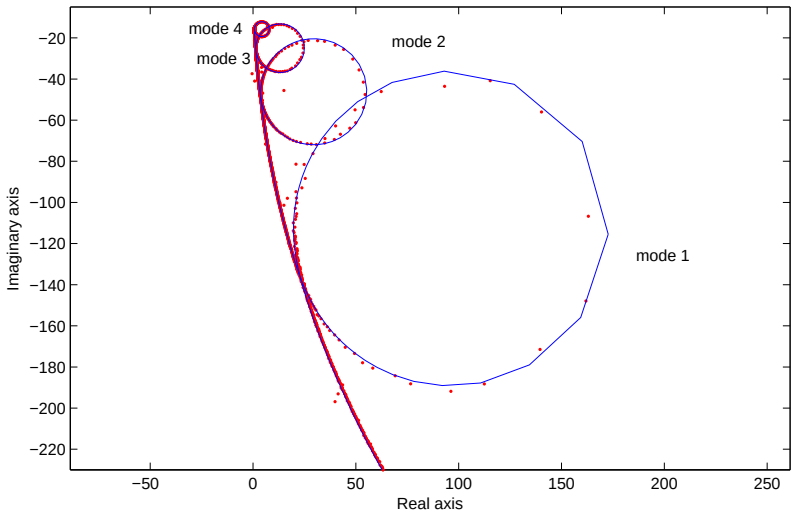


Figure IV.16: Nyquist plot of impedance of the third piezoelectric transducer and curve fit.

using the following relation

$$\Gamma_{jr} = \sqrt{-\beta_{jr}^2 + \sqrt{\beta_{jr}^4 + \frac{\left(\omega_T^2 - \omega_S^2\right)^2}{\omega_j^4}}} \tag{IV.8}$$

where β_{jr} is the ratio of the electric resonance of the RLC shunt circuit on the r-th piezoelectric transducer and the mechanical eigenfrequency ω_j. The frequencies ω_S and ω_T are the fixed points as depicted in figure IV.17. The inductance is tuned to have a ratio β_{jr} equal to one. The obtained results are shown in table IV.5. In table IV.6 are shown the coupling coefficients obtained via a finite element model and the comparison between direct measurement and prediction.

Table IV.5: Normalised piezoelectric coupling coefficients.

	piezo 1	piezo 2	piezo 3
mode 1	-0.095 ± 0.007	0.12 ± 0.02	-0.105 ± 0.007
mode 2	0.083 ± 0.005	-0.09 ± 0.01	-0.090 ± 0.009
mode 3	-0.068 ± 0.007	-0.09 ± 0.01	-0.078 ± 0.008
mode 4	-0.05 ± 0.01	-0.14 ± 0.03	0.06 ± 0.01

Table IV.6: Predicted normalised piezoelectric coupling coefficients.

	piezo 1	Δ1 (%)	piezo 2	Δ2 (%)	piezo 3	Δ3 (%)
mode 1	-0.1106	14	0.1327	9	-0.1105	5
mode 2	0.0965	14	-0.0973	7	-0.0987	9
mode 3	-0.0802	15	-0.1025	12	-0.0828	6
mode 4	-0.0637	21	-0.1417	1	0.0610	2

IV.3 Control Validation

IV.3.1 The Control System

To test the proposed control, laboratory experiments carried out in real time. Specifically, the MathWorks xPC Target is used to create a real-time

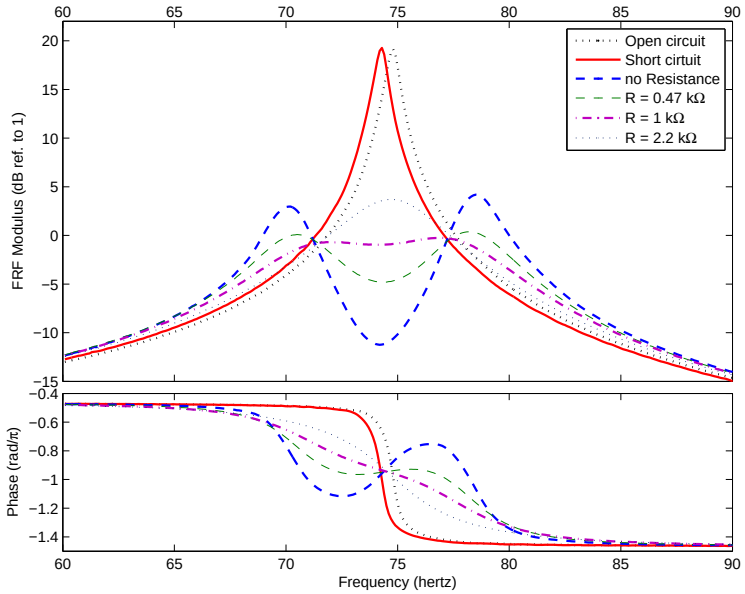


Figure IV.17: *FRF* of the beam with shunt circuit on the central piezoelectric pair close to the first beam mode to measure coupling coefficients by fixed points, ω_S and ω_T.

controller using a standard PC. The xPC Target is an environment that uses a target PC, separate from a host PC, for running real-time applications. In this environment a desktop computer is used as a host PC with Matlab and Simulink to create a model using Simulink blocks. After creating this model with I/O blocks, it is possible to use the host PC with a C/C++ compiler to create executable code. It is downloaded from the host to the target PC running the xPC Target real-time kernel. Target applications created with xPC Target run in real time on target PC without using a Windows operating system. It should be noted that model size, complexity, and target PC hardware affect maximum speed or minimal sample time of execution. The model employed, see figure IV.18, can run with a sample time as fast as 33.3 µs, *i.e.* 30 kHz.

IV.3.2 Results

This section presents the results obtained applying the control technique described in chapter I. To check the validity of control, a dual channel *FFT* analysis is performed to calculate a transfer inertance function which describes the dynamic behaviour of the system. The disturbance actuator is the

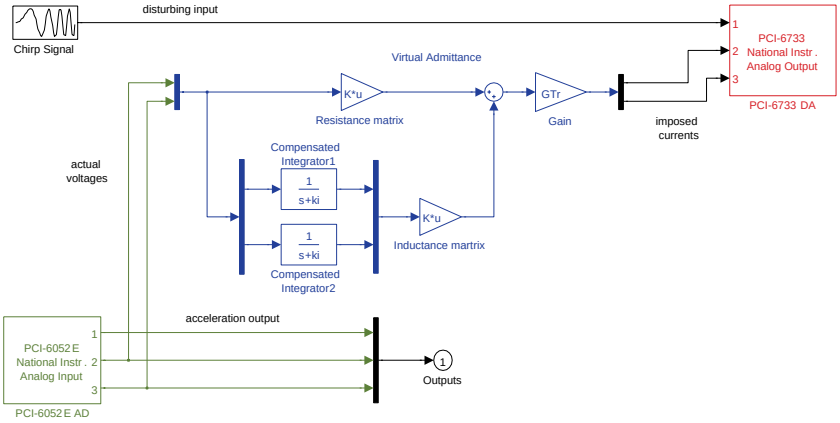


Figure IV.18: Simulink diagram for the real-time application.

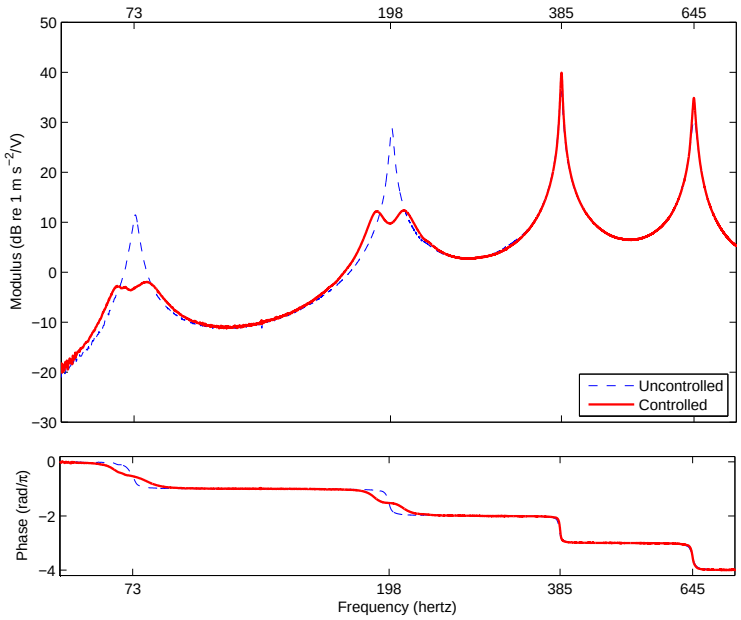


Figure IV.19: Inertance function of the beam and comparison with proposed control for the first and the second modes.

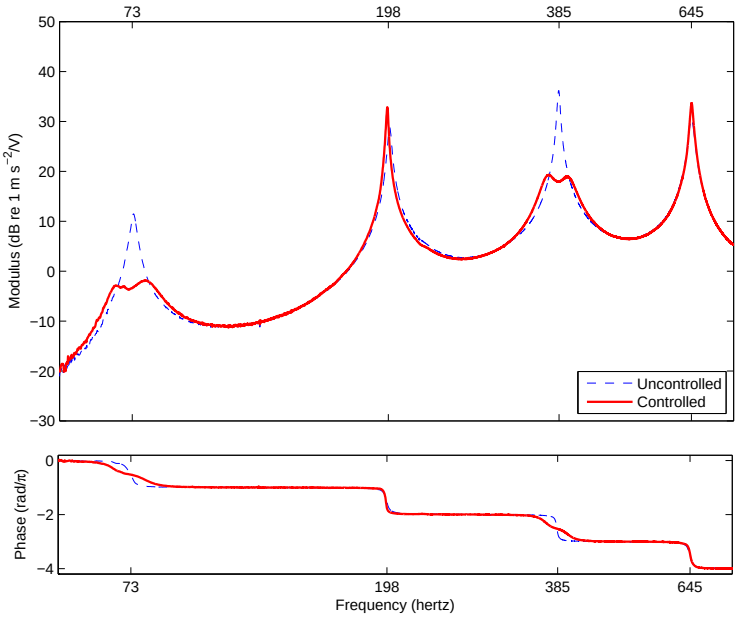


Figure IV.20: Inertance function of the beam and comparison with proposed control for the first and the third modes.

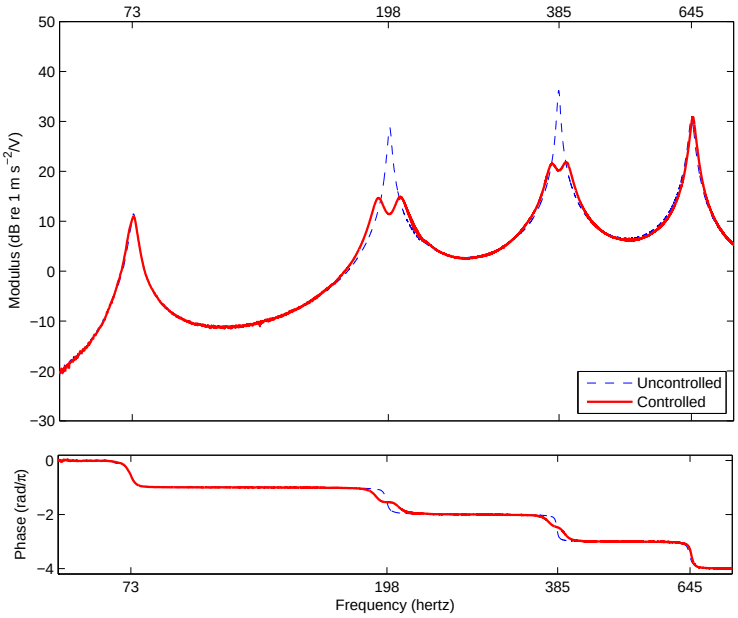


Figure IV.21: Inertance function of the beam and comparison with proposed control for the second and the third modes.

first piezoelectric pairs driven by a linear chirp waveform with a frequency range from 50 Hz to 800 Hz and an amplitude equal to 3 V. This kind of excitation is chosen instead of a random signal, because the real time application is not stable for long time acquisition. Therefore, a random analysis, that required a long time to be representative, is not suitable for this experiment. The National Instruments PCI-6733 board is used to imposed the forcing inputs. The analog outputs of this board have a resolution of 16 bits with an update rate of 1 megasample per second, a maximum voltage range of $\pm 10\,\mathrm{V}$ and a range accuracy of 2.24 mV. A Brüel & Kjær accelerometer is used to measure the response of the system and, therefore, to estimate inertances. The National Instruments PCI-6052E board is the data acquisition device that have a resolution of 16 bits with a memory on board of 512 samples, a range accuracy of 4.747 mV and a sampling rate of 333 kilosample per second. The other two piezoelectric transducers are utilised to control the beam vibrations. To implement the shunt control network, voltage-controlled current sources are employed in conjunction with the PCI-6733 board as shown in figure IV.18. The measurement time is 10 s, hence the frequency analysis has a frequency resolution $\Delta f = 0.1$ Hz. The figures from IV.19 to IV.21 shows the transfer inertance functions and the comparison between the system without control and with the control applied on two modes. It is shown also as the *virtual passive network system* used to control two modes acts over different pair of modes attesting to be equally able to accomplish the purpose of reducing vibrations.

Conclusions

This research work is concerned with modelling and analysis of devices for control of mechanical structure vibrations using piezoelectric transducers. It casts into the framework of advanced technology and engineering science and a special attention is devoted to the control of vibrations of one or two dimensional elastic continua as beam or plate equipped with piezoelectric transducers connected to electric network systems. The main result of this thesis is an extension of the known piezoelectric shunt damping techniques.

A specific technique has been presented for controlling a certain number of structural modes by an identical amount of piezoelectric transducers shunted with a multi-terminal electric network system. The design of the system for control vibrations is based on the intent to make the whole considered system equivalent to a set of independent, single resonant piezoelectric shunting systems, referred to as *generalised piezoelectric shunting systems*. A particular attention is devoted to a passive approach using different kinds of generalised piezoelectric shunting system with resistive-inductive circuits, parallel and series configurations. Two methods are considered for optimising the generalised electrical circuit of control: (i) the fixed points theory and (ii) pole allocation. Comparisons of the results are discussed in details. Differing from existing approaches which consider several shunts separately, the proposed shunting technique consider a multi-terminal network which interconnects the piezoelectric transducers for a spatial, simultaneous control of different mechanical modes. In the case of the passive approach, the shunting network forms, with the inherent piezoelectric capacitances at blocked modal deflections, a multi-degrees of freedom electric system having the following modal properties: (i) the same natural frequencies of the set of mechanical modes to be controlled, (ii) optimal damping ratios to absorb the mechanical

energy, (iii) eigenvectors that maximise the spatial coupling with the original mechanical modes having the same eigenfrequency.

Two optimization problems were shown. By introducing a proper transformation of electric coordinates, a one to one correspondence between the modal mechanical and new electric degree of freedom is approximately attained in order to regard the whole system as a set of the generalised piezoelectric shunting systems. Further, the distribution of the piezoelectric transducers is improved to maximise the damping performance. Two numerical cases, a double clamped beam and a fully clamped plate, was developed to validate the technique. Specifically, mobility functions are computed for the mechanical systems with piezoelectric transducers connected to optimal electric shunt networks and comparisons to uncontrolled systems place the efficiency of the control in evidence. The numerical simulations, performed with Simulink, show that the damping performance is considerably increased with respect to existing techniques for reducing vibrations in a wide range of frequencies. This is mainly due to two reasons: the effective optimal use of all the transducers for all the modes, the avoidance of the usage of additional external capacitors, which decrease the electromechanical couplings.

Besides, an experimental test case was accomplished in order to test the effectiveness of the proposed control: an aluminium double clamped beam with rectangular cross section and equipped with three pairs of piezoelectric elements. In experimental implementations, the required shunting network was obtained by an active feedback control, measuring the voltages at piezoelectric electrodes and using multiple voltage-controlled current sources to impose the forcing signal in order to mimic the behaviour of the designed network. This control was carried out on real time with the help of a desktop computer and Matlab and Simulink software. The present damping technique can be classified as a *virtual passive damping* in the sense of [Juang and Phan, 1992]. The main advantage with respect to purely active approaches is the unconditionally stability of the system. The formulation is model-independent in the sense that a very accurate knowledge of the system dynamics, linear or non-linear, is not an essential requisite in the design process, therefore this approach is robust with respect to parameter variations. An important feature of this formulation is that the controller gains have physical

interpretation. Therefore, one can visualise how the controller is removing energy from the system and tune the controller gains accordingly. Since piezoelectric elements exhibit actuation and sensing abilities within a single transducer, this approach is feasible considering it requires the collocation of sensors and actuators.

Suggestions for Future Works

Herein most attention is devoted to a passive approach even for the provided advantages. On the other hand, the suggested technique can be applied for active structural control which, in spite of a major control effort and stability issues, allows to obtain better performance. In section III numerical simulations involving active controllers are performed and comparisons of the results are commented but now, to check the validity of this active approach experimental test cases are needed.

The proposed technique for designing control systems reducing vibrations is based on a good understanding of the mechanical structure endowed with piezoelectric transducers and its environment. However, in a number of instances, the structure to be controlled is too complicated and the basic physical processes in it are not fully understood. Control design techniques then need to be augmented with an identification technique aimed at obtaining a progressively better understanding of the structure to be controlled. It is, thus, intuitive to aggregate system identification and control. In this dissertation, the two steps are taken separately. Therefore, I suggest as line of approach for further development the use of adaptive controllers that is centred around a fixed-structure controller of the same kind presented herein but with adjustable parameters, *i.e.* controllers possess a mechanism for automatically adjusting parameters based on system identification and posterior information. The use of adaptive control is justified on complex systems exhibiting non-linear and time-varying dynamics or when the use of a fixed controller cannot achieve a satisfactory compromise between robust stability and performance.

Finally, as a further application, it is possible to consider the problem of acoustic radiation. Noise reduction of panels is increasingly required in aircrafts, cars, ships, buildings, *etc.*, to provide a comfortable living environment.

APPENDIX A

Rectangular Plates

A.1 Newtonian Formulation

In order to write the governing equation of the plate take a rectangular element, $ABCD$, out of plate, whose sides are parallel to coordinate axes and having lengths arbitrary small, respectively Δx_1 and Δx_2, and corner A with coordinates $(\tilde{x}_1, \tilde{x}_2)$. In this case the only significant loads are: the shear forces V_1 and V_2; the bending moments M_1 and M_2; the twisting moment M_{12}. They are considered per unit of length. Single subscripts are representative for the normal to side on which they act. See the figure A.1 for agreements with signs. Let f_3 be an arbitrary load per unit of surface acting orthogonally to middle surface. The basic tool in applying Newton's second law is the free-body diagram. Free-body diagram allows to write the equilibrium of the forces along the x_3 axis for the element $ABCD$

$$\begin{aligned} &\int_{\tilde{x}_2}^{\tilde{x}_2+\Delta x_2} [V_1(\tilde{x}_1 + \Delta x_1, x_2, t) - V_1(\tilde{x}_1, x_2, t)]\, dx_2 + \\ &+ \int_{\tilde{x}_1}^{\tilde{x}_1+\Delta x_1} [V_2(x_1, \tilde{x}_2 + \Delta x_2, t) - V_2(x_1, \tilde{x}_2, t)]\, dx_1 + \\ &+ \int_{\tilde{x}_2}^{\tilde{x}_2+\Delta x_2} \int_{\tilde{x}_1}^{\tilde{x}_1+\Delta x_1} f_3(x_1, x_2, t)\, dx_1\, dx_2 = 0 \end{aligned} \tag{A.1}$$

taking in account the definition of partial derivative and grouping together the terms, it can be shown that

$$\int_{\tilde{x}_2}^{\tilde{x}_2+\Delta x_2} \int_{\tilde{x}_1}^{\tilde{x}_1+\Delta x_1} \left(\frac{\partial V_1(x_1, x_2, t)}{\partial x_1} + \frac{\partial V_2(x_1, x_2, t)}{\partial x_2} + f_3(x_1, x_2, t) \right) dx_1 dx_2 = 0 \tag{A.2}$$

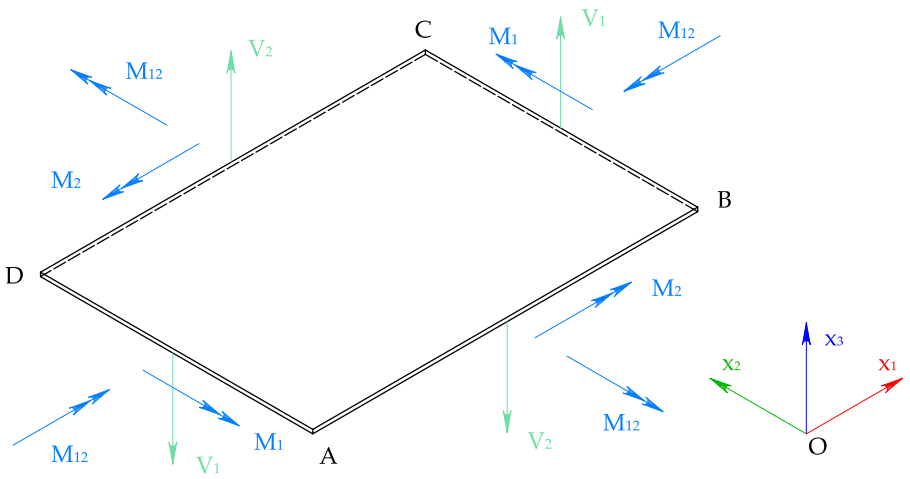


Figure A.1: Free-body diagram. Agreements with positive signs of load per unit of length acting on arbitrary plate element.

owing to the arbitrary chosen of Δx_1 and Δx_2 and because the integrand function is continuous the (A.2) is equivalent to the equation at any point into $\mathscr{A}$

$$\frac{\partial V_1(x_1,x_2,t)}{\partial x_1} + \frac{\partial V_2(x_1,x_2,t)}{\partial x_2} + f_3(x_1,x_2,t) = 0 \quad \forall\, x_1,x_2 \in \mathscr{A} \tag{A.3}$$

Equilibrium of the moments with respect to the pole A projected on the x_1 axis can be developed in this way

$$\begin{aligned}
&\int_{\tilde{x}_1}^{\tilde{x}_1+\Delta x_1} [M_2(x_1,\tilde{x}_2+\Delta x_2,t) - M_2(x_1,\tilde{x}_2,t)]\, dx_1 + \\
&+ \int_{\tilde{x}_2}^{\tilde{x}_2+\Delta x_2} [M_{12}(\tilde{x}_1+\Delta x_1,x_2,t) - M_{12}(\tilde{x}_1,x_2,t)]\, dx_2 + \\
&- \int_{\tilde{x}_2}^{\tilde{x}_2+\Delta x_2} V_1(\tilde{x}_1+\Delta x_1,x_2,t)(x_2-\tilde{x}_2)\, dx_2 + \\
&+ \int_{\tilde{x}_2}^{\tilde{x}_2+\Delta x_2} V_1(\tilde{x}_1,x_2,t)(x_2-\tilde{x}_2)\, dx_2 + \\
&- \Big[\int_{\tilde{x}_1}^{\tilde{x}_1+\Delta x_1} V_2(x_1,\tilde{x}_2+\Delta x_2,t)\, dx_1\Big]\Delta x_2 + \\
&- \int_{\tilde{x}_2}^{\tilde{x}_2+\Delta x_2}\int_{\tilde{x}_1}^{\tilde{x}_1+\Delta x_1} f_3(x_1,x_2,t)(x_2-\tilde{x}_2)\, dx_1 dx_2 = 0
\end{aligned} \tag{A.4}$$

using the (A.3) and integrating by parts the last addend of the (A.4) it obtains

$$\int_{\tilde{x}_2}^{\tilde{x}_2+\Delta x_2}\int_{\tilde{x}_1}^{\tilde{x}_1+\Delta x_1} \left(\frac{\partial M_2(x_1,x_2,t)}{\partial x_2} + \frac{\partial M_{12}(x_1,x_2,t)}{\partial x_1} - V_2(x_1,x_2,t)\right) dx_1 dx_2 = 0 \tag{A.5}$$

and likewise said for the (A.3)

$$\frac{\partial M_{12}(x_1, x_2, t)}{\partial x_1} + \frac{\partial M_2(x_1, x_2, t)}{\partial x_2} - V_2(x_1, x_2, t) = 0 \quad \forall\, x_1, x_2 \in \mathscr{A} \tag{A.6}$$

Proceeding in the same way for the equilibrium of the moments along the x_2 axis with respect to the pole A, it can be written

$$\frac{\partial M_1(x_1, x_2, t)}{\partial x_1} + \frac{\partial M_{12}(x_1, x_2, t)}{\partial x_2} - V_1(x_1, x_2, t) = 0 \quad \forall\, x_1, x_2 \in \mathscr{A} \tag{A.7}$$

At this point differentiating the (A.7) with respect to x_1, the (A.6) with respect to x_2, summing term to term and using the (A.3), the governing equation of plate in terms of moment is

$$\frac{\partial^2 M_1}{\partial x_1^2} + 2\frac{\partial^2 M_{12}}{\partial x_1 \partial x_2} + \frac{\partial^2 M_2}{\partial x_2^2} + f_3 = 0 \quad \forall\, x_1, x_2 \in \mathscr{A} \tag{A.8}$$

The relationships between considered loads and the stress tensor components are given by

$$\begin{aligned} M_1 &\triangleq \int_{-\frac{h}{2}}^{\frac{h}{2}} T_{11}\, x_3\, dx_3, \quad M_2 \triangleq \int_{-\frac{h}{2}}^{\frac{h}{2}} T_{22}\, x_3\, dx_3 \\ M_{12} &\triangleq \int_{-\frac{h}{2}}^{\frac{h}{2}} T_{12}\, x_3\, dx_3 \end{aligned} \tag{A.9}$$

$$V_1 \triangleq \int_{-\frac{h}{2}}^{\frac{h}{2}} T_{13}\, dx_3, \quad V_2 \triangleq \int_{-\frac{h}{2}}^{\frac{h}{2}} T_{23}\, dx_3 \tag{A.10}$$

Remark A.1. It is important to note from the (A.10) that if T_{13} and T_{23} are identically null along the thickness, h, shear forces will be zero. It is absolutely essential, however, to hold that they are different from zero for the above. Actually, considering the (II.1), it is clear that the terms of order zero and first, in which it is possible to expand such components of the stress tensor in a Taylor series, are null. Hence, it is necessary to consider the terms of higher order, that, albeit small, it is not allowed to neglect with respect to zero. It can establish by some elementary considerations that the quadratic term is, on the contrary, different from zero.

◇ ◇ ◇

Using the (II.4) and the (II.3), the relationships between displacements and moments can be written as

$$\begin{aligned} M_1 &= -B\left(\frac{\partial^2 w}{\partial x_1^2} + \nu\,\frac{\partial^2 w}{\partial x_2^2}\right) \\ M_2 &= -B\left(\frac{\partial^2 w}{\partial x_2^2} + \nu\,\frac{\partial^2 w}{\partial x_1^2}\right) \\ M_{12} &= -B\,(1-\nu)\left(\frac{\partial^2 w}{\partial x_1 x_2}\right) \end{aligned} \tag{A.11}$$

where B is the flexural modulus and it is defined by

$$B = \frac{Yh^3}{12\,(1-\nu^2)}$$

In accord with the D'Alembert's principle, to obtain the motion equation is sufficient to relate f_3 with the inertial force per unit of surface. It is given by

$$f_3 = -\rho\,h\frac{\partial^2 w}{\partial t^2} + p(x_1, x_2, t)$$

where ρ is the mass density, constant for the homogeneity and $p(x_1, x_2, t)$ is any external pressure. Substituting the (A.11) into (A.8), finally the governing equation of the plate assumes the form

$$B\,\nabla^4 w(x_1, x_2, t) + \rho\,h\frac{\partial^2 w}{\partial t^2}(x_1, x_2, t) = p(x_1, x_2, t) \quad \forall\, x_1, x_2 \in \mathscr{A} \tag{A.12}$$

The boundary conditions are given by

$$\begin{cases} w(x_1, x_2, t) = 0 & \forall\, x_1, x_2 \in \partial\mathscr{A} \text{ and } \forall\, t \geq 0 \\ \dfrac{\partial w}{\partial \hat{n}}(x_1, x_2, t) = 0 & \forall\, x_1, x_2 \in \partial\mathscr{A} \text{ and } \forall\, t \geq 0 \end{cases} \tag{A.13}$$

and to complete the partial differential problem, the initial conditions take the following form

$$\begin{cases} w(x_1, x_2, 0) = w_0(x_1, x_2) & \forall\, x_1, x_2 \in \mathscr{A} \\ \dfrac{\partial w}{\partial t}(x_1, x_2, 0) = \dot{w}_0(x_1, x_2) & \forall\, x_1, x_2 \in \mathscr{A} \end{cases} \tag{A.14}$$

Into (A.13) and (A.14), the $\hat{n}$ indicates the normal to $\partial\mathscr{A}$, w_0 and $\dot{w}_0$ represent the initial configuration and the initial velocity, respectively.

A.2 Hamiltonian Formulation

Hamilton's principle, so as many other equivalent principles, called of minimum action, on the contrary of Newtonian formulation reduces dynamic problems to the investigation of a scalar integral. Such approach, also named *weak*, not only are easier to employ, but are invariant with respect to the reference frame used. A variational principle, furthermore, provides the boundary conditions compatible with made hypotheses. For instance, think with regard to the generalised transverse shear force of the plate with the boundary conditions completely free [Vasiliev, 2000]. In some cases the Newtonian formulation, also called *strong*, is not applicable because it is not at all easy to find a law that expresses correctly the acting force model. In the strong formulation, if any term has discontinuities, it is not allowed to look for the solution that satisfies the problem at all points, because does not exist. On contrary, it is allowed to search solutions for the weak problem, in which weaker properties are required.

At this point, Hamilton's principle needs of greater investigation. In section II.1.2, the expressions of the kinetic energy (II.7), the strain one (II.11) and the virtual work of external forces (II.12) for a flexible thin plate are derived. Maintaining the same meaning for symbols, if one introduces them into the expression of the Hamilton's principle (II.6) obtains

$$\begin{aligned}
\int_{t_0}^{t_1} \Big\{ & \iint_{\mathscr{A}} \rho\, h \frac{\partial w}{\partial t}\, \delta\left(\frac{\partial w}{\partial t}\right) d\mathscr{A} + \\
& - \iint_{\mathscr{A}} B \left[\frac{\partial^2 w}{\partial x_1^2}\, \delta\left(\frac{\partial^2 w}{\partial x_1^2}\right) + \frac{\partial^2 w}{\partial x_2^2}\, \delta\left(\frac{\partial^2 w}{\partial x_2^2}\right)\right] d\mathscr{A} + \\
& - \iint_{\mathscr{A}} B\, \nu \left[\frac{\partial^2 w}{\partial x_2^2}\, \delta\left(\frac{\partial^2 w}{\partial x_1^2}\right) + \frac{\partial^2 w}{\partial x_1^2}\, \delta\left(\frac{\partial^2 w}{\partial x_2^2}\right)\right] d\mathscr{A} + \\
& - \iint_{\mathscr{A}} 2B\,(1-\nu) \left[\frac{\partial^2 w}{\partial x_1 \partial x_2}\, \delta\left(\frac{\partial^2 w}{\partial x_1 \partial x_2}\right)\right] d\mathscr{A} + \\
& + \iint_{\mathscr{A}} p\, \delta w\, d\mathscr{A} \Big\}\, dt \;=\; 0
\end{aligned} \tag{A.15}$$

Assuming the operator δ and the derivatives, both spatial and temporal, are commutative, that it is possible to interchange the integrations made with respect to the time and these with respect to spatial variables, it can integrate

by parts and obtain

$$\mathscr{I}_K = -\iint_{\mathscr{A}} \left(\int_{t_0}^{t_1} \rho\, h \frac{\partial^2 w}{\partial t^2}\, \delta w \, dt \right) d\mathscr{A} \tag{A.16}$$

where $\mathscr{I}_K$ indicates the first addend of the (A.15) related to the kinetic energy. Here, δw is assumed equal to zero at $t = t_0$ and $t = t_1$ considering synchronous varied paths. Indicating with $\mathscr{I}_{\Pi_i}$ the five terms of the (A.15) related to the strain energy, it can be written

$$\begin{aligned}\mathscr{I}_{\Pi_1} = & \int_{t_0}^{t_1} \int_0^{L_2} \left[-B \frac{\partial^2 w}{\partial x_1^2}\, \delta \left(\frac{\partial w}{\partial x_1} \right) + \frac{\partial}{\partial x_1} \left(B \frac{\partial^2 w}{\partial x_1^2} \right) \delta w \right]_{x_1=0}^{x_1=L_1} dx_2\, dt + \\ & - \int_{t_0}^{t_1} \left[\iint_{\mathscr{A}} \frac{\partial^2}{\partial x_1^2} \left(B \frac{\partial^2 w}{\partial x_1^2} \right) \delta w \, d\mathscr{A} \right] dt \end{aligned} \tag{A.17}$$

$$\begin{aligned}\mathscr{I}_{\Pi_2} = & \int_{t_0}^{t_1} \int_0^{L_1} \left[-B \frac{\partial^2 w}{\partial x_2^2}\, \delta \left(\frac{\partial w}{\partial x_2} \right) + \frac{\partial}{\partial x_2} \left(B \frac{\partial^2 w}{\partial x_2^2} \right) \delta w \right]_{x_2=0}^{x_2=L_2} dx_1\, dt + \\ & - \int_{t_0}^{t_1} \left[\iint_{\mathscr{A}} \frac{\partial^2}{\partial x_2^2} \left(B \frac{\partial^2 w}{\partial x_2^2} \right) \delta w \, d\mathscr{A} \right] dt \end{aligned} \tag{A.18}$$

$$\begin{aligned}\mathscr{I}_{\Pi_3} = & \int_{t_0}^{t_1} \int_0^{L_2} \left[-B\nu \frac{\partial^2 w}{\partial x_2^2}\, \delta \left(\frac{\partial w}{\partial x_1} \right) + \frac{\partial}{\partial x_1} \left(B\nu \frac{\partial^2 w}{\partial x_2^2} \right) \delta w \right]_{x_1=0}^{x_1=L_1} dx_2\, dt + \\ & - \int_{t_0}^{t_1} \left[\iint_{\mathscr{A}} \frac{\partial^2}{\partial x_1^2} \left(B\, \nu \frac{\partial^2 w}{\partial x_2^2} \right) \delta w \, d\mathscr{A} \right] dt \end{aligned} \tag{A.19}$$

$$\begin{aligned}\mathscr{I}_{\Pi_4} = & \int_{t_0}^{t_1} \int_0^{L_1} \left[-B\nu \frac{\partial^2 w}{\partial x_1^2}\, \delta \left(\frac{\partial w}{\partial x_2} \right) + \frac{\partial}{\partial x_2} \left(B\nu \frac{\partial^2 w}{\partial x_1^2} \right) \delta w \right]_{x_2=0}^{x_2=L_2} dx_1\, dt + \\ & - \int_{t_0}^{t_1} \left[\iint_{\mathscr{A}} \frac{\partial^2}{\partial x_2^2} \left(B\, \nu \frac{\partial^2 w}{\partial x_1^2} \right) \delta w \, d\mathscr{A} \right] dt \end{aligned} \tag{A.20}$$

$$\begin{aligned}\mathscr{I}_{\Pi_5} = & \int_{t_0}^{t_1} \left[\left[-2B(1-\nu) \frac{\partial^2 w}{\partial x_1 \partial x_2}\, \delta w \right]_{x_1=0}^{x_1=L_1} \right]_{x_2=0}^{x_2=L_2} dt + \\ & + \int_{t_0}^{t_1} \int_0^{L_2} \left[2B(1-\nu) \frac{\partial^3 w}{\partial x_1 \partial x_2^2}\, \delta w \right]_{x_1=0}^{x_1=L_1} dx_2\, dt + \\ & + \int_{t_0}^{t_1} \int_0^{L_1} \left[2B(1-\nu) \frac{\partial^3 w}{\partial x_1^2 \partial x_2}\, \delta w \right]_{x_2=0}^{x_2=L_2} dx_1\, dt + \\ & - \int_{t_0}^{t_1} \left[\iint_{\mathscr{A}} 2B(1-\nu) \frac{\partial^4 w}{\partial x_1^2 \partial x_2^2}\, \delta w \, d\mathscr{A} \right] dt \end{aligned} \tag{A.21}$$

where $[f(x_1)]_0^{L_1} = f(L_1) - f(0)$. Substituting the (A.16)-(A.21) into (A.15) and remembering that they are defined $\forall w \in \mathcal{F}$, it leads to the equation

$$B\left(\frac{\partial^4 w}{\partial x_1^4} + 2\,\frac{\partial^4 w}{\partial x_1^2 \partial x_2^2} + \frac{\partial^4 w}{\partial x_2^4}\right) + \rho h \frac{\partial^2 w}{\partial t^2} = p \tag{A.22}$$

this equation being defined into open set $\mathscr{A} \times \mathbb{R}_0^+$. It also can be written

$$\int_0^{L_2} B\left[\left(\frac{\partial^3 w}{\partial x_1^3} + (2-\nu)\frac{\partial^3 w}{\partial x_1 \partial x_2^2}\right)\delta w\right]_{x_1=0}^{x_1=L_1} dx_2 = 0 \tag{A.23a}$$

$$\int_0^{L_1} B\left[\left(\frac{\partial^3 w}{\partial x_2^3} + (2-\nu)\frac{\partial^3 w}{\partial x_2 \partial x_1^2}\right)\delta w\right]_{x_2=0}^{x_2=L_2} dx_1 = 0 \tag{A.23b}$$

$$\int_0^{L_2} -B\left[\left(\frac{\partial^2 w}{\partial x_1^2} + \nu\frac{\partial^2 w}{\partial x_2^2}\right)\delta\left(\frac{\partial w}{\partial x_1}\right)\right]_{x_1=0}^{x_1=L_1} dx_2 = 0 \tag{A.23c}$$

$$\int_0^{L_1} -B\left[\left(\frac{\partial^2 w}{\partial x_2^2} + \nu\frac{\partial^2 w}{\partial x_1^2}\right)\delta\left(\frac{\partial w}{\partial x_2}\right)\right]_{x_2=0}^{x_2=L_2} dx_1 = 0 \tag{A.23d}$$

$$\left[\left[-2B(1-\nu)\frac{\partial^2 w}{\partial x_1 \partial x_2}\,\delta w\right]_{x_1=0}^{x_1=L_1}\right]_{x_2=0}^{x_2=L_2} = 0 \tag{A.23e}$$

from which all possible boundary conditions can be derived. It is opportune to note that the equation (A.23e), only defined on the corners of the plate, takes in account the twisting moment that is not important all times that on the $\partial\mathscr{A}$ is zero δw, as in the case completely clamped.

A.3 Vibration of Fully Clamped Plates

The transverse vibrations of a thin plate have a behaviour described by the equation (II.13). This last, for free vibrations, assumes the form

$$B\,\nabla^4 w(x_1, x_2, t) \;+\; \rho\, h \frac{\partial^2 w}{\partial t^2}(x_1, x_2, t) \;=\; 0 \quad \forall\, x_1, x_2 \in \mathscr{P} \tag{A.24}$$

being $\mathscr{P}$ the open set equal to $(0, L_1) \times (0, L_2)$. The boundary conditions on all $\partial\mathscr{P}$, that is the border of $\mathscr{P}$, are given by a clamped edges for all t in $\mathbb{R}_0^+$ and more precisely, they are

$$\begin{cases} w(x_1, x_2, t) = 0 \\ \dfrac{\partial w}{\partial \hat{n}} = 0 \end{cases} \tag{A.25}$$

where $\hat{n}$ represents the unit normal at the domain boundary $\partial\mathscr{P}$. The initial conditions are

$$\begin{cases} w(x_1, x_2, 0) = w_0(x_1, x_2) & \forall\, x_1, x_2 \in \mathscr{P} \\ \dfrac{\partial w}{\partial t}(x_1, x_2, 0) = \dot{w}_0(x_1, x_2) & \forall\, x_1, x_2 \in \mathscr{P} \end{cases} \tag{A.26}$$

With the intention to use the Fourier's method to solve the differential problem (A.24), (A.25) and (A.26), let the generic stationary wave be expressed by

$$w = W(x_1, x_2)\eta(t) \tag{A.27}$$

Substituting the particular solution (A.27) into the equation (A.24), assuming that $w \neq 0$ there where w is defined, one finds

$$-\frac{\ddot{\eta}(t)}{\eta(t)} = \frac{B}{\rho\, h}\frac{\nabla^4 W(x_1, x_2)}{W(x_1, x_2)} = \omega^2 \tag{A.28}$$

where ω^2 represents an eigenvalue of the problem obtained from the last relation of the (A.28)

$$\begin{cases} \dfrac{B}{\rho\, h}\nabla^4 W = \omega^2 W & \forall\, x_1, x_2 \in \mathscr{P} \\ W = 0 & \forall\, x_1, x_2 \in \partial\mathscr{P} \\ \dfrac{\partial W}{\partial \hat{n}} = 0 & \forall\, x_1, x_2 \in \partial\mathscr{P} \end{cases} \tag{A.29}$$

The operator ∇^4 is self-adjoint[1] and positive definite[2] thus the problem (A.29) has the same properties and its eigenvalues are a numerable infinite spectrum of values all positive, *i.e.* ω^2.

Exact solutions for the problem (A.29) are not representable with an elementary closed form; only when at least one pair of opposite sides is simply

[1] A linear operator, L, is self-adjoint in $\mathscr{P}$ if and only if $\forall\, u(x_1, x_2)$ and $v(x_1, x_2)$ functions opportunely smooth is valid

$$\iint_{\mathscr{P}} v\, L(u)\; dx_1\, dx_2 = \iint_{\mathscr{P}} u\, L(v)\; dx_1\, dx_2$$

[2] A linear operator, L, is positive definite in $\mathscr{P}$ if and only if $\forall\, u(x_1, x_2)$ opportunely smooth is valid

$$\iint_{\mathscr{P}} u\, L(u)\, dx_1\, dx_2 \geq 0$$

and the integral is equal to zero if and only if u is identically null.

supported, it is suitable to look for exact solutions in closed form. For other edge constrains approximate methods are to be employed which at least consent to satisfy the geometric boundary conditions. It is crucial to note that if eigenfunctions are representable only with proper series of the some orthogonal and complete system, it is very hard to handle them for whatever purpose though they are suitably truncated. In order to find approximate solutions, utilisable with ease, the Rayleigh's principle can be employed. It asserts: "*The vibration frequency of a conservative system close to a configuration of stable equilibrium has a stationary value in the neighbourhood of a natural mode*". In other words, given a harmonic motion in the form (A.27), the first variation of $\mathscr{E}$, computed as the difference between the maximum strain energy, Π_{Max}, and the maximum kinetic energy, K_{Max}, must be null $\forall$ eigenfunction W, that is a natural mode. More precisely, $\mathscr{E}$ has this aspect

$$\mathscr{E}(W) = \frac{1}{2}\iint_{\mathscr{P}} \Big\{ B \Big[\Big(\frac{\partial^2 W}{\partial x_1^2}\Big)^2 + \Big(\frac{\partial^2 W}{\partial x_2^2}\Big)^2 + 2\,\nu \frac{\partial^2 W}{\partial x_1^2}\frac{\partial^2 W}{\partial x_2^2} + \\ + 2(1-\nu)\Big(\frac{\partial^2 W}{\partial x_1 \partial x_2}\Big)^2 \Big] - \omega^2 \rho h W^2 \Big\} d\mathscr{P} \tag{A.30}$$

The equation

$$\delta\mathscr{E} = 0 \tag{A.31}$$

is equivalent to the problem (A.29), indeed, if the variational calculation is developed, then the same problem is obtained. In order to determine an approximate solution, it is reasonable to search for the optimum separable solutions of the type $W(x_1, x_2) = \alpha(x_1)\beta(x_2)$. The factor functions are called *plate characteristic functions*. This allows to write, from the equation (A.31), two ordinary differential equations to solve simultaneously, with considerable simplifications because the linearity of the equations and the constancy of their coefficients. For more details the reader is referred to [Rajalingham et al., 1996, 1997]. In general, this factorisation is not at all allowed, here there is the approximation. The variational formulation aids to understand what it is doing. In truth, the solutions of these two ordinary equations are the best approximations of the natural modes taking in account the constrain referred to the factorisation. That is to say, defining an appropriate distance into the space of the considered functions, this approximation minimises the errors.

In order to put the problem in dimensionless form, it needs execute a proper chance of variables. Let the new variables be

$$\xi_1 = x_1/L_1 \qquad \xi_2 = x_2/L_2 \tag{A.32}$$

developing the (A.31) with the new variables, as above specified, two ordinary differential equations are obtained

$$\begin{cases} \dfrac{1}{\lambda^2}B^{(00)}\alpha^{IV} + 2B^{(02)}\alpha^{II} - (\varpi^2 B^{(00)} - \lambda^2 B^{(04)})\alpha = 0 \\ \lambda^2 A^{(00)}\beta^{IV} + 2A^{(02)}\beta^{II} - (\varpi^2 A^{(00)} - \dfrac{1}{\lambda^2}A^{(04)})\beta = 0 \end{cases} \tag{A.33}$$

where $\varpi = \omega L_1 L_2(\rho h/B)^{1/2}$ is the dimensionless circular frequency, whilst $\lambda = L_1/L_2$ is the aspect ratio and the coefficients are defined by

$$A^{(mn)} = \int_0^1 \frac{d^m\alpha}{d\xi_1^m}\frac{d^n\alpha}{d\xi_1^n}d\xi_1 \qquad B^{(mn)} = \int_0^1 \frac{d^m\beta}{d\xi_2^m}\frac{d^n\beta}{d\xi_2^n}d\xi_2 \tag{A.34}$$

The boundary conditions become

$$\begin{cases} \alpha(0) = 0 & \alpha'(0) = 0 & \alpha(1) = 0 & \alpha'(1) = 0 \\ \beta(0) = 0 & \beta'(0) = 0 & \beta(1) = 0 & \beta'(1) = 0 \end{cases} \tag{A.35}$$

The general solution of the system (A.33) is representable in the following way

$$\begin{aligned} \alpha(\xi_1) &= C_1\cos(p_1\xi_1) + C_2\sin(p_1\xi_1) + C_3\cosh(p_2\xi_1) + C_4\sinh(p_2\xi_1) \\ \beta(\xi_2) &= D_1\cos(q_1\xi_2) + D_2\sin(q_1\xi_2) + D_3\cosh(q_2\xi_2) + D_4\sinh(q_2\xi_2) \end{aligned} \tag{A.36}$$

The characteristic parameters, p_1, p_2, q_1 and q_2, can be calculated by the imposition of the boundary conditions (A.35) and by the congruence relations obtained enforcing the (A.36) to be solutions of the (A.33) by means of the (A.34). At this point, it is opportune to observe that for the symmetry of the plate and of the boundary conditions, the two solutions (A.36) can be subdivided each in two subset: symmetric, (S), or antisymmetric, (A), with respect to $\xi_1 = 1/2$ and $\xi_2 = 1/2$. In other words, the solutions assume this shape

$$\alpha(\xi_1) = \begin{cases} \dfrac{\cosh[p_2(\xi_1 - 1/2)]}{\cosh(p_2/2)} - \dfrac{\cos[p_1(\xi_1 - 1/2)]}{\cos(p_1/2)} & (S) \\ \dfrac{\sinh[p_2(\xi_1 - 1/2)]}{\sinh(p_2/2)} - \dfrac{\sin[p_1(\xi_1 - 1/2)]}{\sin(p_1/2)} & (A) \end{cases} \tag{A.37}$$

along the ξ_1 axis. Similar expressions can be found for the solutions in the variable ξ_2, substituting p_1 and p_2 with q_1 and q_2, respectively. The integration constants C_j and D_j are been computed imposing the condition of null displacement on all the perimeter of the plate, separating the odd and the even terms in order to obtain the solutions (S) and (A). Keep in mind that eigenfunctions are defined unless of the multiplicative constant. Besides, imposing the conditions on the first derivatives on all the perimeter of the plate, one finds

$$P(p_1, p_2) = 0 \tag{A.38}$$

where

$$P(p_1, p_2) = \begin{cases} p_2 \tanh(p_2/2) + p_1 \tan(p_1/2) & (S) \\ p_1 \tanh(p_2/2) - p_2 \tan(p_1/2) & (A) \end{cases} \tag{A.39}$$

The congruence relations, mentioned above, assume the appearance

$$p_2{}^2 - p_1{}^2 = 2\,\lambda^2\,\mathscr{B}(q_1, q_2) \tag{A.40}$$

in particular, it has

$$\mathscr{B}(q_1, q_2) = \frac{\mathscr{B}_* + \frac{1}{2}(q_2{}^2 - q_1{}^2)}{\left[\frac{(q_2{}^2 - q_1{}^2)}{2 q_2{}^2 q_1{}^2}\right] \mathscr{B}_* - 1} \tag{A.41}$$

where

$$\mathscr{B}_* = \begin{cases} 1 - [1 - p_2 \tanh(p_2/2)]^2 & (S) \\ 1 - \left[1 - \dfrac{p_2}{\tanh(p_2/2)}\right]^2 & (A) \end{cases} \tag{A.42}$$

Operating in the same manner for $\beta(\xi_2)$, from the conditions on the first derivatives, it arrives to

$$Q(q_1, q_2) = 0 \tag{A.43}$$

being, as it is easy to prove, $Q(q_1, q_2) = P(q_1, q_2)$. Moreover, the congruence relations allow to write

$$q_2{}^2 - q_1{}^2 = \frac{2}{\lambda^2}\,\mathscr{A}(p_1, p_2) \tag{A.44}$$

with $\mathscr{A}(p_1, p_2) = \mathscr{B}(p_1, p_2)$. Again, from the congruence relations, it can be written

$$\varpi^2 = \frac{1}{\lambda^2}\, p_2{}^2 p_1{}^2 + \lambda^2 q_2{}^2 q_1{}^2 - \frac{1}{2}(p_2{}^2 - p_1{}^2)(q_2{}^2 - q_1{}^2) \tag{A.45}$$

From the equations (A.38) and (A.40) as well as from the (A.43) and (A.44), it is possible calculate the characteristic parameters, and again, from these with the (A.45), the approximate values for the natural circular frequencies can be computed. It should be noted that if $(\tilde{p}_1, \tilde{p}_2)$ are characteristic parameters, even $(\tilde{p}_1, -\tilde{p}_2)$, $(-\tilde{p}_1, \tilde{p}_2)$ and $(-\tilde{p}_1, -\tilde{p}_2)$ are possible parameters; however, the sign of these is not crucial considering the (A.37). Thus, without loss of generality, the characteristic parameters are assumed positive.

In order to computing the characteristic parameters it is possible to follow the iterative scheme given below:

1) the equation (A.40) is solved with respect to p_2;

2) the expression of p_2 is introduced into the (A.38), thus p_1 is calculated and afterward p_2;

3) knowing the couple (p_1, p_2), it can compute $\mathscr{A}$;

4) the equation (A.44) is solved for q_2, that is substituted in the (A.43) to calculate the couple (q_1, q_2);

5) with this last $\mathscr{B}$ is calculated and then, the points 1) and 2) as well as 3) and 4) are repeated up to convergence;

6) setting $\mathscr{B}$ equal to zero as first step, the (A.38) becomes equivalent to the frequency equation of the fully clamped beam.

Characteristic functions of a rectangular plate having aspect ratio, λ, a sufficient difference from one denote a good approximation for the eigenfunctions of the problem (A.29). On contrary, in the case in which the aspect ratio is close to one, it should be remarked some detail in addition. The reader more careful has, of course, seen that characteristic functions have nodal lines straight and parallel to Cartesian axes; but there can be vibrational modes having nodal lines very bending. This occurs because the square plate has eigenvalues with algebraic multiplicity greater than one, hence, the eigenfunctions referred to these eigenvalues constitute a space with dimension greater than one. In other words, modal shapes correlated to these eigenvalues can be defined not in unique manner, as a set of functions linearly

dependent, but with whatever set of functions mutually orthogonal in number equal to the dimension of the eigenfunction space. Linear combinations of functions with nodal lines straight can have got nodal lines bending. On the other hand, in these cases so as to improve the approximation, it possible to use the Rayleigh-Ritz method proper with the characteristic functions, that assure a faster convergence.

Table A.1: SS mode parameters for aspect ratio $\lambda = \sqrt{2}$.

mode	p_1	p_2	q_1	q_2	ϖ
(1, 1)	4.0774	8.0738	4.4914	5.652	39.305
(3, 1)	10.831	12.774	3.8334	10.638	103.15
(1, 3)	3.4834	20.184	10.952	11.435	178.07
(5, 1)	17.21	18.442	3.5638	16.629	227.14

Table A.2: SA mode parameters for aspect ratio $\lambda = \sqrt{2}$.

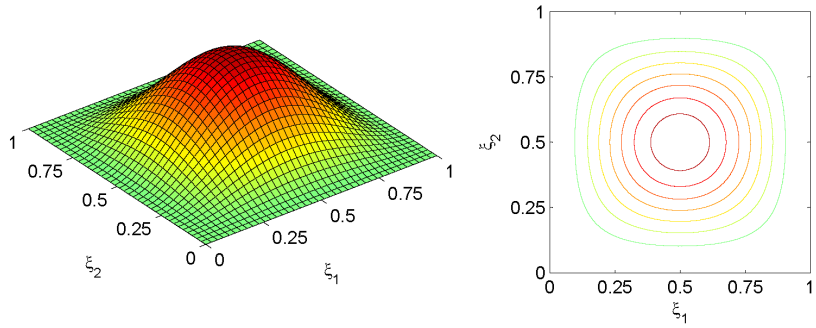
mode	p_1	p_2	q_1	q_2	ϖ
(1, 2)	3.651	14.024	7.7688	8.4565	94.447
(3, 2)	10.533	17.016	7.3615	12.304	154.24
(5, 2)	17.046	21.551	7.0412	17.681	274.97
(1, 4)	3.3974	26.413	14.111	14.482	289.68

Table A.3: AS mode parameters for aspect ratio $\lambda = \sqrt{2}$.

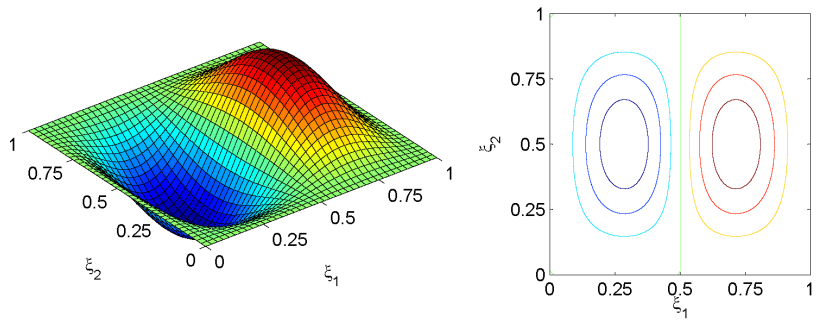
mode	p_1	p_2	q_1	q_2	ϖ
(2, 1)	7.5572	10.213	4.1022	7.8794	63.247
(4, 1)	14.035	15.548	3.6689	13.593	157.95
(2, 3)	6.9192	21.02	10.84	12.667	199.58
(4, 3)	13.599	23.959	10.55	16.736	287.37

Table A.4: AA mode parameters for aspect ratio $\lambda = \sqrt{2}$.

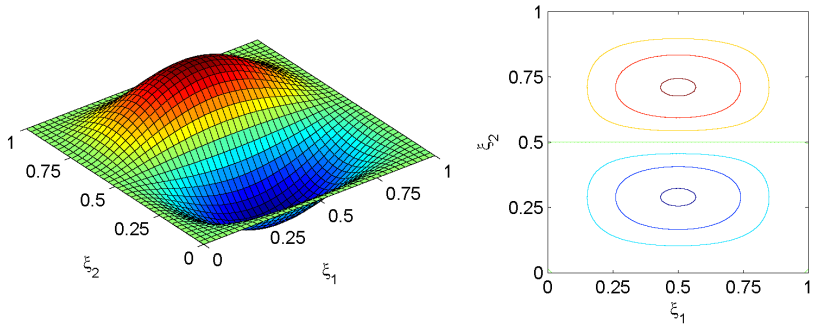
mode	p_1	p_2	q_1	q_2	ϖ
(2, 2)	7.1614	15.248	7.5733	10.065	116.62
(4, 2)	13.816	19.156	7.1817	14.895	207.17
(2, 4)	6.7741	27.04	14.04	15.472	310.93
(6, 2)	20.246	24.123	6.9331	20.579	357.33



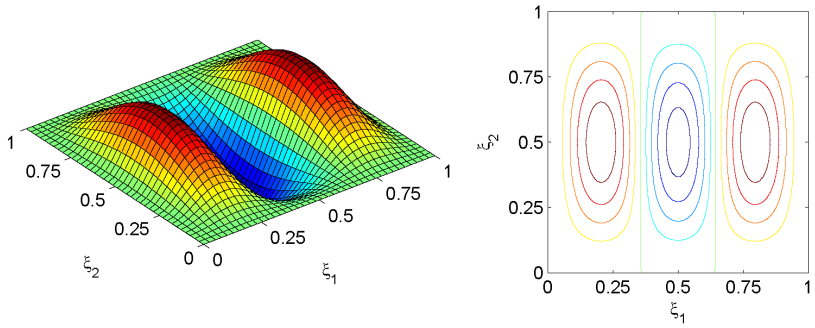
A.2.1: SS plate characteristic function with $\varpi = 39.305$.



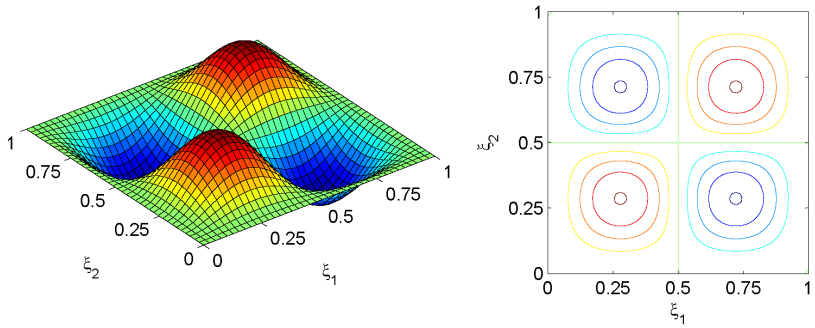
A.2.2: AS plate characteristic function with $\varpi = 63.247$.



A.2.3: SA plate characteristic function with $\varpi = 94.447$.



A.2.4: SS plate characteristic function with $\varpi = 103.15$.



A.2.5: AA plate characteristic function with $\varpi = 116.62$.

Figure A.2: Plate characteristic functions with aspect ratio $\lambda = \sqrt{2}$. On the left hand side are exhibited the graph of the first five characteristic functions. On the right hand side are displayed their isolines.

A.4 Modal Analysis with the Finite Element Model

The following figures are the first five mode shapes of the plate introduced in section III.2 computed with the finite element model of section II.4. Soon afterward the mode rotations around axes X and Y are showed for their importance. They, specifically, are used to determine the entries of the coupling matrix Γ computing the integrals of the relation (II.48). Performing a modal analysis of an undamped plate with the finite element model above mentioned, it is fairly straightforward to determine natural frequencies and mode shapes. Besides, modal rotations around the axes x_1 and x_2, respectively $ROTX_i$ and $ROTY_i$, for each mode are available and given the following relations

$$\begin{cases} \dfrac{\partial W_i}{\partial x_1} = -ROTY_i \\ \dfrac{\partial W_i}{\partial x_2} = \quad ROTX_i \end{cases} \tag{A.46}$$

it is possible, finally, to compute the above integrals numerically on the grid of the nodal points.

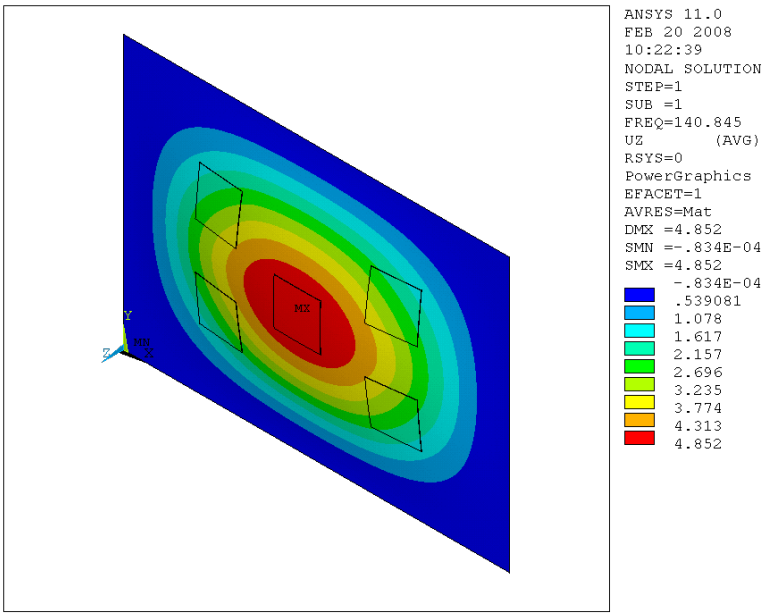


Figure A.3: The first mode shape for a plate in study.

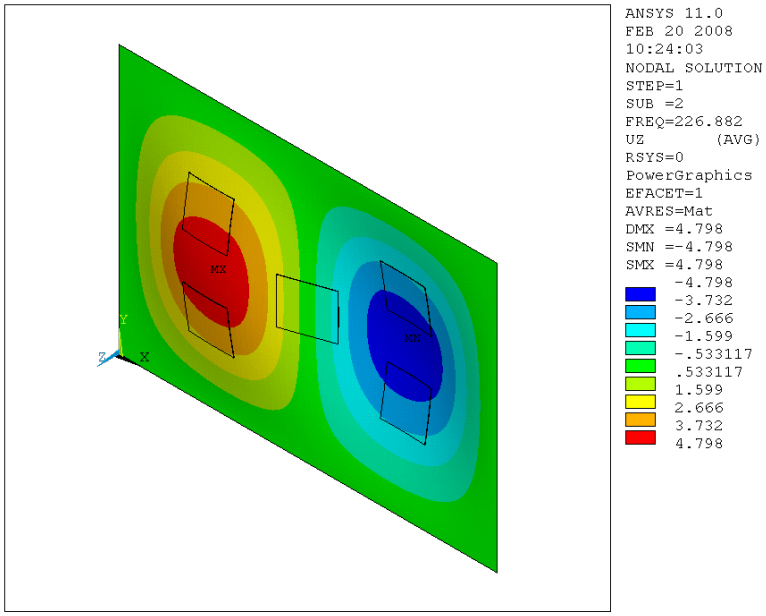


Figure A.4: The second mode shape for a plate in study.

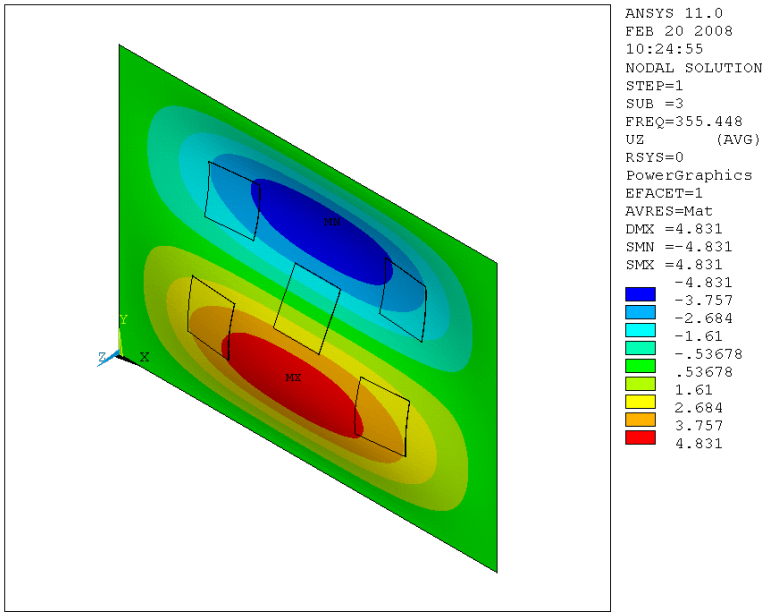


Figure A.5: The third mode shape for a plate in study.

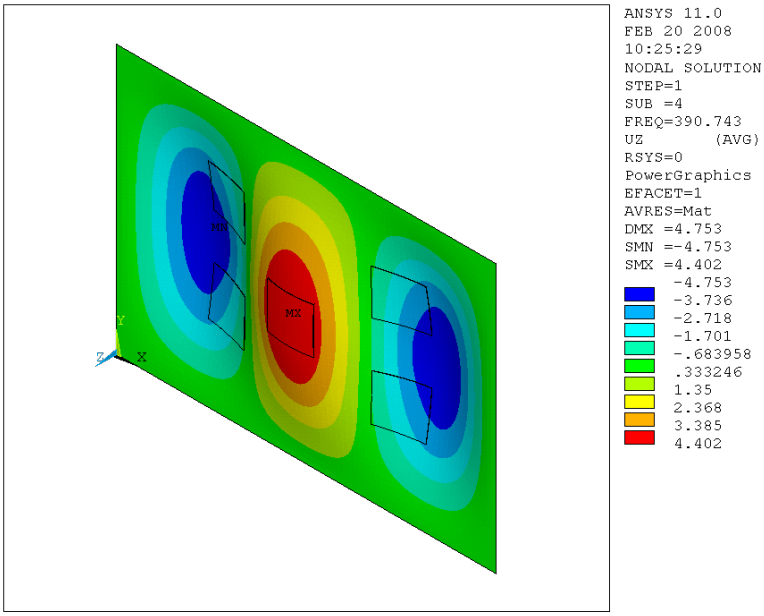


Figure A.6: The fourth mode shape for a plate in study.

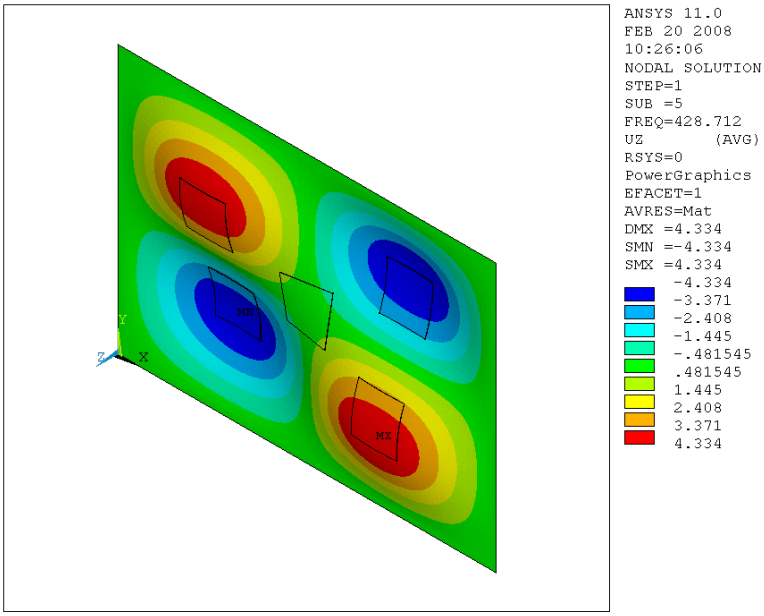


Figure A.7: The fifth mode shape for a plate in study.

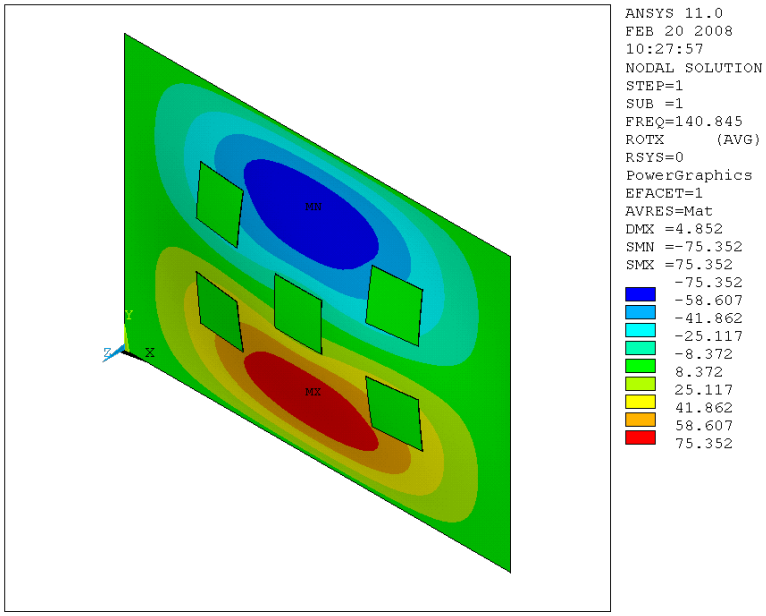


Figure A.8: The first mode rotation around the axis X.

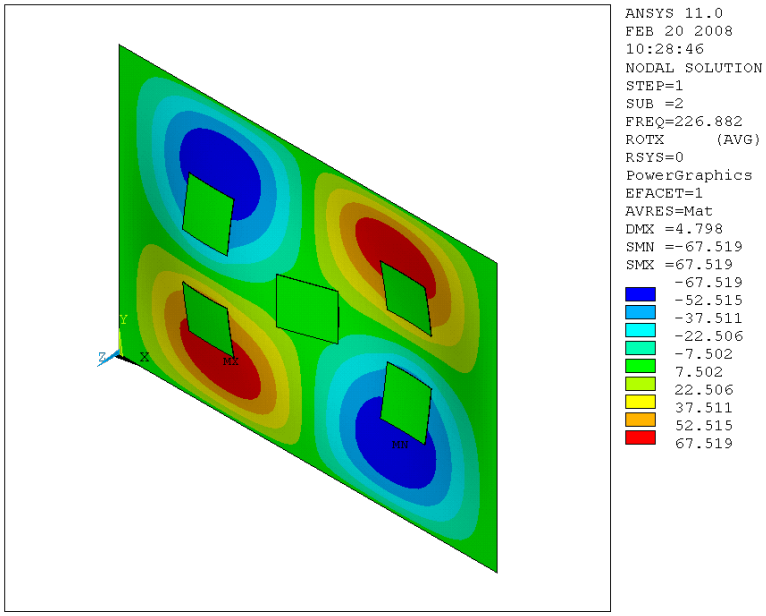


Figure A.9: The second mode rotation around the axis X.

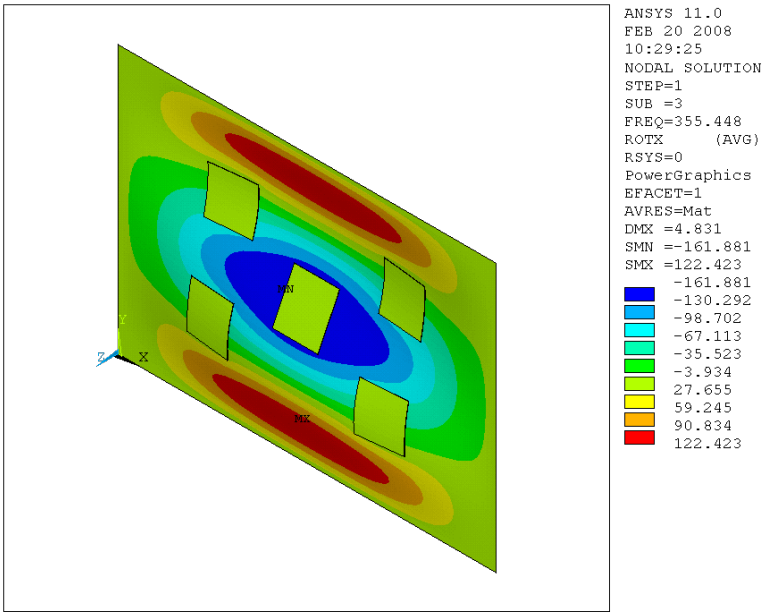


Figure A.10: The third mode rotation around the axis X.

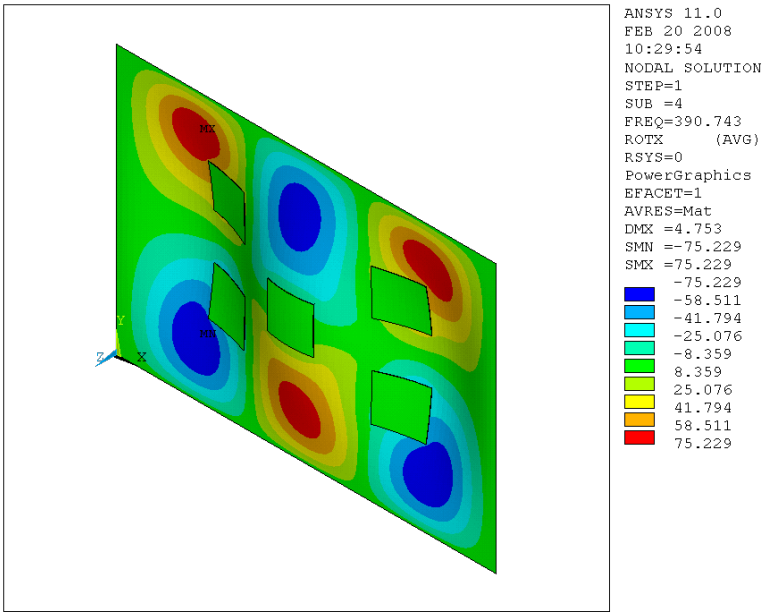


Figure A.11: The fourth mode rotation around the axis X.

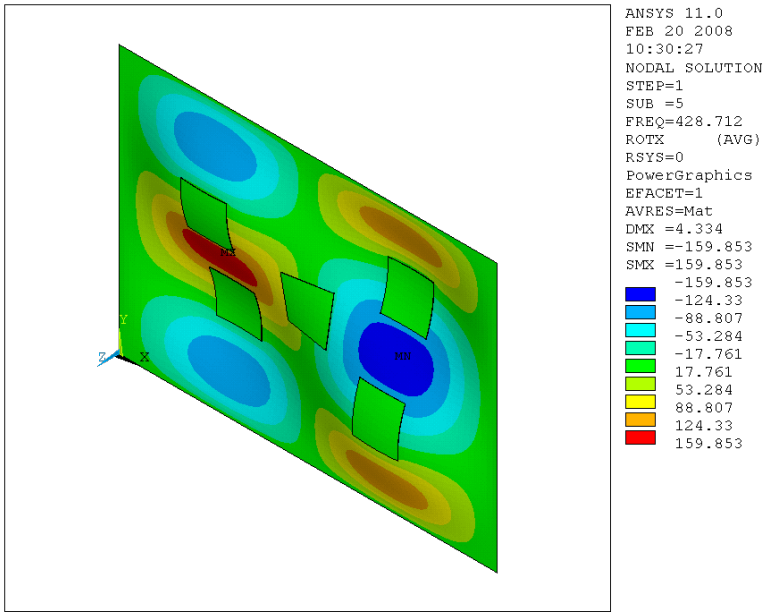


Figure A.12: The fifth mode rotation around the axis X.

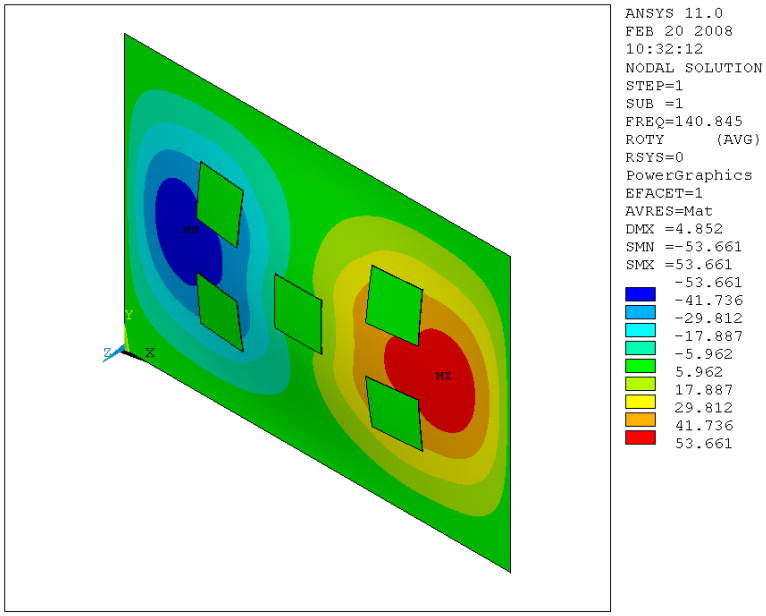


Figure A.13: The first mode rotation around the axis Y.

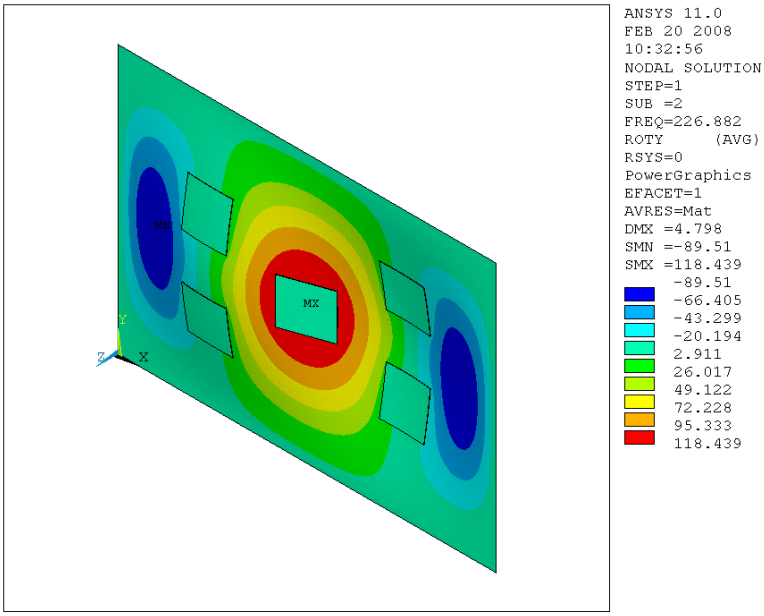


Figure A.14: The second mode rotation around the axis Y.

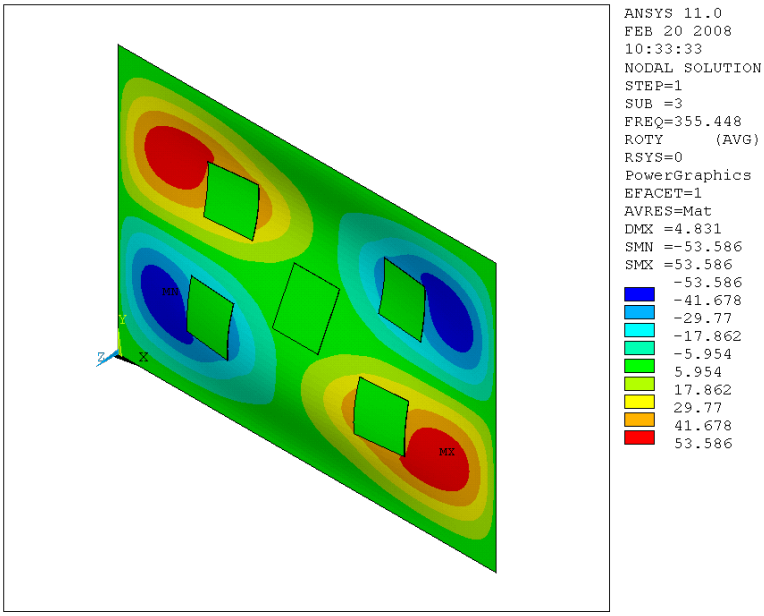


Figure A.15: The third mode rotation around the axis Y.

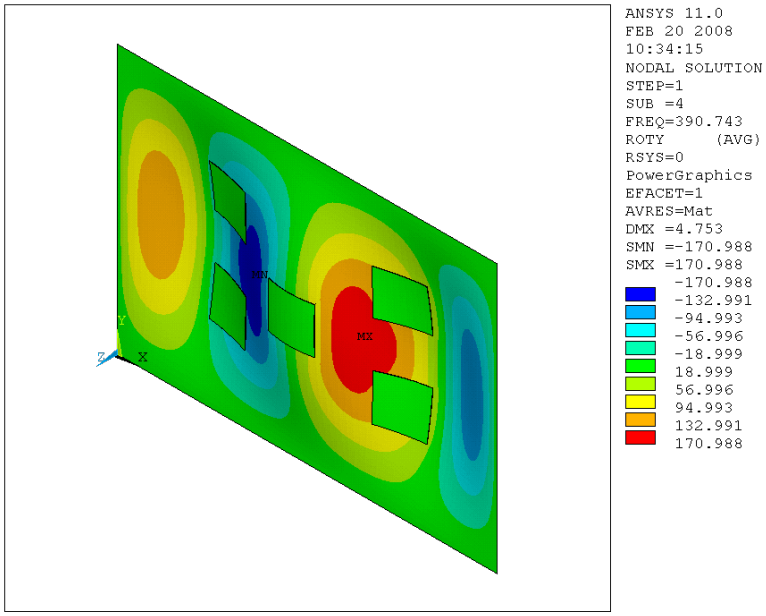


Figure A.16: The fourth mode rotation around the axis Y.

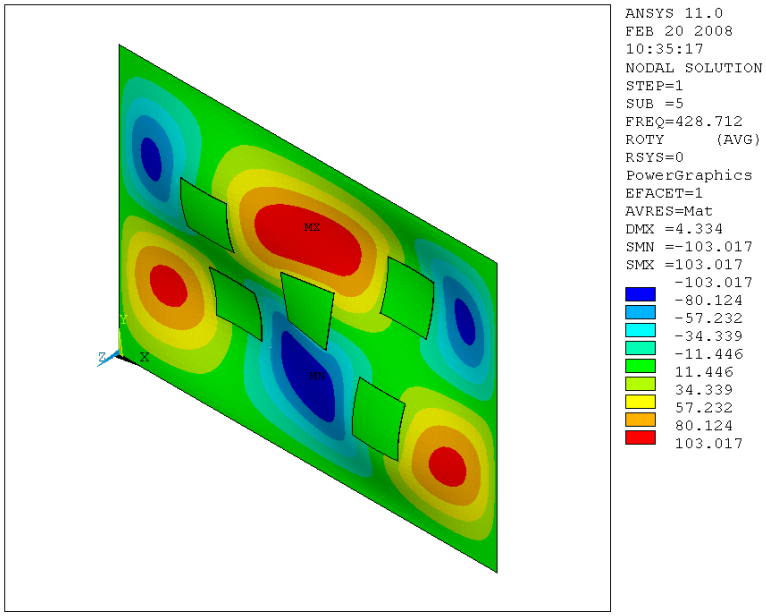


Figure A.17: The fifth mode rotation around the axis Y.

Bibliography

M. Al-Bassyiouni and B. Balachandran. Sound transmission through a flexible panel into an enclosure: structural-acoustics model. *Journal of Sound and Vibration*, 284:467–486, 2005.

S. Alessandroni, U. Andreaus, F. dell'Isola, and M. Porfiri. Piezo-Electro-Mechanical (PEM) Kirchhoff-Love plates. *European Journal of Mechanics - A/Solids*, 23:689–702, 2004. (Cited on page 64.)

S. Alessandroni, U. Andreaus, F. dell'Isola, and M. Porfiri. A passive electric controller for multimodal vibrations of thin plates. *Computers and Structures*, 83:1236–1250, 2005. (Cited on pages 1, 2, and 3.)

E. H. Anderson and N. W. Hagood. Simultaneous piezoelectric sensing/actuation: analysis and application to controlled structures. *Journal of Sound and Vibration*, 174:617–639, 1994. (Cited on page 1.)

U. Andreaus, F. dell'Isola, and M. Porfiri. Piezoelectric passive distributed controllers for beam flexural vibrations. *Journal of Vibration and Control*, 10 (5):625–659, 2004. (Cited on pages 2 and 3.)

ANSI/IEEE Std 176-1987. IEEE standard on piezoelectricity. The Institute of Electrical and Electronics Engineers, Inc, 1987. (Cited on page 61.)

A. Badel, G. Sebald, D. Guyomar, M. Lallart, E. Lefeuvre, C. Richard, and J. Qiu. Piezoelectric vibration control by syncronized switching on adaptive voltage sources: Towards wideband semi-active damping. *Journal of the Acoustical Society of America*, 119(5):2815–2825, 2006. (Cited on pages 1 and 3.)

S. Behrens, S. O. R. Moheimani, and A. J. Fleming. Multiple mode current

flowing passive piezoelectric shunt controller. *Journal of Sound and Vibration*, 266:929–942, 2003. (Cited on pages 42 and 90.)

Julius S. Bendat and Allan G. Piersol. *Engineering Applications of correlation and spectral analysis*. John Wiley & Sons, Inc., Los Angeles, California, 1980. (Cited on page 95.)

D. Bondoux. Piezo-damping: a low power consumption technique for semi-active damping of light structures. In *Proc. SPIE, Smart Materials and Structure*, volume 2779, pages 694–699, 1996. (Cited on page 42.)

I. Chopra. Review of state of art of smart materials structures and integrated systems. *AIAA Journal*, 21:1087–1091, 2002. (Cited on page 3.)

M. Dalaei and A. D. Kerr. Natural vibration analysis of clamped rectangular orthotropic plates. *Journal of Sound and Vibration*, 189(3):399–406, 1996.

F. dell'Isola and S. Vidoli. Continuum modelling of piezoelectromechanical truss beams. *Archive of Applied Mechanics*, 68:1–19, 1998. (Cited on pages 1 and 2.)

F. dell'Isola, C. Maurini, and M. Porfiri. Passive damping of beam vibrations through distributed electric networks and piezoelectric transducers: prototype design and experimental validation. *Smart Materials and Structures*, 13 (2):299–308, 2004. (Cited on page 3.)

J. Dosch, D. Inman, and E. Garcia. A self-sensing piezoelectric actuator for collocated control. *Journal of Intelligent Material Systems and Structures*, 3: 166–185, 1992. (Cited on page 1.)

D. J. Ewins. *Modal Testing: Theory and Practice*. Research Studies Press, Ltd., London, England, 1984. (Cited on page 97.)

Amâncio Fernandes and Joël Pouget. An accurate modelling of piezoelectric multi-layer plates. *European Journal of Mechanics - A/Solids*, 21:629–651, 2002. (Cited on page 64.)

A. J. Fleming, S. Behrens, and S. O. R. Moheimani. Reducing the inductance requirements of piezoelectric shunt damping systems. *Smart Materials and Structures*, 12:57–65, 2003.

C. R. Fuller, S. J. Elliott, and P. A. Nelson. *Active control of vibration*. Academic press Inc., 1996.

Senthil V. Gopinathan, Vasundara V. Varadan, and Vijay K. Varadan. A review and critique of theories for piezoelectric laminates. *Smart Materials and Structures*, 9:24–48, 2000. (Cited on page 64.)

N. W. Hagood and A. Von Flotow. Damping of structural vibrations with piezoelectric materials and passive electrical networks. *Journal of Sound and Vibration*, 146:243–268, 1991. (Cited on pages 2, 16, 17, 27, and 31.)

J. P. Den Hartog. *Mechanical Vibrations*. McGraw-Hill Book Company, Inc., New York, 1956. (Cited on page 29.)

J. J. Hollkamp. Multimodal passive vibration suppression with piezoelectric materials and resonant shunts. *Journal of Intelligent Material Systems and Structures*, 5:49–57, 1994. (Cited on pages 2 and 90.)

J. J. Hollkamp and T. F. Starchville. A self-tuning piezoelectric vibration absorber. *Journal of Intelligent Material Systems and Structures*, 5:559–566, 1994. (Cited on page 1.)

T. Ikeda. *Fundamentals of piezoelectricity*. Oxford University Press, 1990.

J. N. Juang and M. Phan. Robust controller design for second-order dynamic systems: a virtual passive approach. *Journal of Guidance, Control and Dynamics*, 15:1192–1198, 1992. (Cited on pages 11 and 113.)

J. Kim and J. H. Kim. Multimode shunt damping of piezoelectric smart panel for noise reduction. *The Journal of the Acoustical Society of America*, 116(2): 942–948, 2004.

S. Koshigoe and J. W. Murdock. A unified analysis of both active and passive damping for a plate with piezoelectric transducers. *The Journal of the Acoustical Society of America*, 93(1):346–355, 1993. (Cited on page 13.)

W. P. Mason. *Piezoelectric Crystals*. Van Nostrand, Princeton, 1950.

C. Maurini. *Piezoelectric composites for distributed passive electric control: beam modelling, modal analysis, and experimental implementation*. Phd thesis, Uni-

versité Pierre et Marie Curie and Università di Roma La Sapienza, 2005. (Cited on page 73.)

C. Maurini, F. dell'Isola, and D. Del Vescovo. Comparison of piezoelectronic networks acting as distributed vibration absorbers. *Mechanical Systems and Signal Processing*, 18(5):1243–1271, 2004. (Cited on pages 2 and 3.)

C. Maurini, M. Porfiri, and J. Pouget. Numerical methods for modal analysis of stepped piezoelectric beams. *Journal of Sound and Vibration*, 298:918–933, 2006. (Cited on page 73.)

Kenneth G. McConnell. *Vibration Testing*. John Wiley & Sons, Inc., Ames, Iowa, 1995.

L. Meirovitch. *Dynamics and control of Structures*. A Wiley-Interscience publication, 1990.

V. V. Meleshko. Bending of an Elastic Rectangular Clamped Plate: Exact Versus 'Engineering' Solutions. *Journal of Elasticity*, 48:1–50, 1997.

J. A. Mitchell and J. N. Reddy. A refined hybrid plate theory for composite laminates with piezoelectric laminae. *International Journal of Solids and Structures*, 32(16):2345–2367, 1995. (Cited on page 64.)

S. O. R. Moheimani, A. J. Fleming, and S. Behrens. Dynamics, stability, and control of multivariable piezoelectric shunts. *IEEE/ASME Transactions on Mechatronics*, 9(1):87–99, 2004. (Cited on page 2.)

S. O. Reza Moheimani. A survey of recent innovezions in vibration damping and control using shuntend piezoelectric transducers. *IEEE Transactions on Control Systems Technology*, 11(4):482–494, July 2003. (Cited on pages 3, 9, and 11.)

D. Niederberger and M. Morari. An autonomous shunt circuit for vibration damping. *Smart Materials and Structures*, 15(2):359–364, 2006. (Cited on page 3.)

D. Niederberger, A. Fleming, S. O. R Moheimani, and M. Morari. Adaptive multi-mode resonant piezoelectric shunt damping. *Smart Materials and Structures*, 13(5):1025–1035, 2004.

J. F. Nye. *Physical Properties of Crystals: Their representation by Tensors and Matrices*. Oxford, New York, 1957.

C. H. Park. Dynamics modelling of beams with shunted piezoelectric elements. *Journal of Sound and Vibration*, 268:115–129, 2003. (Cited on page 73.)

G. Pavić. Numerical study of vibration damping, energy and energy flow in a beam-plate system. *Journal of Sound and Vibration*, 291:902–931, 2006.

M. Porfiri, C. Maurini, and J. Pouget. Identification of electromechanical modal parameters of linear piezoelectric structures. *Smart Materials and Structures*, 16:323–331, 2007. (Cited on page 103.)

C. Rajalingham, R. B. Bhat, and G. D. Xistris. Vibration of rectangular plates using plate characteristic functions as shape functions in the Rayleigh-Ritz method. *Journal of Sound and Vibration*, 193(2):497–509, 1996. (Cited on page 123.)

C. Rajalingham, R. B. Bhat, and G. D. Xistris. Vibration of rectangular plates by reduction of the plate partial differential equation into simultaneous ordinary differential equations. *Journal of Sound and Vibration*, 203(1):169–180, 1997. (Cited on page 123.)

J. N. Reddy. On laminated composite plates with integrated sensors and actuators. *Engineering Structures*, 21:568–593, 1999.

N. Rizet, M. Brissaud, and P. Gonnard. Modal control of beam flexural vibration. *Journal of the Acoustical Society of America*, 107(4):2061–2067, 2000. (Cited on page 3.)

A. M. Sadri, J. R. Wright, and R. J. Wynne. Modelling and optimal placement of piezoelectric actuators in isotropic plates using genetic algorithms. *Smart Materials and Structures*, 8:490–498, 1999.

C. C. Sung and J. T. Jan. The response of and sound power radiated by a clamped rectangular plate. *Journal of Sound and Vibration*, 207(3):301–317, 1997.

J. Tang and K. W. Wang. Active-passive hybrid piezoelectric networks for vibration control: comparisons and improvement. *Smart Materials and Structures*, 10:794–806, 2001. (Cited on pages 1, 3, 17, 42, and 43.)

O. Thorp, M. Ruzzene, and A. Baz. Attenuation and localization of wave propagation in rods with periodic shunted piezoelectric patches. *Smart Materials and Structures*, 10:979–989, 2001. (Cited on page 1.)

Stephen P. Timoshenko and S. Woinowsky-Krieger. *Theory of Plates and Shells*. McGraw-Hill, New York, 2 edition, 1959. (Cited on page 54.)

S. Tliba and H. Abou-Kandil. Modélisation et contrôle actif des vibrations d'une structure intelligente. In *Actes du 7e Colloque National en Calcul des Structures*, 2005. (Cited on page 70.)

V. V. Vasiliev. Modern conceptions of plate theory. *Composite Structures*, 48: 39–48, 2000. (Cited on page 119.)

L. Weinberg. *Network analysis and Synthesis*. Mc-Graw-Hill, New York, 1962. (Cited on page 32.)

S. Y. Wu. Piezoelectric shunts with a parallel R-L circuit for structural damping and vibration control. In *Proc. SPIE, Smart Materials and Structure*, volume 2720, pages 259–269, 1996. (Cited on pages 2, 17, and 27.)

S. Y. Wu. Method for multiple-mode shunt damping of structural vibration using a single pzt transducer. *Smart Structures and Materials 1998: Passive Damping and Isolation*, 3327:159–168, 1998. (Cited on pages 1 and 90.)

S. M. Yang and C. A. Jeng. Structural vibration suppression by concurrent piezoelectric sensor and actuator. *Journal of Smart Materials and Structures*, 5:806–813, 1996. (Cited on page 13.)

K. Zhou, J. C. Doyle, and K. Glover. *Robust and optimal control*. Prentice Hall, New Jersey, 1996.